MECHANICAL BEHAVIOUR OF ADHESIVE ANCHORS INSTALLED IN CONCRETE

KONSTANTINOS D. ZAVLIARIS

VOLUME 1

A thesis submitted for the degree of Doctor of Philosophy

Department of Civil Engineering
City University London
June 1990

C O N T E N T S

VOLUME 1

VOLUME 2

LIST OF TABLES

LIST OF FIGURES

a resin, after Furr /45/.

Fig.5.1. The components of an adhesive anchor system.

Fig.5.2. Internal axial forces and displacements of the components of an adhesive anchor slice.

Fig.5.3. Envelopes of shear interfacial bond $\tau_{c,r}(z)$, steel tension $P_s(z)$ and resin tensile strain $\varepsilon_r(z)$.

Fig.5.4. System of coordinates used by Mindlin /55/ and simulation of the forces acting on the concrete by pulling out the anchor.

Fig.5.5. Distribution of steel, resin and concrete strains and of interfacial concrete-resin shear stresses derived from theoretical analysis of a particular system.

Fig.6.1. The model analysed by finite element elastic analysis.

Fig.6.2. The slip elements used in the finite element elastic analysis.

Fig.6.3. Results obtained from the linearly elastic finite element analysis (steel and resin strain distribution due to an axial pull-out load P=10 kN).

Fig.6.4. Results obtained from the linearly elastic finite element analysis (interfacial shear stress and concrete strain distribution due to an axial pull-out load P=10 kN).

Fig.6.5. Results obtained from the linearly elastic finite element analysis (steel and resin strain distribution due to an axial pull-out load P=10 kN).

of resin and the eccentricity of the anchor.

Fig.7.141. Specimen 3.15 (injection of resin). Resin strains.

Fig.7.142. Specimen 3.15 (splitting mode). Steel strains.

Fig.7.143. Specimen 3.17 (non shrink grout). Point C1. Concrete strains.

Fig.7.144. Specimen 3.17 (Non shrink grout). Point C2. Concrete strains.

Fig.7.145. Specimen 3.17 (Non shrink grout). Point C3. Concrete strains.

Fig.7.146. Partially bonded anchors. $P=P(\delta)$ and $\tau=\tau(\delta)$ relationships, obtained experimentally.

Fig.7.147. Local bond - local slip law for concrete to concrete adhesive joints.

Fig.7.148. Local bond - local slip for concrete to steel adhesive joints.

Fig.7.149. Local bond - local slip for steel to steel adhesive joints.

Fig.7.150. Resin tensile test for C1380 type of resin.

Fig.7.151. Resin tensile test for LV type of resin.

Fig.8.1. Comparison of the steel strains and displacement and the resin strains derived from theoretical and finite element analyses with those obtained experimentally.

Fig.8.2. Comparison of interfacial concrete-resin shear stresses calculated by theoretical analysis with those computed by finite element analysis, and of concrete strains derived from both analyses with those obtained experimentally.

LIST OF PLATES

Plate 26:Resin failure at the bottom.

Plate 27:Resin failure at the bottom.

Plate 28:Detail of resin failure at the bottom.

Plate 29:Detail of resin failure at the bottom.

Plate 30:Detail of resin failure at the bottom of split specimen.

Plate 31:Detail of bond failure at the bottom of anchor.

Plate 32:Resin failure at the bottom.

Plate 33:Details of the ribbed bar-resin interface.

Plate 34:Details of the ribbed bar-resin interface. Close-up.

Plate 35:Failure of resin in the case of threaded anchor.

Plate 36:Detail of the threaded anchor-resin interface.

Plate 37:Details of the threaded anchor-resin interface.

Plate 38:Pull-out test of partially bonded anchor.

Plate 39:Pull-out test of partially bonded anchor.

Plate 40:Pull-out test of partially bonded anchor.

Plate 41:Pull-out test of partially bonded anchor.

LIST OF APPENDICES

A THREADED BAR IN RELATION TO THAT OF PLAIN CYLINDER.

Appendix H CALCULATIONS FOR NORMALIZATION WITH RESPECT TO CONCRETE STRENGTH OF DIFFERENT TEST RESULTS IN ORDER TO OBTAIN COMPARABLE VALUES.

Appendix I CALCULATIONS TO CORRECT THE VALUES OBTAINED FROM TESTS 4.01, 4.03.

Appendix J CALCULATED DESIGN EXAMPLE OF A PARTICULAR ADHESIVE ANCHOR.

ACKNOWLEDGMENT

The most sincere gratitude is expressed to Dr P.R.S. Speare, Senior Lecturer in the Department of Civil Engineering, City University London, for his guidance, advice and continuous support throughout the course of this work.

Gratitude is also given to Dr St. Kollias, Assistant Professor in Civil Engineering Department of N.T.U. Athens and Head of the Laboratory of the Greek Cement Industry Association for his advice and encouragement relating to the experimental part of the work.

The experimental part of this research was carried out in the laboratory of the Association of Greek Cement Industry and the author wishes to express his thanks for the facilities made available to him.

Finally, thanks must be expressed to the administrative and workshop staff of ETAN SA who helped out in the preparatory, drawing and typing work, for their willing help and cooperation.

DECLARATION

The author grants power of discretion to the City University Librarian to allow the thesis to be copied in whole or in part without further reference to the author.

ABSTRACT

The thesis presents the main characteristics of the mechanical behaviour of adhesive anchors installed in concrete. They are the mechanisms of failure, the relationship between applied pull-out load and slip of the anchor and the stresses and strains in each of the three components (steel-resin-concrete).

The study is primarily experimental but theoretical and finite element analyses are also included.

These main characteristics are dependent on the adhesion and wetting phenomena across the resin-concrete and resin-steel interfaces, and on a series of parameters relating to geometry, properties of materials and methods of installation.

The principal conclusions obtained are:

a) The combined mode of failure involving concrete, resin tensile and interfacial bond failure, is the most probable provided that the resin has a high adhesive strength and that the anchor diameter is larger than the minimum value necessary to prevent steel failure, which can be calculated.

b) The sequence of failure in the combined mode is concrete failure in the upper part, bond failure in the remaining part of the anchor and resin tensile fracture at the bottom of the anchor.

c) The values of pull-out load normalized with respect to concrete strength, $P_u/\sqrt{f_{cc}}$, can be

regarded as independent of concrete strength. Therefore, a limit state design criterion for adhesive anchors in any concrete substrate can be established.

d) The values of anchor displacement normalized with respect to concrete strength, $\delta.\sqrt{f_{cc}}$, vary linearly with it. Based upon this, a simple mathematical function can be determined, which allows the calculation of the displacement of any adhesive anchor. This can be used as a design criterion for the limit state of serviceability of the particular system.

N O T A T I O N

A	: section area
C	: compliance of a body
D	: height of a joint
$D_a = G_a$	: shear modulus of adhesive
E	: modulus of elasticity
EP	: Epoxy
F	: applied external force
G	: fracture energy
G_a	: shear modulus of adhesive
G_c	: critical fracture energy
K_c	: fracture toughness
PMMA	: Polymethylmethacrylate
PU	: Polyurethane
P_c	: concrete axial force
P_r	: resin axial force
P_s	: anchor steel axial force
P_{u1}	: resin tensile ultimate strength in the combined mode
P_{u2}	: interfacial ultimate strength in the combined mode
P_{u3}	: concrete cone ultimate strength in the combined mode
Q_s	: strain energy per unit volume
T	: shear force across an interface
UPR	: unsaturated polyester resin
VE	: Vinylester
$W_{1,2}$	: work of adhesion between phases 1,2
W_a	: work of adhesion

W_p : plastic work

a : coefficient of $\delta=a.\tau$ relationship

b : width

c : concrete cone height

c_r : concentration of functional groups in a resin

c_a : overlapping length

f_{cc} : concrete strength measured on cubes

f_r : resin tensile strength

f_t : concrete tensile splitting strength

h : capillary height

k : numerical factor

l : embedment length

m : E_s/E_g ratio of moduli of elasticity of steel and grout

r,d : anchor radius, diameter

r_0, d_0 : borehole radius, diameter

s : length of the concrete cone generating line

t : thickness

$w_{c,r,s}$: displacements of concrete, resin, steel along the z axis

$\Phi_{1,2}$: fractional length of the phases 1 and 2 of an adhesive joint

α : flaw size

β : stress concentration factor

γ : safety factor

γ_{1D}, γ_{1P} : surface energy of phase 1, dispersion and polar component respectively

δ : slip

δ_{jin1} : slip of the anchor at load level j, on concrete with cube compressive strength i,normalized with respect to concrete strength of specimen 1

(19.56 MPa)

$\delta_{c,r}$: differential slip between steel and resin

ε : strain

$\theta[^0]$: concrete cone failure inclination, contact angle between two phases

$\varkappa$: $\sqrt{[(1/\mu)[(1/\lambda_c)+(1/\lambda_s)]\pi d_o]}$

$\lambda_{e1}-\lambda_{e11}$: factors to take into account the effect of different variables on the $\delta_1\sqrt{f_{cc}}$ values

$\lambda_{c,s,r}$: $[(E_{c,s,r})(A_{c,s,r})]$ for concrete, steel, resin respectively

μ : $a[1+(d_o/d)]+(t/G_a)$

$\mu_1-\mu_{11}$: factors to take into account the effect of different variables on $P_u/\sqrt{f_{cc}}$ values

ν : Poisson's ratio of concrete

ξ : E_2/E_1, ratio of moduli of elasticity of the substrate and adhesive

ρ : density

ρ_o : $a(d_o/d)+(t/G_a)$

ρ_{12} : $(\xi+1)/(\varphi_{12}+1)$

σ : normal stress

σ_f : ultimate externally applied normal stress

τ : interfacial shear strength

τ_f : ultimate externally applied shear stress

φ : shear rotation

φ_{12} : $1+(E_2/2)[(1+\nu_1)/E_1-(1+\nu_2)/E_2]$

ψ : E_c/G_A :ratio of concrete modulus of elasticity to adhesive shear modulus

ω : dimensionsless factor

1. INTRODUCTION

In everyday concrete construction the demand for reliable anchoring systems is rapidly increasing, as a result of the tendency either to strengthen or to alter existing concrete structures.

One method for anchoring to concrete is to install into a predrilled hole a bolt, a threaded rod or a reinforcing steel bar by means of adhesives, Fig 1.1. Adhesives commonly used include Polymers (Epoxy, Polyurethane, Polyester or Polymethylmethacrylate resins) pure or mixed with fillers or aggregates to obtain predetermined mechanical and physical properties.

In this way, independent anchors capable of transferring loads in the concrete with acceptable deformations are obtained. Independent anchors can be combined to form more complex systems or devices, to adapt to local geometrical data of the structural member and the conditions of anchorage position.

The understanding of the behaviour of installed anchors in terms of their basic failure mechanisms, the load - displacement relationship, the stresses and strains in the surrounding concrete, and the influence of the parameters involved is very important in selecting and designing the anchor correctly.

The existing information on the stress and strain distribution in all structural components involved in an anchor (bolt, adhesive, concrete) is limited in extent. Besides, doubt exists regarding the value of some critical parameters of the problem. The existing literature mainly includes either experimental work leading to proposals for the value of the load carrying capacity at failure, in

relation to the possible modes of failure, Fig 1.2, or load-displacement diagrams. However useful such a tool can be, it does not give any comprehensive knowledge about the influence of the parameters involved (geometry, materials, technique of installation), and the stress and strains development in the anchoring materials (steel, resin and concrete) at any stage of loading.

1.1. Scope of the investigation

The possible types of loading on an anchorage are tension, shear and combined tension and shear. Bending can be regarded as a combination of tension (on anchors) and pressure (on concrete or anchor).

The subject of this work is tensile anchors only and the aim is to provide some reliable criteria for designing such anchors according to modern structural concepts (Limit state of load-carrying capacity and limit state of serviceability) by examining the influence of all primary parameters. To achieve this, it is necessary to carry out both analytical and experimental research, which is the approach chosen here, Fig 1.3.

- The analytical approach, has three possible strands:
  - Examination of the fundamental mechanisms contributing to adhesion, namely the primary (chemical) adhesion, secondary (physical) adhesion and the mechanical interlocking effect. Understanding of these, together with the phenomenon of wetting, is necessary to express the relationship between the thermodynamic work of adhesion and the ideal bond strength and also its

loss. This leads to the theoretical bond strength.

- Theoretical analysis, studying the stress and strains of the structural components of the system. In addition to this, a numerical analysis of the real specimens is made using finite elements in the form of a parametric analysis of the problem.
- Fracture mechanics analysis, which is based on the hypothesis of pre-existing flaws across an interface. This is where the understanding of wetting phenomena is crucial, since incomplete wetting results in more extensive pre-existing flaws. By fracture mechanics theories the mechanisms of failure can be explained and quantitative expressions of the ultimate strength obtained.
- The experimental approach involves laboratory work with a set up enabling a study to be made of the parameters involved in the problem, and a comparison with the results of the theoretical and finite element analysis.

As the adhesive is a crucial "link" of the system, a relatively large part of the present work is devoted to a discussion of the physical and mechanical properties of the polymer materials and the adhesion mechanisms governing their bond to concrete substrate.

1.2 The failure mechanisms

The possible mechanisms of failure for an adhesive anchor are, Fig 1.2 :

(I) Concrete failure (cone failure - splitting)

(II) Bond failure across the adhesive - concrete interface. This interface is more critical than the resin-steel interface in the majority of cases, because the mechanical interlocking across it is relatively lower.

(III) Failure of steel bolt.

(IV) Combined failure involving a partial-depth concrete cone, bond failure at the adhesive-concrete interface and possibly tensile failure at the lower part of the adhesive.

The objective of a design should be to ensure failure by mode (III).

From the rest of failure mechanisms the most general is that of failure mode (IV) which is usual for relatively deep anchors.

The failure mode which occurs on each occasion depends mainly on:

- the embedment length of the anchor
- the diameter of the anchor and of the bore
- the strength of the concrete
- the physical and mechanical properties of the adhesive
- the texture of the surface of the bolt or bar to be anchored.

The forces involved in a combined mode of failure are

shown in Fig.1.2.(e) :

- The ultimate tensile load of resin at section CC1 (Pu_1).
- The ultimate shear resistance of the lateral (quasi cylindrical) surface BB_1C_1C (Pu_2) from the tip of the cone down to the bottom of the anchor.
- The ultimate resistance of the truncated cone surface AA_1B_1B (Pu_3).
- The lateral pressure (P_1) due to macro or micro roughness of the interface.

Therefore:

$$Pu_1 = \pi(r_o^2 - r^2)(f_{res}) \quad \text{.....(1.1)}$$

$$Pu_2 = 2\pi r_o(1-c)(\tau) \quad \text{.....(1.2)}$$

$$Pu_3 = [\pi r_c s((f_t)\cos\theta) - \pi r_o s_o((f_t)\cos\theta)] =$$

$$= [\pi r_c(s\cos\theta)f_t - \pi r_o(s_o\cos\theta)f_t] =$$

$$= [\pi r^2{}_c f_t - \pi r_o{}^2 f_t] = \pi(r^2{}_c - r_o{}^2)f_t \quad \text{.....(1.3)}$$

where:

f_{res}: the tensile strength of the adhesive

τ: the bond strength between adhesive and concrete

f_t: the tensile strength of concrete

and dimensions as shown in Fig 1.2.

And if all the links failed simultaneously:

$$P = P_{u1} + P_{u2} + P_{u3} \quad \text{.....(1.4)}$$

Under incremental static loading, at a certain level, a crack occurs near the hole, in the area where the failure

criterion (e.g. the principal tensile stress) reaches its critical value (crack 1, Fig 1.4). Generally this crack does not appear in the external surface as the "critical area" is very limited in extent, since the load level is relatively low.

By increasing the load in the new structural system derived after the formation of the first crack, the critical value of failure is again reached and a new crack "2" is formed and so on until a load level, at which the area where the failure criterion exerts its critical value reaches the concrete surface, thus resulting in a visible crack.

By further increasing the load it is obvious that only the mechanisms of bond failure and resin tensile failure are possible, since the new cracks cannot reach the surface.

If:

$$P_{u,1} + P_{u,2} + P_{u,3} > A_s f_y$$

this mechanism cannot be fully developed because at a previous stage of loading the bolt would have failed itself.

Given that:

$$A_s f_y > P_{u,1} + P_{u,2} + P_{u,3}$$

the mechanism of combined failure takes place.

At the level of first cracking it is always:

$$P_{u,1} + P_{u,2} > P_{u,3}$$

since the maximum value of shear stress at the interface which controls the cracking of concrete is expected at the top, and therefore the cone height c,Fig 1.2, is relatively small.

If this relationship continues to be valid under incremental loading, this will mean that the formation of a cone is possible and thus the anchor will fail by cone

failure.

The combined failure (concrete, resin and bond failure) will occur at a load level at which this inequality reverses,

$$P_{u,1} + P_{u,2} < P_{u,3}$$

The failure will take place at that value of c, at which the sum of the critical mechanisms, Eq.(1.1), becomes minimum i.e. where, as James et al /1/ reported by explaining the failure mechanisms of such anchors:

$$dP_u / dc = 0$$

or

$$(d/dc)[(r_o^2 - r^2) f_{res} + 2r_o(1-c)\tau + (r_c^2 - r_o^2) f_t] = 0 \quad (1.5)$$

and because $r_c = (c/\tan\theta) + r_o$ ..... (1.6)

$$(d/dc)[(r_o^2 - r^2) f_{res} + 2r_o(1-c)\tau +$$

$$+ \{(c^2/\tan^2\theta) + r_o^2 + (2cr_o/\tan\theta) - r_o^2\} f_t] = 0 \quad (1.7)$$

or

$$-2r_o\tau + [(2c/\tan^2\theta) + (2r_o/\tan\theta)] f_t = 0 \quad (1.8)$$

or

$$c/r_o = \tan^2\theta [(\tau/f_t) - (1/\tan\theta)] \quad (1.9)$$

The above value c/r_o is theoretical. Some factors which can affect the mechanisms a great deal are not considered. Among them are the "double cone", which leads to greater values of c/r_o, and the penetration of concrete by resin which increases the apparent r_o at the interface, also resulting in greater values of c/r_o. If the real surface, as found by experiment, is to be considered, then Eq.(1.9) can be converted in Eq.(1.10):

$$C_{real} = \Delta c + c = \Delta c + (r_o)\tan^2\theta[(\tau/f_t) - (1/\tan\theta)] \quad (1.10)$$

where:

Δc = the increase in the height of cone of failure due to the double conical lateral surface, Fig 1.2

The above concept is based on the simplified principal plain tensile stress criterion for concrete, Fig 1.4 . This, however, is not exactly the case as can be seen from Fig. 1.5.

It is obvious that apart from the vertical stress σ_z, the radial stress σ_y, the shear stress τ_{yz}, and the tangential stress σ_x may also be crucial under certain circumstances for the failure mechanism. In the cases in which the failure is governed by the tangential stress σ_x, the failure mode is splitting of the concrete, Fig.1.6.

In the case where a threaded bar is used, σ_x is increased because the radial component of pressure P_i (due to inclined contact surface concrete-resin) is causing considerably higher σ_x stresses, Fig.1.7.

It is interesting to examine initially the influence of the different parameters involved in the combined mode (embedment length, thickness of annulus, strength of resin), assuming there is no interaction among them:

By increasing embedment length, l, only the contribution of $P_{u,2}$ (bond mechanism) will increase, since $P_{u,1}$ (resin tensile) and $P_{u,3}$ (concrete tensile) mechanisms are not influenced. For common values of τ, f_{resin}, f_t, d, d_o, the contribution of $P_{u,2}$ is generally about 25% of P_{ult}. So, by increasing l, there is a linear increase in a term accounting for approximately one quarter of P_{ult}, as long as steel is not critical. After that value, further increase

in l gives no increase in the ultimate pull-out load because the steel fails.

By increasing d and keeping t and l constant, there is a linear increase in $P_{u,2}$, a linear increase in $P_{u,1}$, (because $\pi(r_o^2-r^2)f_{res} = \pi(r_o+r)(r_o-r)f_{res} = \pi(r_o+r)tf_{res}$) and $P_{u,3}$ has little effect (for constant angle θ), according to Eq.(1.3). However, there is also an increase in the tangential stress σ_x, which is dependent on the quantity $(P_i.d)$, Fig 1.7. So the splitting mode of failure becomes more likely.

By increasing the thickness of the annulus, there is a second order increase in $P_{u,1}$, a linear increase in $P_{u,2}$, whereas $P_{u,3}$ changes only a little (for constant angle θ). Besides, there is also a more uniform distribution of the shear and radial forces along the boreface in the case of threaded and ribbed bars, Fig.1.7, which contributes to higher P_{ult}.

There might be, however, in this case an increase in the total slip, since, provided that $G_{resin} << G_{concrete}$, as is always the case, the differential shear deformation of the annulus might contribute to higher final displacements, despite the more favourable stress distribution and subsequently lower concrete deformation.

By higher f_{res}, and f_t, there is an increase in $P_{u,1}$ and $P_{u,3}$ respectively.

The role of the shear bond strength τ, however, is not so simple that it only contributes to higher $P_{u,2}$. It also causes higher values of c, Equ.(1.9), thus resulting in considerably higher $P_{u,3}$, and improving the greatest part of P_{ult}, $(P_{u,3} + P_{u,2})$, and, most importantly, without any side effect (as the increase of diameter has by causing an

increase in σ_x). It is, therefore, the most important controlling factor of the performance of the bolt.

1.3. Concluding remarks

By equilibrium analysis at failure, the factors contributing to the ultimate tensile load of an adhesive anchor can be identified. The analysis shows that for the combined mode of failure (resin failure at the bottom, adhesive failure across the concrete-resin interface and concrete cone failure) there is a strong dependence of the ultimate pull-out load on the adhesive shear stress across the concrete-resin interface.

2. REVIEW OF THE EXISTING STUDIES ON ADHESIVE ANCHORS

The extensive use of adhesive anchors is largely associated with the development in the resin production and, to a lesser degree, with the enhancement of the additives to cement mortars and grouts, which have taken place over the last two decades.

This is why the first studies to evaluate the structural behaviour of adhesive anchors appeared in the early 1970's whereas there is an increase in the frequency of their use after approximately a decade, when the first tentative recommendations or guidelines for using adhesive anchors were also published.

Adhesive (or grout or resin) anchors as they were called, used to be, and still are, in use in mines and underground works for supporting the roof strata. As adhesives, unsaturated polyester resin or cement modified grouts were mainly used. The first recorded use of chemical anchors in underground work was in W.Germany in 1959 (TITAN-system) by the K.Krupp Mining Co. Since then different systems have been developed with the earliest in France (Selfix system), the USA (Cyanamid System) and in the U.K. (Nobel system). Now the use of adhesive anchors in the mining industry is a fully accepted and well proven technique.

Applications in civil engineering came later and the first were in tunnel projects. Among them were the Fish Tunnel Project (S.Africa-late 1960's), the Manx Pool Project (U.K.-1968) and the M8 Road at Jeffrey's Mount (U.K.-1969). Then the applications in concrete structures came, firstly as shear connectors or starter bars on the extension of existing concrete structures.

2.1. Biviridge R.L.W

Biviridge /2/in 1973, in a paper intended to be a guide for design of adhesive anchors, reported tests carried out in Newcastle University by pulling out anchors fixed in concrete blocks by polyester resin mortar and presented the results in load-displacement curves, Fig.2.1., for an embedment length of 450mm, bar diameter 20mm and hole diameter 28mm cast in the block or, drilled by percussive equipment.

In relation to modern anchors, the ratio of embedment length to bar diameter was huge (450/20=22.5) but was estimated according to the belief that "this must be half of the relative length valid for anchoring rebars to fresh concrete".

He also gave some creep performance data for a 20 mm bar in sandstone with 350 mm bond length for an 18 day loading period under 73 kN load, in the form of increase in the initial displacement, Table 2.1.

Table 2.1. Time dependence of the anchor displacement, after Biviridge /2/

δ_t/δ_o	Time elapsed
1.8	5 days
2.0	10 days
2.2	15 days
2.3	18 days

The design criteria (In fact"rules of thumb") proposed by Biviridge were:

$$P_{ult} = [l/25], \text{ for } l<300mm$$

$$P_{ult} = (l-50)/25 \text{ for } l>300mm$$

Where:

l: embedment length (mm)

P_{ult}: ultimate pull-out load [tones]

Hole diameter: d + (8-12)mm

For cracked material, 30% should be allowed for resin losses in the cracks.

In a further article, /3/ in 1974, Biviridge completed the report by giving some data on the softening of polyester resin by elevated ambient temperature and described a structural application of such anchors in columns at Melbourne University.

2.2. Sell R.

In 1973 Sell /4/ summarized the results of a series of tests carried out on polyester resin with concrete. The constitutive law of the anchor relating the load to displacement for a range of the embedment lengths, is illustrated in Fig.2.2.

2.3. Eibl J. - Franke L. - Hjorth D.

In 1972, Eibl Franke and Hjorth, /5/ experimented with resin mortars to study the bond behaviour of steel anchored to concrete. The set up they designed is illustrated in Fig.2.3. They used epoxy (EPR) and unsaturated polyester resin (UPR) mortars with varying resin to aggregate ratio.

EPR. mortar: 1 : 5.00 - 1 : 7.00

UPR. " : 1 : 5.25 - 1 : 7.25

The properties of pure resins were:

	EPR.	UPR.	
• Flexural strength :	80.0	95.0	[N/mm²]
• Modulus of Elasticity:	3,000	3,900	["]

The aggregates had a grading based approximately on the Fuller law which was the basis for grading used in concrete mixes in Germany.

The rebars used were cold worked ribbed bars, but some experiments were made on plain bars for comparison. The rate of loading was 0.125 N/mm²/s. The results in terms of local bond-local slip relationship are given in Fig.2.4. Because the bond length they designed was small they could calculate the local bond stress as the average value of the shear stress along the bonding length.

They also gave the influence of high temperatures on the bond behaviour in the form of curves of Fig.2.5.

2.4. Farmer I.W.

The aim of Farmer /6/, 1975 was the comparison of theoretical with actual shear stress distribution along the anchor axis. He chose 20mm anchors placed in 28mm holes with lengths of 350 and 500mm.

His theoretical consideration involved the formation of equilibrium and compatibility conditions for a slice with infinitesimal length between x and x+δx, Fig.2.6.

By setting the boundary conditions:

$x = 0 \qquad \sigma = \sigma_o = P/A_s$

$x = L \qquad \sigma = 0$

he derived the basic equation:

$$\tau_x = (\sigma_o / E_s)(1/a)e^{-ax} \quad \text{.....(2.1.)}$$

where:

τ_x : the interfacial stress

$\sigma_o = P/A_s$

E_s : modulus of elasticity of steel

$a^2 = k/r(R-r)$ for thin annulus, i.e. t/r<1

$a^2 = k/r^2 \ln(R/r)$ for thick annulus, i.e. t/r>1

$K = 2G_r / E_s$

r,R= radius of the bar and the hole respectively

G_r : The shear modulus of resin

Because for ax=4.6, $e^{-ax}=0.01$ and thus $\tau_x/\tau_o=0.01$, where τ_o the shear stress at the free end of the anchor, he termed as the transfer length of the anchor (l_t) the x coordinate for which:

$$l_t = x_{0.01} = 4.6/a$$

That is the point at which the shear stress is reduced to 1% of its value at the free end.

The distribution of shear stresses calculated in this way, is shown in Fig.2.7.

For the experimental shear stress distribution Farmer used strain gauges to measure the steel strain. The strain gauges were placed in a groove cut in one half of the bar. The loading rate was 5 kN/min. The shear stresses were computed from the measured steel strains, according to the equilibrium of an elementary length of the steel anchor:

$$2\pi rl(\Delta\tau) = (E_s)(\Delta\varepsilon)\pi r^2$$

$$\tau_{i,i+1} = (rE_s/2l)\,[\varepsilon_i - \varepsilon_{i+1}] \quad \text{.....(2.2)}$$

The experimental shear stresses so obtained are plotted in Fig.2.7 against the theoretical values, whereas the steel strain along the axis is plotted in Fig.2.8.

It is important to note here that Farmer's experimental results were possibly affected by the closeness of the anchor to the bearing forces of the jack. The effect of these forces is not reported.

2.5. Rehm G. - Franke L.

The main aim of Rehm and Franke /7/ was to present a proposal for the necessary anchorage length of reinforcing ribbed bars. They made use of the results of existing pull-out tests of ribbed bars anchored by means of resins or polymer grout. The corresponding experimental set ups matched those for determination of the bond law commonly used in OPC concrete (local bond - local slip tests).

The first conclusion of this work was that, in principle, the bonding performances are the same. The local bond - local slip law for resin mortar they proposed is illustrated in Fig.2.9 for polyester and EP.Resin mortars with resin/aggregates ratio 1/5 - 1/8.5 and compressive strengths of 70-100 N/mm^2.

The temperature and creep effects are illustrated in Fig.2.10.

Accepting that the slip, which is a function of many variables including the anchorage length, must be kept below certain limits, they made a proposal for the calculation of the necessary development length of every type of ribbed reinforcing bar anchor under any temperature and creep effect. This is illustrated in Fig.2.11 and allows the determination of the embedment length in relation to the expected value of slip.

2.6. Daws G.

Daws /8/, in 1980, recommended a method for calculation of ultimate pull-out load, based on tests on 21 N/mm^2 concrete.

He described the mechanism of concrete failure which involved firstly a shear cone formed at a depth of approximately 0.2L, Fig.2.12. By increasing load there was an increase in the failure cone until a point X was reached, such that the remaining embedment length Lx had a pull-out load value less that the force required to shear the concrete mass.

He also reported creep data for resin anchors showing an increase in the initial displacements by a factor of 2.0 after 300 hours of loading and 1.5 after 150 hours respectively, Fig.2.13.

2.7. Lee N.K - Mayfield B. - Snell C.

In 1980, Lee, Mayfield and Snell /9/ made an extensive analysis of the mechanical performance of polyester resin bonded bars by approaching it experimentally and by finite element analysis. They tested 16mm diameter high yield reinforcing bars and block end bolts made of steel with a yield strength of 710 N/mm^2 and embedment depths of 75, 100 and 125mm (4.7d, 6.25d, 7.81d). The concrete block dimension and its anchoring were in accordance with BS 5080.

Their tests showed the "double coned" profile for concrete failure, Fig.2.14, with the average depth of the cone of failure being about 25% of the anchor depth for reinforcing bars, which is far lower than all the other researchers have till now reported, 50-75% being the usual range. The ultimate and the so called service pull-out

loads (at a slip of 0.1mm), are given in Fig.2.14.

The most important outcome of their work is a simple mathematical expression for the interaction of two adjacent block end-anchors based on the model of a linear reduction in the ultimate pull-out load of a group of anchors in proportion to the reduction of the total projected area of the independent cones.

As the interaction relationship does not depend so much on the anchor pull-out mechanism as on the intersection of cone surfaces, it could be used for chemical anchors also:

$$P_{gr} = f_t [\pi v(\tan^2\theta+1)[(D/2\tan\theta) + (v/4)] + + (f_t/2)\ [2v/\sin(2\theta) + D]s \quad \ldots\ldots\ldots\ (2.3)$$

where:

P_{gr} : the ultimate load of the independent anchor as one of the two anchors of the group.

f_t : the tensile strength of concrete.

v : the embedment length.

θ : the cone semi-angle measured from the vertical line.

D : diameter of the hole

s : distance between the two bolts

The first term in the bracket expresses the contribution of the external semicone and the second the contribution of the internal symmetric semisurface between the two anchors.

They tested also the creep performance of bonded anchors and their results, which are very similar to those of Biviridge /2/ and Daws /8/, are illustrated in Fig.2.15.

2.8. Canon R.W. - Godfrey D.A. - Moreadith R.L.

In 1981, Canon, Godfrey and Moreadith /10/ stated general design rules for the design of anchor bolts and other steel embedments. They stressed that:

- The basic philosophy of anchorage requirements must be consistent with the ultimate design philosophy of concrete structures. This means that the failure mechanism should be controlled by requiring yielding of the steel anchor prior to brittle failure of concrete, Fig 2.16.

- The calculation of the ultimate pull-out load of the surrounding concrete can be based on a nominal inclination of the failure cone of 45° against the horizontal plane.

- The inclination of the lateral cone surface is reduced as the crack propagates toward the free surface, as a result of the influence of the compressive stresses which occur in the vicinity of the perimeter.

- The edge effect, or the cone intersection effect of adjacent anchors, must be taken into consideration by reducing linearly the ultimate load carrying capacity in accordance with the reduction of the total lateral surface.

2.9. Wachtsmuth P.P. - Eligehausen R.

In 1982 P.P.Wachtsmuth and R.Eligehausen /11/ presented a state of the art report, according to which:

- The cone depth by concrete failure is about 70% of the anchor depth.
- The failure surface is inclined at 35° - 40° to the horizontal plane.
- Exposure to temperatures higher than 20°C resulted in a decrease in shear strength, as is illustrated in Fig.2.17 and the time dependent increase in

total displacement was almost linear, as is shown in Fig. 2.18.

2.10. Kobarg J.

In 1982 Kobarg /12/ carried out a major experimental programme in the University of Karlsruhe. The whole project was designed to take advantage of unpublished results of similar tests conducted previously, so that a large number of parameters could be taken into consideration. These parameters were:

- The embedment length.
- The concrete strength.
- The curing conditions of concrete.
- The type of loading.
- The diameter of the hole.

In the majority of tests only the load and the anchor slip were measured. However, some tests were gauged for strain measurement in the anchor and the surrounding concrete as well.

The concrete block was reinforced and had the form illustrated in Fig.2.19, the diameters of the anchors were 20 and 28 mm made of steel St.42/50 and 26.5 and 36 mm made of steel St.83/103 (high yield prestressing steel). The hole diameters were 30, 40, 40 and 50 mm respectively.

Kobarg first examined the dependence of bond length on the concrete strength in order to achieve the max pull-out load, Fig.2.20.

Starting from the formulation of equilibrium and compatibility conditions, Kobarg came by integration to the well known expression

$$\delta(x) = \int_{x\,i}^{x\,j} \varepsilon_s(x)dx - \int_{x\,i}^{x\,j} \varepsilon_b(x)dx + \delta_o \quad \ldots\ldots\ldots\ldots \quad (2.4)$$

Where:

$\delta(x)$: The slip between concrete and steel anchor at the section of x coordinate.

$\varepsilon_s(x)$: The strain of steel.

$\varepsilon_b(x)$: The strain of concrete.

δ_o : The initial slip.

By adopting a law for the distribution of concrete strain as shown in Fig.2.21., Kobarg could calculate the second integral and thus by taking the measured values of $\delta_o(x=0)$ and of $\varepsilon_s(x)$ at characteristic sections, on the one hand, and the calculated values of

$$U_b(x) = \int_{x\,i}^{x\,j} \varepsilon_b(x)dx$$

on the other, formed the strain and displacement distribution along the axis of the anchor Fig.2.22.

By combining these values of $\delta(x)$ at characteristic sections with the values of $\tau(x)$ calculated from the fundamental equation of equilibrium,

$$d\sigma_e/d_x = (2/r)\tau(x) \quad \ldots\ldots\ldots\ldots\ldots\ldots \quad (2.5)$$

he could establish the $\tau=(\delta)$ law in the form illustrated in Fig.2.23.

Kobarg also calculated the critical embedment length, which is the length for which there is a simultaneous failure of steel and concrete, as a function of the concrete strength, the ratio of hole diameter to anchor diameter and

the ratio of maximum particle size of concrete to anchor diameter as shown in Fig.2.24.

The type of bond stress and steel stress distribution he obtained are shown in Fig.2.25 and 2.26. The curves are different from those of Farmer (Fig. 2.7, 2.8). However, the curves are not comparable because:

- the shear stress of steel to resin according to Farmer is a different stress from Kobarg's bond stress of steel to concrete.
- the differences in the ratio of embedment length to anchor diameter were large (Farmer ≈ 17.5, Kobarg ≈ 9.0).
- Farmer based his model on homogeneous elastic analysis whereas Kobarg took into consideration the concrete cracking state, Fig 2.21, and its influence on the stress and strain distributions.
- the strain gauge lay-out of Kobarg was more dense than Farmer's, so there is a difference in the accuracy of calculation.
- in Kobarg's experiments, and this is a remarkable point of his work, there was a certain contribution of the lateral boundary conditions to the stress of the structural components of the system, since the lateral dimension of the concrete block was very small in relation to the embedment length and the anchor diameter:

2b/l=500/(240..500)=(2.1)..(1.0) (common values 6.0)

2b/d=500/(20..36) =(25)..(14) (common values 32.0)

Yet, this set-up resulted in increase in the lateral pressure at the interface which became evident from the tangential strains of concrete he measured.

So it was expected that, even for deep anchors, the concrete failure mode was unlikely to occur and that the concrete splitting mode of failure was on the point of starting or actually took place in most cases.

2.11. Peier W.H.

Peier /13/ analysed the strain and stress distributions in the concrete surrounding the adhesive anchor by means of a sophisticated finite element analysis which:

- was based on the real, non linear $\sigma = \sigma(\varepsilon)$ behaviour of concrete
- could take into account the triaxial stress situation in the concrete.
- by gradually incrementing the load, could determine the failure surface by calculating the relative principal stress and, in the event of it reaching its ultimate value, could reduce the stiffness of the element for the analysis of the next stage.

The problem is that the anchors analysed by Peier were extraordinarily shallow (l=80mm, d=25mm, l/d=3.2d). He also did not consider the resin as a structural element of the system. The failure cone determined by Peier is illustrated in Fig.2.27.

2.12. Eligehausen R. - Mallee R. - Rehm G.

In 1984 Eligehausen, Mallee and G.Rehm /14/ made a very extensive review of existing studies and formed a report which could be used as a comprehensive guide for design of adhesive anchors. They concentrated on capsule anchors with unsaturated polyester resin with aggregates as adhesive and

based all their study upon these.

They describe first the possible failure mechanisms and clearly state that, for common anchors with an average embedment length of v=9d, if the anchor is to fail by pull-out the average bond strength, τ, must be greater than 8.0 N/mm² for a concrete compressive strength greater than 20 N/mm².

The crack which finally results in failure starts at a depth of approximately 60-75% of the bond length. They further report that in the remaining bond length, the bond strength between resin mortar and concrete is exceeded. For this mode of failure, provided that the tensile strength of concrete is linearly dependent on f_{cc}, they proposed:

$$P_{ult} = 0.85\ v^2 \sqrt{f_{cc}} \qquad \text{.....(2.6)}$$

where:

P_{ult} : ultimate failure load [N]

v : embedment length [mm]

f_{cc} : compressive strength of concrete [N/mm²]

The loads calculated from Eq.(2.6.) are plotted in Fig.2.28. against the 5% and 95% fraction curves of the experimental results.

By increasing v beyond 9d, however, there is no substantial increase in the ultimate failure load, so Eq. (2.6) is valid for ratios of embedment length to diameter of anchor less than 9.

They further devote a whole section to the effects of group of adjacent anchors and that of an anchor near the edge of concrete member. Based upon the concept of the reduction of the lateral concrete surface of cone failure if the centres of adjacent anchors lie closer than a critical distance dk= 2v they proposed:

$$P_{u,gr} = (K_a)P_{ult} \quad \text{..... (2.7)}$$

where:

$P_{u,gr}$: the real failure load of the group

P_{ult} : nP_{ult} calculated according to Eq.(2.6)

n : the number of the anchors of the group

K_a : reduction factor= $(K_{ax})(K_{ay})$

$K_{ax,y}$: $0.5(1 + a_{x,y}/d_k)$

d_k : 2v

$a_{x,y}$: actual centre to centre distance

In the same way, they proposed the calculation of the ultimate pull-out load for anchors placed near the edges, by using Eq.(2.6.).

In this case:

$$P_{u,e} = K_{a,e}P_{ult} \quad \text{..... (2.8)}$$

$K_{a,e} = a_e/d_e$

a_e :actual distance of the centre of the anchor from edge

d_e = v

Should the edge effect on a group of adjacent anchors be taken into consideration, then $P_{u,e,gr}$ is to be calculated as:

$$P_{u,e,gr} = K_a K_e P_{ult} \quad \text{..... (2.9)}$$

They also give some data on the behaviour of adhesive anchors with 10-24 mm diameter at high ambient temperatures combined with long term loading effects. Fig.2.29.

The data given for normal ambient temperature (23° C), are less than those of Daws /8/. However, at elevated temperatures there is an increase in the values of Eligehausen et al and a tendency towards agreement.

The effect of the cracked state of the concrete is also examined. They collected unpublished data from various tests undertaken on different systems of chemical capsule anchors in order to obtain a licence for their use and presented the influence of crack width on the reduction of pull-out load in the form of Fig.2.30., with very wide scatter, which is attributed to the random path of the artificially formed cracks over the embedment length.

It may be the right place here to point out the advantages of using the injected adhesive anchors for structural applications over the capsule anchors and the coated bolts or rebars. The common capsule anchors consist of two glass cylinders one inside the other, each containing the two component of resin. The cylinders are broken after having been put in the bore, by the anchor stud which is driven by the same drilling device used to drill the bore. By breaking of the cylinders the two components come into contact and are mixed by the rotating anchor stud. Although the volume of the mixed resin is usually greater than the volume of the gap it must fill, the filling of the possible cracks crossing the drill is uncertain. Conversely, the injection fills up the possible cracks crossed by the anchor's hole and simultaneously saturates with resin all the voids and gaps in the surrounding concrete down to 10μ, provided there is a connection between them, so contributing to a higher ultimate pull-out load and reducing anchor displacement. As a result, in the cases where there is a need for anchoring in concrete under tensile or reversed stresses, it can be deemed as imperative to use injection as the proper means of installing the resin.

2.13. James R.W. et al /1/

In 1987, James et al /1/ made a review of the possible failure mechanisms of adhesive anchors and they reported that for a combined mode of failure the ultimate resistance of the anchor is the sum of the contributions of the concrete, resin and bond shear strength along the interface down to the tip of the concrete cone, assuming simultaneous failure of the three mechanisms. They stated that the theoretical depth of spall can be derived from the requirement for the minimum ultimate pull-out load of the anchor and they showed that this depth, for a constant angle of the lateral conical surface, is dependent on the bond strength across the concrete - adhesive interface, the concrete strength and the hole diameter.

They further made a linear and a non-linear finite element analysis. From the linear analysis they obtained contours representing constant values of τ_{max}/τ_{crit} for the Mohr-Coulomb criterion they adopted, in the form shown in Fig.2.31, which represent the boundary of the concrete failed corresponding to the particular bolt stress level indicated in Fig.2.31

From the nonlinear analysis, which enabled to be taken into consideration the progressive cracking of the concrete, they could predict the bolt tensile stress-slip relationship, Fig.2.32, and the conic angle $\theta=45^{\circ}$ (in contrast with linear analysis according to which $\theta=60^{\circ}$).

2.14. Concluding remarks

The majority of the existing literature on adhesive anchors is devoted to the possible failure mechanisms and the resulting geometry of failure. Most of the existing

papers mention the anchor pull-out, the steel failure, the concrete cone failure and the concrete splitting mode of failure. However, that closest to what happens in reality is James et al /1/, who clearly define the combined concrete cone failure involving the failure of resin near the bottom and the shear failure across the concrete resin interface. Lee et al /9/ did not discuss the combined mode but do report the double cone profile of the failed concrete.

There are some mathematical expressions for the ultimate pull-out load of adhesive anchors as function of the geometry of the anchor and some expressions which take into consideration the properties of all materials involved. The most comprehensive analytical proposal is that of James et al /1/, according to which, at the first stage, the depth of concrete cone expected must be calculated.

Most of the experimental work has led to P-δ (pullout force - total anchor slip) relationships. The relationships reported are illustrated in Fig 2.33. There is a very wide gap between the different curves drawn because of the different condition of the tests. It seems, however, at first sight, that the diameter and the embedment length are among the decisive factors.

The same wide gap exists among the τ-δ (interfacial shear stress-local slip) relationships, reported, Fig 2.34, which cannot be regarded as comparable, because of the quite different materials, geometry and conditions of the tests.

There are few theoretical analyses of the stress and strain distributions of the anchor components. They are combined with experimental work in order to have feed back

from tests to formulate the boundary conditions. Although there is no significant divergence in the theoretical aspects used, the results are different owing mainly to different test conditions being modelled.

The finite element analyses reported are based on either linear or nonlinear laws for the concrete stress-strain relationship, but in none of them the differential slip across the adhesive-concrete is taken into account.

The time and temperature dependent properties of the anchors are reported in several works which are in general agreement.

Finally, the group and edge effects are handled by some authors who proposed formulae for the reduction of the ultimate pull-out load of anchors belonging to a group of anchors or placed near to existing edges as mathematical function of the geometry of their lay-out.

3. ADHESION AND BOND

3.1 The Science of Adhesion

In reality the typical adhesive anchor system which consists of:

- the concrete
- the resin
- the bolt or the ribbed bar

is an adhesive joint, in which the resin has the ability to withstand and transfer significant stresses between the materials it joins by means of adhesion.

In order to have the data necessary to evaluate the strength of this adhesive joint the fundamental mechanisms and basic theories of adhesion should be discussed.

As will be seen later, the criteria for interfacial adhesive failure are strongly dependent on such characteristics as the surface tension of the substrate and the adhesive and the thermodynamic work of adhesion. The dependencies for ideally brittle and elastic tensile and shear joints are as follows:

<u>Tensile joint</u>

$$\sigma_{1,2} = \sigma_{1,2}\ (G_c,\ \alpha)$$

$$G_c = G_c\ (W_{1,2})$$

$$\alpha = \alpha\ (\alpha_0,\ \gamma_1,\ \gamma_2)$$

$$W_{1,2} = W_{1,2}\ (\gamma_{1d}, \gamma_{2d}, \gamma_{1p}, \gamma_{2p},)$$

$$\gamma_{1,2} = \gamma_{1,2,d} + \gamma_{1,2,p}$$

Shear joints

$$\tau_{1,2} = \tau_{1,2}\ (K_c, a)$$

$$K_c = K_c\ (G_c)$$

$$G_c = G_c\ (W_{1,2})$$

$$\alpha = \alpha\ (\alpha_o,\ \gamma_1,\ \gamma_2)$$

$$W_{1,2} = W_{1,2}\ (\gamma_{1d}, \gamma_{2d}, \gamma_{1p}, \gamma_{2p},)$$

Where:

$\sigma_{1,2}$, $\tau_{1,2}$: ultimate adhesive strength between the two phases,the adhesive (1) and the substrate (2)

G_c : critical fracture energy

α : pre-existing flaw across the interface

$W_{1,2}$: thermodynamic work of adhesion

$\gamma_{1,2}$: surface energy of adhesive-substrate respectively.

γ_{1d}, γ_{2d} : dispersion intermolecular component of γ_1 , γ_2

γ_{1p}, γ_{2p} : polar intermolecular components of γ_1 , γ_2

K_c : critical stress intensity factor

The above mean that a brief review of existing theories on the following is necessary to understand the mechanisms and express quantitatively the ultimate bond strength of an adhesive joint:

a) adhesion forces operating across an interface
b) the wetting phenomena, including the aspects of surface energy and the thermodynamic work of adhesion, and
c) the fracture mechanics principles.

3.1.1 The mechanisms of adhesion

In all the joints of this type the adhesive joins the solid parts by attaching to their surfaces within a layer of molecular dimensions i.e. of the order of 0.1 to 0.5 nm. Because adhesives are liquid in their early stage, in the ideal cases they wet the solids and flow into the surface irregularities of the solid substrate, and, if the surface is free of contaminations, come into intimate contact with it. As a result, they interact with it on atomic or molecular scale.

Wetting the substrate (which is also referred to as adherent) implies the formation of a thin film of liquid spreading uniformly, without breaking into droplets on the surface, Fig.3.1.

Once interfacial contact between substrate and adhesive has been established and the adhesive solidified, the link generated by the adhesive is capable of transferring forces.

This link involves various types of intrinsic forces which may operate across the interface. These types of interfacial forces are broadly referred to as mechanisms of adhesion.

The modern state of the art permits classification of adhesion mechanisms into:

- mechanical interlocking effects and
- specific adhesion, which involves:
    - adsorption (the accumulation of molecules or atoms of a gas or liquid on a solid) and wetting
    - chemical bond
    - electrostatic phenomena
    - diffusion

3.1.2 The theories of adhesion

Mechanical theory (Mechanical interlocking effects)

The idea of the mechanical interlocking is that the liquid adhesive penetrates the pores or flows into the irregularities of the substrate implementing in this way connectors with it.

The **Adsorption theory** explains adhesion in terms of surface forces. According to this theory, provided that intimate molecular contact is achieved across the interface, interatomic and intermolecular forces are established, which result in strong adhesive bond. The forces which are involved in this model are the well known Van der Waals forces (Keeson, Debye, London forces), referred to as secondary bonds.

Chemical (or **primary**) bonding, which may sometimes be formed at interfaces, provided that molecular contact has already been established, increases adhesion and contributes positively to the durability of the joint. It generally involves covalent, ionic and metalic bonds.

The **Electrostatic theory** arose from observations obtained from peel tests which could not be explained adequately by existing theories (crackling noises and flashes of light during rapid peeling). Kinloch /15/, criticising this theory, states that it generally appears that the electrostatic forces involved in this theory do not contribute significantly to the strength of typical adhesive joints.

Alner /16/, in a review paper, reported that the fundamental concept of the **diffusion theory** is that adhesion is the result of interdiffusion of the adhesive and the adherent, and that this theory has been applied principally

to joints between polymeric materials .

In general, the adsorption theory has the broadest applicability whereas each of the others may be appropriate in certain circumstances. Because any contribution of these forces to the strength of an adhesive joint is very difficult to isolate from other contributions (e.g. rheological energy losses in the adhesive and the substrate as well geometrical and loading factors, etc.), the only way to obtain information about their magnitude is indirectly or by fracture mechanics concepts. From the possible adhesion mechanisms the mechanical interlocking and absorption will be discussed below as the only ones applicable to chemical anchoring.

3.2. Mechanical Adhesion

3.2.1. The mechanisms

The mechanical interlocking mechanisms between phases are affected by two factors, as Fiebrig /17/ reports:

- the microtopography of the substrate, Fig 3.2.
- the size of molecules of the adhesive,

which means that some chain segments which fit into the micropores of the adherent effect an interlocking action different from that of greater molecules.

Adhesion cannot be expressed by taking into consideration only these factors, since the effective contact surface, Fig.3.2.b, is influenced by the wetting phenomena and the chemical interaction between the two phases.

However incomprehensible the effect of the contribution of mechanical interlocking to the adhesion across an interface might be, the following points must be noted:

- A strong bond may be formed even in the absence of strong molecular attraction.
- The bond is especially strong under shear stress.
- Most of the transformation of the fluid to solid state of the adhesive is accompanied by volume changes which affect the final result.

It has been suggested in the literature that the increase in joint strength due to the mechanical "keying" might be attributed to the additional interfacial area provided by the mechanical interlocking (Fig 3.2) and the more beneficial stress distribution across the interface, promoting the plastic deformation.

3.2.2. The role of shrinkage

It is unfortunate that most changes of state in adhesives are associated with shrinkage, (all polymerization or cross linking processes exhibit shrinkage because they establish stronger bonds between molecules than in fluid state).

Apart from the fact that the shrinkage rates of most adhesives are rather low and in the case of small dimensions their effect negligible, the possibility of using shrinkage reducers, usually fillers of different kind, is of great importance. Their effect depends on the nature and the mixing ratio of the polymer and the aggregates and will be discussed in Chapter 4.

3.3. Specific adhesion

There are two broad categories involving chemical (primary) and physical (secondary) forces, as can be seen in Table 3.1. illustrating their range of magnitude.

Table 3.1: Linkage energy of primary and secondary bonds after Fiebrig /27/

	Linkage Energies in kJ/mol	Adhesion Strength in N/mm2	
Type of Forces		Theoretical Adhesion	Technical Adhesion
<u>Primary Bonding Forces</u>			
Covalent	60..700	17500	
Ionic	600..1000	30	
			15..25 in general
<u>Secondary Bonding Forces</u>			
Permanent Dipoles	<20	200..1750	
Induced Dipoles	<2	35..300	
Dispesion Forces	0.1..40	60..360	
Hydrogen Bridge	<50	500	

The terms "primary" and "secondary" imply the relative strength of these forces. The primary forces concern only atomic interaction. If this is to occur, an intimate contact of the two phases across the interface must have been achieved. This is because the primary bond forces are all short range (2-3 A° at most). The secondary forces are much weaker but are effectively of considerably greater range (up to 10 A° at least).

An interatomic primary bond can be covalent, ionic or metallic, Fig.3.3.

There are several types of the intermolecular (secondary) forces but all arise from interactions between electrostatically unbalanced molecules, which are the results of electrostatic attraction between dipoles. A dipole describes an electrically neutral molecule with a

pair of opposite charges whose weight centres do not coincide. This can be explained by the theory of Pauling.

The different types of Van der Waals forces arise from different types of dipole interaction, which are described below.

3.3.1. Dipoles and polar molecules

Keesom (or dipoles) forces arise from the direct interaction of permanent dipoles in neighbouring molecules of two or more polar compounds, where the dipoles orientate themselves to minimize internal energy Fig.3.4.a.

Debye (or induced dipole) forces may exist between polar and non polar molecules, the dipole moment of the former inducing a dipole in the latter by means of its electrostatic field. Then an attraction takes place between the polar molecules and the induced dipoles, Fig.3.4.b.

London (or dispersion) forces are attributed to instantaneous dipoles. The perpetual motion of electrons gives random instantaneous displacement of the electrons from the theoretical positions at which they give non polarity, so that there is always an instantaneous dipole set up in any molecule (even in non-polar one). These instantaneous dipoles will be established in different molecules across an interface and each tends to induce a corresponding dipole in the other. There is therefore a force of attraction between the instantaneous and induced dipoles, Fig 3.4.c.

The important characteristic of this kind of force is that they are not dependent on the permanent dipoles of polar molecules, but exist on any surface.

The **Hydrogen bond** is not a chemical bond but a special

case of dipole - interaction. It represents the forces of attraction between a highly electronegative atom or group, such as oxygen or chlorine and one or more hydrogen atoms, Fig 3.4.d. Hydrogen bonds can also be formed when there are highly polar groups such as hydroxyls (-OH) and carboxyls (-COOH) on polymeric structures, which play a significant role in many adhesives.

In all the above types of attraction it is common that the attractive forces vary with the inverse seventh power of the distance between molecules, Fig 3.5, as Elley /18/ and Fiebrig /17/ reported.

3.3.2 Adhesion and cohesion

It is possible to use existing formulae for calculating the attractive energy or forces between molecules due to each of the aforementioned interactions. The summation of the various molecular energies results in the total attractive energy between two molecules, Good /19/.

If in this integration of the pairwise interaction, to every molecule of phase 1 only the influence of all the molecules of the same phase are calculated, this results in the cohesive strength of the phase 1.

If, on the contrary, on the molecules of the one phase only the forces due to their interaction with molecules of the other phase are calculated up to a determined depth, this gives the adhesive strength.

So, regarding the possible modes of failure there is a distinction between:

- adhesion failure (at the adhesive - adherent interface), and

- cohesion failure (within the adherent or the adhesive).

For the resin-concrete case this is illustrated in Fig. 3.6.

Van der Waals forces are operative over very small distances only. Therefore the atoms of the two surfaces must be brought close enough together to enable these forces to become active. Adhesion, however, is only one of the requirements to achieve a strong adhesive joint. Additionally an increase in the real contact area , Fig 3.7, and the absence of weak boundary layers are essential factors.

To achieve a large contact area means that the one material must fit into the irregularities of the other, which, in a practical sense, implies that one of the materials must be fluid when it comes in contact with the other. This, however, although necessary, may not be a sufficient condition. If, for example, a high viscosity fluid makes a sizeable contact angle with the solid (which is the angle formed by the intersection of the fluid-solid and the fluid-air interfaces), Fig.3.7.b, there is only slight probability of creating a large contact area with the substrate. This, in turn, leads to entrapped air voids, Fig.3.8, and thus in little penetration of the irregularities of the solid. In contrast, if the liquid phase spontaneously spreads on the solid Fig.3.7.a, the contact area increases as the fluid penetrates more completely the pores and the cavities of the solid. As a result, the bond forces become greater because the integration of the molecular forces applies over a larger area.

A proper adhesive, apart from flowing into the crevices, must also displace the more loosely absorbed molecules, e.g. the air and water molecules attained by any fresh surface immediately after its exposure to air, and come intimately close to the molecules of the solid to bond effectively to them.

3.4. Wetting

In order to assess the ability of a given combination of substrate-adhesive to meet the aformentioned requirements, it is necessary to examine:

- the wetting equilibria, determining the extent of possible flaws at interface,
- the values of the free energy of both substrate and adhesive,
- the correlation between adhesive strength and thermodynamic work of adhesion.

Wetting is the ability to cover the substrate completely. This ability is governed by both the driving force which tends to produce the spreading of the adhesive over the substrate, and the resistance to spreading which is controlled by the viscosity of the adhesive, the surface irregularities and the presence of contaminants. The most important factor is the driving force which is controlled by the relationship between the surface energy of the liquid adhesive and the solid substrate. (The surface energy of a phase is attributed to the inward attraction of the molecules of a phase as a result of the inbalance of intermolecular forces, Fig.3.9).

When a liquid and a solid meet, the angle formed by the

intersection of their respective interfaces with air is their contact angle, which is dependent on the surface tension of the liquid and the surface energy of the solid. Since any system tends to adopt the state of the lowest energy, a solid of high surface energy will encourage the spreading of lower surface energy materials over its own surface, so giving rise to adsorption. A low surface tension liquid will, in the same way, tend to spread as much as possible on solids, whereas a high surface tension liquid will minimize its spreading by forming spherical droplets (minimizing its surface/volume ratio). Thus, in general, low surface tension liquids tend to spread over or wet high surface energy solids.

3.4.1. Wetting equilibria

Whenever one phase adjoins another, at the boundary of separation conditions prevail which are different from those in the mass of each of the phases because the molecules in the surface layers are in a field of inwardly directed forces, Fig.3.10. As a result, the situation of deformation in each boundary shows a greater intermolecular distance along their new deformation line. To extend the area of the surface extra energy is required, which is normally described in terms of surface tension parallel to the surface opposing any attempt to extend the surface. The surface tension for liquids is defined as the increase in free energy per unit increase in the surface.

$$\gamma_L = dG/dA \quad \text{.....(3.1)}$$

So, surface tension is a direct measure of intermolecular energy.

For liquid-liquid systems, interfacial tensions can be

directly measured and can be identified with free surface energies. For solid - liquid systems, however, it is not possible to measure directly the free energies of the solids but a concept similar to that for liquids can be used.

The method of calculation in this case follows. It must be noted here that free energy is the energy which must be supplied to form 1 cm^2 of new surface in a reversible manner, so that it is one half of the free energy which is gained when two identical surfaces of 1 cm^2 each are annihilated, as in adhesion.

The attempts to explain these solid - liquid systems are focused on the problem of wetting. The basic concepts is that of Young /20/, that is the contact angle by a drop on a plane solid surface. By adopting the static equilibrium condition for the resting drop at the joint of the three phase boundaries, the YOUNG equation can be obtained, Fig 3.11

$$\gamma_{sV} = \gamma_{sL} + \gamma_{LV} \cos\theta \quad \ldots\ldots\ldots\ldots\ldots\ldots\ldots\ldots (3.2)$$

If $\theta>0$ the liquid is said to be non-completely spreading, whereas if $\theta=0$ the liquid is completely spreading and wetting the solid.

Dupre /21/ in addition showed that the reversible work of adhesion required to separate one surface unit of solid - liquid interface is the sum of the free surface energies of solid and liquid minus the free interfacial energy:

$$W_a = \gamma_s + \gamma_{LV} - \gamma_{sL} = \gamma_{LV} (1 + \cos\theta) + \pi \quad \ldots\ldots\ldots (3.3)$$

where γ_s refers to the solid surface tension in absolute vacuum, and π is the spreading pressure.

Kinloch /22/, referring to the estimation of the values of surface tension, reports that an approach to estimate the values of γ_s, γ_L is in the proposal of Fowkes, that the

surface free energy of a single phase may be represented by the sum of contributions of the different types of intermolecur force components. In addition, he reports that Schultz et al suggested that γ can be expressed by two terms, the dispersion component γ_D and the polar γ_P, such that:

$$\gamma = \gamma_{,D} + \gamma_{,P} \quad \ldots\ldots\ldots\ldots\ldots\ldots\ldots\ldots\ldots\ldots(3.4)$$

and then, that the geometric mean of the dispersion force components is a good approximation for the interaction energies at the interface caused by dispersion forces.

He further reports that Owens and Wendt have proposed a similar geometric mean for the polar force interactions, although currently not fully acceptable, so that:

$$\gamma_{1,2} = \gamma_{1,D} + \gamma_{2,D} - 2\sqrt{[(\gamma_{1,D})(\gamma_{2,D})]} \quad \ldots\ldots\ldots(3.5)$$

if only dispersion forces are operative, and:

$$\gamma_{1,2}=(\gamma_{1,D}+\gamma_{1,P})+(\gamma_{2,D}+\gamma_{2,P}) - 2\sqrt{[(\gamma_{1,D})\ (\gamma_{2,D})]}-$$
$$-2\sqrt{[(\gamma_{1,P})\ (\gamma_{2,D})]} \quad \ldots\ldots\ldots\ldots\ldots\ldots\ldots(3.6)$$

if there are also polar forces involved across the interface.

Combining the first of above equations with Eq.(3.2) by setting

$_1$ instead of $_{SV}$ and $_2$ instead of $_{LV}$, for the case of non polar phases:

$$\cos\theta = [-\gamma_{LV} + 2\sqrt{[(\gamma_{SD})(\gamma_{LD})]}/\gamma_{LV} \quad \ldots\ldots\ldots(3.7)$$

In the same way by combining (3.6) and (3.2) the following is obtained:

$$\cos\theta=[-\gamma_{LV}+2\sqrt{[(\gamma_{S,D})(\gamma_{L,D})]}+2\sqrt{[(\gamma_{S,P})(\gamma_{L,P})]}/\gamma_{LV} =$$
$$-1+(2/\gamma_{LV})[\sqrt{(\gamma_{S,D})(\gamma_{L,D})]}+\sqrt{[(\gamma_{S,P})(\gamma_{L,P})]} \quad (3.8)$$

Taking into account that γ_{LV}, γ_{LD} , γ_{LP} are known for

many liquids, if the contact angles of two liquids on a solid surface are measured, a set of 2 equations (3.8) can be formed and solved to obtain values of $\gamma_{S,D}$, $\gamma_{S,P}$. Then the surface energy of the solid can be calculated as

$$\gamma_S = \gamma_{S,D} + \gamma_{S,P}$$

It is obvious that by using Eq. (3.3) and (3.6) the expression for W_a becomes:

$$W_a = 2\sqrt{[(\gamma_{S,D})(\gamma_{L,D})]}+2\sqrt{[(\gamma_{S,P})(\gamma_{L,P})]}+\pi \quad .....(3.9)$$

Following the expression (3.3) the work of cohesion for $\pi=0$ becomes:

$$W_{cL} = 2\gamma_{LV}, \; W_{c,s} = 2\gamma_s \quad .....(3.10)$$

Mouton /23/ defines the condition for a liquid to spread on a surface in terms of the work of spreading (or spreading coefficient) S:

$$S = W_a - W_c = \gamma_S - \gamma_{LV} - \gamma_{SL} > 0 \quad .....(3.11)$$

That means that spreading is enhanced by:

a high value of γ_S

a low value of γ_{LV}

a low value of γ_{SL}

or in other words, spreading readily takes place in the case of high energy solids by low surface tension liquids.

The Dupre equation in free air conditions is:

$$W_{a1} = \gamma_{SV} + \gamma_{LV} - \gamma_{SL} \quad .....(3.12)$$

whereas the difference $W_a - W_{a1} = \gamma_S - \gamma_{SV}$ expresses the decrease in the free surface energy due to adsorption of the vapour film. This means that the adsorption of a vapour film produces a surface of lower free energy. Values of W_{a1} for series of interfaces are given in Table 3.2.

Table 3.2. Work of adhesion in air, W_{a1} [mJ/m^2] after Kinloch /22/

Interface	
Epoxy-SiO_2	178
Epoxy-Al_2O_3	232
Epoxy-Fe_2O_3	291
PMMA-Al_2O_3	216
PMMA-Fe_2O_3	270

3.4.2 Critical surface tension of a solid substrate

The above results, Eq.(3.3-3.11), are most meaningful when viewed in terms of the critical surface tension for the solid substrate. This parameter was derived from the observation that there is a relationship between $\cos\theta$ and the surface tension of the wetting liquid γ_{LV}.

Zisman /24/ defined the critical surface tension γ_c as

$$\gamma_c = \lim_{\theta \to 0} \gamma_{LV} = \lim_{\theta \to 0} (\gamma_S - \gamma_{SL}) \quad \text{.....(3.13)}$$

According to his concept, if a number of liquids of a homologous series of known but different surface tensions are placed on a given solid, each will achieve its own contact angle. Then for each of these liquids:

$$W_a = \gamma_s + \gamma_{LV} - \gamma_{SL} = \gamma_{LV}(1+\cos\theta) + \pi \quad \text{.....(3.14)}$$

Then, if a graph is drawn of the cosines of the contact angles as a function of the γ_{LV}, a curve is produced, (ZISMAN's plot). The critical surface tension of the solid is the maximum value of γ_{LV} for which $\theta=0$ (complete wetting), Fig 3.12.

Any liquid with surface tension greater than this causes S, Eq.3.11, to decrease and gives incomplete wetting on this solid.

It must be stressed here that γ_c is not the surface free energy of the solid but just a parameter indicating its behaviour in wetting by liquids.

Table 3.3: Surface free energies [mN/m] after Kinloch /22/

Solid surface	γ_{sD}	γ_{sP}	γ_s	γ_c
SiO_2	78	209	287	40
Al_2O_3	100	538	638	45
Fe_2O_3	107	1250	1357	46

Liquid surfaces	$\gamma_{LV,D}$	$\gamma_{LV,P}$	γ_L
Water	22.0	50.2	72.2
DGBEA epoxy	41.2	5.0	46.2
Rubber-thougened epoxy	37.2	8.3	45.5
PMMA	35.9	4.3	40.2

A criterion for wetting, therefore, is that the surface tension of the adhesive should be equal to or less than the critical surface tension of the solid substrate. Another feature of the adhesive is that it must also be able to flow into capillaries that may constitute the rough surface, as is the case with concrete, in order to promote adhesion. This means that it must have a minimum value of surface tension which is necessary to rise in a capillary (because the height is directly proportional to the liquid surface tension, Fig. 3.13).

$$h = 2[(\gamma_L)\cos\theta]/(\rho r) \quad \ldots\ldots\ldots\ldots\ldots\ldots\ldots\ldots (3.15)$$

Thus, the best results are obtained in the case where the surface tension γ_{LV} is high enough to encourage the resin to rise in the capillaries, but not higher than the critical surface tension.

3.4.3. The concrete-epoxy resin interface

In the case of adhesive anchors, epoxy resins are mostly used as bonding material. Across a concrete-epoxy resin interface all the aforementioned mechanisms of adhesion are active.

3.4.3.1. Mechanical interlocking.

Mechanical interlocking is initiated by:

- The macro-roughness of the interface due to drilling of the bore in concrete. For theoretical bore diameters up to 20 mm drilled by hand held electric percussive units, deviations up to 0.5 mm from the ideal cylindrical surface are reported, Wachstmuth /25/.
- The microroughness of the concrete which involves the pores and cracks of the aggregates, those of cement gel and the pores at the aggregate-gel interface, varying in size as follows:

  - Gelpores : 0.5-30nm, full of water bound physically.
  - Capillary pores: 30nm-50 μm.
  - Air pores : 0.1-1 mm

Capillaries, although partially occupied by calcium hydroxide solution and airpores, are available to be filled by resin and, as a result, form shear connectors across the concrete-resin interface.

3.4.3.2. Secondary (Van der Waals) forces.

Among the products of hydration of the concrete gel, there are many hydrated minerals which are polar and many of them contain OH-, as Mlodecki/26/ reports. These polar components can interact with the polar components of resins (Hydroxyls, Carboxyls, and phenolic groups) resulting in permanent dipole forces.

From the point of view of wetting equilibria, Fiebrig /27/ referring to the values of surface energy of aggregates and gel of concrete reported the values given by Ramond /28/ for the critical surface tension of quartz, basalt and limestone which are between 29-35 mJ/m^2, and also their surface energy at much higher values. He also reported values of more than 100 mJ/m^2 for the surface energy of cement gel given by Zorll /29/, and on the estimation of the surface energy of concrete at levels higher than 73 mJ/m^2 made by Rehm and Franke /30/.

All the above values are substantially higher than those for commonly used epoxy resins of 42.0-46.0 mJ/m^2 (Tables 3.3, 4.1). This results in a spontaneous spreading of the low energy resin on the high energy concrete, promoting the wetting of the substrate. This is confirmed by Mouton /23/ who reported a wetting angle of different low viscosity epoxy resins on cement gel between 25° - 30° ($\cos\theta$ = 0.906-0.866).

Finally, there are hydrogen bonds operative at such interfaces as Hewlett /31/ and Charneki and Puterman /32/ reported. They stated that the hydroxyl-containing amines of epoxy resin form hydrogen bonds with the calcium silicate hydrate (Hewlett) or with any inorganic or organic polar substrate (Charnecki and Puterman).

3.4.3.3 Primary forces (chemical bonds)

Chemical bonds have been found between concrete containing quartz aggregates and epoxy resins, Fig 4.6. as Fiebrig /27/ reported referring to the work of Maier /33/. However, there is uncertainty about the existence of chemical bonds across any concrete - resin interface.

3.4.4. The steel-epoxy resin interface

The macro-mechanical interlocking across this interface is formed either by the thread of the bolt or by the ribs of the ribbed bar eventually used. Apart from this, there is also a micro-mechanical interlocking effect due to either the mild oxidation of the lateral surface of the anchor or due to the micropores and micro fissures on the steel surface, which form capillaries, Mlodecki /26/.

Physical adhesion is established mainly by hydrogen bonds between the hydroxyls contained in the epoxy resin and the iron atoms of steel, which are electronegative, Mlodecki /26/.

3.5. Interfacial failure of adhesives

3.5.1. Ideal bond strength

For many years attempts have been made to relate the work of adhesion to the mechanical strength of adhesive joints. Dahlquist /34/ reports that the fracture energy under certain conditions can be directly related to the mechanical work of rupture, which consists of the reversible work of adhesion and irreversible plastic work:

$$G = W_a + W_p \quad \ldots\ldots\ldots\ldots\ldots\ldots\ldots\ldots \quad (3.16)$$

or for perfectly elastic and brittle materials:

$$G = W_a$$

since W_p does not occur in such case.

The above means that for a perfectly elastic material, W_a can also be expressed as a function of bond strength or vice versa, because G can be related to the bond strength.

Good /19/, using the principle that if the potential energy functions and the geometry of all the atoms and molecules in a system were known, it would be possible to

sum up all the forces across an interface, expressed the ideal strength of an adhesive bond as a function of the work of adhesion and the intermolecular distance in equilibrium between adhesive and substrate (r_o), as follows:

$$\sigma_{max} = (16/9\sqrt{3})(W_a/r_o) \quad \text{.....(3.17)}$$

Indicative values of the ideal bond strength in relation to the different intermolecular forces acting across an interface are shown in Table 3.1., Section 3.3.

3.5.2. Loss of strength

As experimental results indicate, the strengths calculated in this way are generally substantially higher than the real, measured bond strength .

Allen /35/ commenting on this fact states that:

-The ideal strength is the maximum of the interfacial strength which can be attained but is never reached in reality.

-A primary loss of strength is due to the failure of the molecules to make intimate contact, which, in turn, means that not all the real surface is in contact. A similar factor comes from incomplete wetting of the substrate by the adhesive. In this way there are intrinsic flaws across the interface and, as a result, the ideal strength results in the inherent strength. Fig.3.14.

-A further reduction is due to the established internal stresses which can arise from shrinkage during the solidification phase, temperature changes, or volume changes due to moisture. In fact, as the adhesive-substrate interface is constrained by the adhesion, the shrinkage will

induce internal stresses on it, which will then reduce the fracture bond energy of the interface. Monitoring the solidification phase will show that, as long as the adhesive remains sufficiently fluid, internal stresses do not occur at all but will start to build up as soon as the adhesive reaches its solidification point. The magnitude of these stresses depends upon the shrinkage rate of the adhesive, the modulus at the solidification point, the geometry of the interface and the substrate, and its mechanical properties. The inherent strength reduced in this way results in the residual strength.

-Finally, there is also the measured strength, which is generally different from the residual strength to a degree which depends on the rheological properties of the adhesive and the apparatus in use.

3.5.3. Fracture of bond

3.5.3.1. The fracture mechanics approach

As stated in 3.5.1., the real bond strength is lower than the ideal (theoretical) one due to the existing defects at the interface, not to mention the internal stresses due to the volume changes of the material. That is a characteristic of adhesive joints, which usually fail by initiation and propagation of flaws. The ideas on which this approach is based were introduced by Griffith /36/ who proposed that every body contains flaws or imperfections and that its failure is governed by them, and occurs at the largest flaw.

The source of the "intrinsic flaws" may be voids, cracks, aggregates or dirt particles, inhomogenities in the adhesive, improperly mixed local areas of the adhesive etc.

Especially for mechanical anchors, where the probability of "intrinsic flaws" due to the injection or pouring or, in general, insertion of resin is high as a result of the commonly involved difficulties in such a work, the fracture mechanics approach becomes very important to explain the mechanisms of failure.

The principle of Griffith's theory for the elastic body has been applied in the recent decades to adhesive joints, as will be discussed below (sections 3.5.3.2 and 3.5.3.5), where first the theoretical background will be considered briefly and then its application to common types of adhesive joints will be stated from the point of view of measuring the parameters G (fracture energy) and K (fracture toughness), which express the two main criteria for fracture.

Actually, the first criterion, proposed by Griffith, is that when a flaw grows or a crack propagates there is a decrease in the potential energy of the body and so energy is released to form the new surfaces of the growing flaw. The latter is termed fracture or critical strain energy, G.

The second criterion expresses the field of stresses around a pre-existing crack tip in terms of the stress intensity factor K and states that fracture occurs when this factor exceeds a critical value Kc (a characteristic of the particular material in question).

The fracture mechanics approach can be applied to the cohesive and adhesive modes of failure. The difference is that, in the former case, the expended energy creates two

similar surfaces, whereas in the latter two dissimilar ones.

3.5.3.2 Energy approach

According to this approach (Griffith /36/) at fracture there must be a balance between the energy release (elastic strain energy and the work done by the movement of the external force) and the energy expended to create fracture surfaces, which means:

$$dU = dW \quad \text{.....(3.18)}$$

where dU is the decrease of potential energy, and dW, the increase of surface energy due to the extension of the crack.

The fracture energy, G, is the energy required to separate one unit of area A (which consists of 2 units of surface area):

Thus for an ideally brittle and elastic material:

$$G = dW/dA = 2(\gamma_s) \quad \text{.....(3.19)}$$

So:

$$(dU/dA) = G \quad \text{.....(3.20)}$$

The analysis for a lamina with thickness t and with an elliptical flaw under uniformly distributed tensile stress σ_o gives the result:

$$\sigma_f = \sqrt{[(EG_c)/(\pi\alpha)]} \quad \text{..... (3.21)}$$

where:

σ_f : Applied failure stress.

E : Modulus of elasticity of the material.

G : Energy release rate which can include the plastic work.

α : The flaw size.

A very important point regarding the above equation is that the failure stress is dependent on the flaw size, which causes the most scatter in failure stress measurements and, of course, on the material property G_c.

With analysis of the energy balance at fracture for two-dimensional bodies, G can be evaluated (Williams /37/) as:

$$G=dW/A = dU_1/dA - dU_3/dA = (u^2/2tC^2)(dC/da) \quad (3.22)$$

where:

dU_1/dA : The energy input to the system

dU_3/dA : The change in potential stored

u : The displacement caused by the applied force along it

t : The thickness of the body

C=u/P : The compliance of the body

This means that G can be found by determining C for a cracked body either by analysis or experimentally. If C(a) is found, then dC/da is known and G may be determined by using the above equation (3.22).

3.5.3.3. Stress intensity approach

It has been shown that G can be calculated for several geometries and thus provide data for the calculation of failure stress.

In many cases, however, the determination of G is not so simple since C is difficult to calculate or deduce experimentally. For these cases there is the alternative of considering the stress field associated with the crack tip.

Irwin /38/ calculated the stresses at the tip of an existing crack in an infinite homogeneous elastic lamina under uniformly applied tension, Fig.3.15, by using the stresses function of Westergaard:

$$\begin{vmatrix}\sigma_x\\ \sigma_y\\ \tau_{xy}\end{vmatrix} = (K/2\pi r) \begin{vmatrix}f_x(\theta)\\ f_y(\theta)\\ f_{xy}(\theta)\end{vmatrix} \quad \text{.....(3.23)}$$

where:

$$f_x(\theta) = [\cos(\theta/2)]\,[(1-\sin(\theta/2)]\,[\sin(3\theta/2)]$$

$$f_y(\theta) = [\sigma os(\theta/2)]\,[(1+\sin(\theta/2)]\,[\sin(3\theta/2)]$$

$$f_{xy}(\theta) = [\sin(\theta/2)]\,[\cos(\theta/2)]\,[\cos(3\theta/2)] \text{...(3.24)}$$

and $K = \sigma\sqrt{(\pi\alpha)}$

K is the stress intensity factor relating the magnitude of the stress intensity local to the crack to the applied loading and geometry of the member in which the crack is located.

From Eq.(3.23) it can be seen that as r->0, $\sigma_x, \sigma_y, \sigma_{xy} \to \infty$ and therefore stress alone does not pose a reasonable local fracture criterion. Since the level of stress field around a crack can be defined by K, Irwin /38/ proposed that fracture occurs when:

$$K = \sigma\sqrt{(\pi\alpha)} = K_C \quad \text{..... (3.25)}$$

where:

$K_C = (Q)(\sigma_{of})(\sqrt{\alpha})$ is a critical value for the crack propagation in the material, and as such is a material property ,

Q : a geometric constant calculated theoretically or determined experimentally.

For a crack in a homogenous material, Kinloch /22/ reported that the geometric factor, Q, may be expressed as a non-dimensional function of crack length and structural geometry in the form of a finite series. Among the many techniques used to obtain it are the direct methods, where equations relating the crack-tip stresses or displacements

to the stress intensity factor are solved by closed form methods.

So for the double shear joint, Fig 3.16 (c) Kinloch /22/ gives:

$$K_c = \tau_c . Q . \sqrt{\alpha}$$

$$\tau_c = F/2bd$$

$$Q = Q_h \ (\sqrt{E_a}/E_s)$$

$$Q_h = d/D \ [0.0325+14.63(\alpha/D)-46.07(\alpha/D)^2 + +(61.03)(\alpha/D)^3 -28.86(\alpha/D)^4] \ldots\ldots\ldots (3.26)$$

where :

F : the applied shear force

b : the width of the joint

d : the thickness of the solid

α : the half length of the flaw

D : the height of the joint

E_a : the modulus of elasticity of the adhesive

E_s : the modulus of elasticity of the solid

G_c, and K_C are two different criteria which can be unified.

By considering a contour around a crack tip and applying the energy balance equation on it, it is possible to deduce the energy release rate, G_c, for the system in relation to K_c. Thus according to Kinloch /22/:

$$G_c = K_c^2 / E \quad \text{for plain stress conditions..} \quad (3.27)$$

or

$$G_c = (K_c^2/E)(1-\nu^2) \quad \text{for plain strain conditions} \quad (3.28)$$

Values of G_c, K_c can be evaluated, Fig 3.16, or obtained experimentally.

3.5.3.4. The adhesive fracture

In terms of the energy concept, cohesive and adhesive fracture are the same. There is, however, a difference in that in cohesive fracture two similar fresh surfaces are formed, whereas in the adhesive the two are dissimilar.

Thus, following Eq. (3.3), the fracture energy for the adhesive fracture is:

$$G = (\gamma_{s1} + \gamma_{s2}) - \gamma_{12} + W_{p1} + W_{p2} \quad \ldots\ldots\ldots (3.29)$$

where:

γ_{s1} : the surface energy of the phase 1

γ_{s2} : the surface energy of the phase 2

γ_{12} : the interfacial energy between 1-2

$W_{p1,2}$: the plastic work in the phases 1,2 respectively.

The condition for the adhesive fracture is:

$$dU/dA > G \quad \ldots\ldots\ldots (3.30)$$

In the same way as by the cohesive fracture, for two orthogonal ideally elastic brittle semi-disks bonded together at their border line, the fracture energy criterion according to Wu /39/is:

$$\sigma_f = \sqrt{[(E_{1,2})(G/\pi\alpha)]} \quad \ldots\ldots\ldots (3.31)$$

where:

$E_{1,2} = (E_1 E_2)/(\Phi_1 E_1 + \Phi_2 E_2)$ with $\Phi_{1,2}$ the fractional length of the phases 1 and 2 respectively.

Similarly for the stress intensity approach for the mode of tensile opening (mode I), Williams /37/ gives:

$$G=(K^2/2)(1/E_1 + 1/E_2)((2\rho_{1,2}-1)/\rho_{1,2}^2) \quad \ldots\ldots (3.32)$$

Where:

$$\rho_{1,2} = (\xi+1)/(\varphi_{1,2}+1)$$

$$\xi = E_2/E_1$$

$$\varphi_{1,2} = 1+(E_2/2)[(1+\nu_1)/E_1 - (1+\nu_2)/E_2)]$$

3.5.3.5. Fracture mechanics concepts and wetting

It is generally possible to combine the energy approach of Griffith with the relations obtained from the wetting equilibria. Wu /39/ reported a relationship between the size of the unwetted interfacial defect and the wetting properties of the joint:

$$\alpha = \alpha_o \ (1-S_{12}/\gamma_2)^n \quad \text{.....(3.33)}$$

where α_o is a constant equal to the size of the unwetted interfacial void when $S_{12}=0$, γ_2 the surface energy of the solid and n is a constant with value 2 in most cases.

Combining then this equation with the relations from Griffith's approach and given that $\gamma_{12} << \gamma_1$, which is usually the case for high energy solids with low energy adhesives (phase 1), he found that:

$$\sigma_f = (km)\gamma_2/(\gamma_1+\gamma_{12}) = km_{.2}/\gamma_1+\gamma_{12} = km_{.2}/\gamma_1 \quad (3.34)$$

where:

$$km = \sqrt{(E.G)/\pi.\alpha_o} \text{ and } k_{m.2} = k_m(\gamma_2).$$

This means that for a given substrate, in order to achieve max σ_f, γ_1 must be minimized.

3.5.3.6 Effect of chemical bonding

Chemical bonding is generally difficult to detect because of the thinness of the interface. However, in some systems chemical bonding has been found, which contributed to the adhesive strength.

In practice, chemical bonding is promoted by using a small amount of appropriate reactive functional groups, which, thus used, do not affect the bulk material properties and the wettability conditions at the interface.

In this case the increase of adhesive strength is given by Wu /39/:

$$\sigma_r = \sigma_{f\,o} + k(c_r)^n \quad \text{..... (3.35)}$$

where:

c_r : is the concentration of functional groups and k,n constants (n=0.6-1.0) and $\sigma_{f\,o}$ the initial adhesive strength.

Functional groups are those promoting chemical bonding or specific hydrogen bonding, which is, as mentioned before, less effective than chemical bonding. They usually are:

- carboxyl groups
- nitrogen containing groups
- hydroxyl and methylol groups
- isocyanate groups

To sum up, the assessment of adhesive strength via the adsorption theory can be calculated for tensile joints:

$$\sigma_f = \sigma_{f\,o} + k(c_r)^n - \sigma_i \quad \text{..... (3.36)}$$

where:

$\sigma_{f\,o}$ = the interfacial fracture tensile stress

σ_i = loss due to shrinkage

and for shear joints:

$$\tau_f = \tau_{f\,o} + k(c_r)^n - \tau_i \quad \text{..... (3.37)}$$

$\tau_{f\,o}$ = the interfacial fracture shear stress

τ_i = loss due to shrinkage

3.5.3.7. Reduction of strength due to shrinkage of the adhesive

During setting, adhesives usually shrink as a result of solidification accompanied by loss of solvent, if any, or cross-linking, or cooling.

In the case of adhesive anchors, because the concrete and the bolt are neutral from the point of view of volume changes at the moment of anchor installation, they induce

internal stresses in the adhesive along the interface, which reduce the strength of the adhesive bond.

Internal stresses cannot reduce the inherent strength as long as the adhesive is in the fluid state, but start to build up as soon as the adhesive reaches its solidification point.

Assuming that $W_o \gg h_o$ and ignoring the adhesion forces at the bottom, Gent/40/ calculated the radial (tensile) and the longitudinal stresses due to shrinkage in a system similar to an adhesive anchor, as follows, Fig 3.17:

$$\sigma = Ee\,[2+(6/h_o^{\,2})(W^2{}_o/4 - x^2)] \quad \ldots\ldots\ldots\ldots \quad (3.38)$$

$$\tau = 3Ee(W_o/h_o) \quad \ldots\ldots\ldots\ldots\ldots\ldots\ldots\ldots \quad (3.39)$$

Where:

W_o : the embedment length of the anchor

h_o : the thickness of the adhesive

d : the anchor diameter

E : the modulus of elasticity of the adhesive

e : the shrinkage rate of the adhesive

x : the x-coordinate of the section, measured from the middle of the embedment length

3.5.4. Failure criteria

It is evident from the above that the parameters G_c and K_c do not provide analytical failure criteria. However, by considering the stress field at the tip of the crack and rearranging it by substitution of the common parameter α from the G_c, K_c expressions,

$$\sigma_{c,el.an} = \sigma(\alpha, Geometry)$$

$$G_c = G(\alpha, Geometry)$$

relations of the following form can be obtained:

$$\sigma_c = \sigma(G_c, Geometry) \quad \ldots\ldots\ldots\ldots\ldots\ldots\ldots \quad (3.40)$$

and in the same way for the critical shear strength:

$$\tau_c = t_c \ (K_c, \ \text{Geometry})$$

Such relations can be used to calculate the ultimate stress for the particular joint.

So, for tensile and shear joints failure criteria are obtained as shown in sections 3.5.4.1 and 3.5.4.2 following.

3.5.4.1. Adhesive joints under tension (Butt Joints)

In the systems of adhesive anchor there are generally two different types of adhesive joints:

a) A joint under tension at the bottom of the metallic bolt (or bar).

b) A joint under shear across the lateral cylindrical surface of the anchor involving the bolt (or bar), the adhesive and the concrete surface of the bore.

The analysis of stresses for a circular tensile adhesive joint (radius r, thickness h - Fig.3.18) based on the assumption that the side groove profile is an ellipse, made by Wu /39/, results in:

$$\beta = \sigma_{max}/\sigma_o = 1 + (8/\pi)(r/h)[\varepsilon/(1+\varepsilon)^2] \ \ldots \ (3.41)$$

where:

$\varepsilon = dh/h$ is the adhesive tensile strain.

The fracture energy per unit of interfacial area of a tensile specimen with a relatively long adhesive layer (based on the lamina model) with thickness h containing an edge crack and loaded in pure tension, Fig.3.18, according to Gent /40/ is:

$$W_a = hQ_s \ \ldots\ldots\ldots\ldots\ldots\ldots\ldots\ldots\ldots\ldots\ldots\ldots\ldots\ldots\ldots\ldots(3.42)$$

for the thin joint, where Q_s is the strain energy per unit volume, or

$$W_a = k\alpha Q_s = [\pi/\sqrt{(1+\varepsilon)}]\alpha Q_s \quad \ldots\ldots\ldots\ldots\ldots\ldots\ldots (3.43)$$

for the thick joint.

Taking into consideration the increase in σ at the edge the overall mean value of Q_s is:

$$Q_s = \sigma^2/[2E(1+ r^2/2h^2)] \quad \ldots\ldots\ldots\ldots\ldots\ldots (3.44)$$

and thus, on the assumption that a critical amount of strain energy is required in the neighbourhood of the edge for the flaw to grow catastrophically, combining Eq.(3.44) with Eq.(3.42) or (3.43) the failure stress becomes:

$$\beta\sigma_f = [(1+r^2/2h^2)/\sqrt{(1+3r^2/2h^2)}]\sqrt{2EQ_s} \quad \ldots\ldots\ldots (3.45)$$

where:

$Q_s = W_a/h$,

according to Eq.(3.42) for a thin joint or

$Q_s = W_a\sqrt{(1+\varepsilon)}/\pi a$

for the thick joint.

The above means that for the first case (thin layer) the adhesive layer governs the fracture whereas in the second (thick layer) the pre-existing flaw does, which confirms experimental findings.

3.5.4.2. Single adhesive joints under shear (lap joints)

For lap joint with negligible influence of load eccentricity, Fig.3.19, the stress analysis made by Volkersen gives a stress concentration factor, β, Wu /39/:

$$\beta = \tau max/\tau = [(\delta/\varepsilon)(2\varepsilon^2 - 1 + \cosh(2\varepsilon\delta))/(\sinh(2\varepsilon\delta)] \quad (3.46)$$

Where:

$$\delta^2 = (2c_a{}^2 D_a)/(E_2 t_2 t_a) \quad \ldots\ldots\ldots\ldots\ldots\ldots (3.47)$$

$$\varepsilon^2 = (E_{1\,t1} + E_{2\,t2})/(2E_{1\,t1}) \quad \ldots\ldots\ldots\ldots\ldots\ldots (3.48)$$

D_a :the shear modulus of adhesive

Following the influence of the adhesive thickness established in the previous section, Gent/40/, examined two

extreme forms of sheared adhesive joint, the thin and the thick joint, as shown in Fig.3.20.

In each case the work W_a comes from the strain energy stored in the adhesive, and is given by:

$$W_a = hQ_s \quad \text{..... (3.49)}$$

$$W_a = k\alpha Q_s \quad \text{..... (3.50)}$$

for the thin and the thick adhesive layer respectively, with h the thickness of the adhesive, k a numerical factor, Q_s the strain energy per unit volume and α the length of the flaw (which in this case is a debond).

Gent /40/ combining equation (3.46) with Eq. (3.49) or Eq. (3.50) derived the expression of fracture shear stress:

$$\tau_f = (1/\beta)\sqrt{[(E_a)(W_a)/h(1+\nu_a)]} \quad \text{.....(3.51)}$$

$$\tau_f = (1/\beta)\sqrt{[(E_a)(W_a)/\pi(1+\nu_a)\alpha]} \quad \text{.....(3.52)}$$

for the case of relatively large and relatively small flaws (in relation to the adhesive thickness), Fig.3.20,

where:

β : the aformentioned stress concentration factor

E_a : tensile modulus of elasticity, of adhesive

ν_a : Poisson's ratio of adhesive

3.5.4.3. The double shear adhesive joint

The maximum of shear stress of a double shear joint can be derived using equation (3.26). This loading type, however, as Kinloch /15/ reported, referring to work of Anandarajah and Vardy, is basically mode II (with mode I/mode II≈0,01) for which no clearly established relationships are available. However, since, according to Kinloch /15/:

$$G_c = [(1-\nu^2)/E]K^2_I + [(1-\nu^2)/E]K^2_{II} + [(1-\nu^2)/E]K^2_{III} \quad \text{.....(3.53)}$$

it is possible to calculate $k_{I}{}_{I}c$ as function of the G_c and thus obtain the ultimate shear strength.

3.5.4.4. Evaluation of the fracture mechanics approach for the case of O.P.C. concrete-epoxy resin joints, (Appendix A).

In Appendix A the tensile strength of a concrete-resin butt joint and the shear strength of a concrete-resin single lap joint and that of a similar double shear joint are calculated.

3.5.4.4.1. Tensile (butt) joint

Given that there is no contribution of chemical bonding and that the joints are ideally brittle and linear elastic, for O.P.C. concrete-epoxy resin interfaces with following properties taken from Table 3.3:

Resin	Concrete
$\gamma_{L\,D}$=41 mN/m	$\gamma_{S\,D}$=78 mN/m
$\gamma_{L\,P}$= 5 mN/m	$\gamma_{S\,P}$=209 mN/m
46 mN/m	287 mN/m

W_a can be calculated in accordance with Eq(3.9):

$$W_a = 2\sqrt{[\gamma_{S\,D}\gamma_{L\,D} + \sqrt{\gamma_{S\,P}\gamma_{L\,P}}] =$$

$$= 2(\sqrt{(78)(41)}+\sqrt{(5)(209)}) = 2(56.5+32.3) =$$

$$= 177.6 \text{ mN/m} = 0.178 \text{ N/mm}$$

Further, for a resin with E_r=3000 N/mm² and ε=0.02 and a concrete with E_c=30000 N/mm² and a thin butt joint with:

r = 10mm, h = 1 mm

it is calculated:

β = 1.489 and

σ_f is obtained combining Eq.(3.42) and (3.45)

σ_f = 6.17 N/mm^2

3.5.4.4.2. Shear (lap) joint

For the same concrete and resin properties and for

$E_{concrete}$ = 30000 MPa

and a single lap joint with

$t_1 = t_2 = 60$mm $\quad t_a = 2$mm

$2c = 60$mm $\quad \nu_a = 0.30$

$a = 0.01$mm $\quad D_a = 3000/2(1+\nu_a) = 1154$ MPa

τ_f can be derived in accordance with Equations (3.46), (3.47), (3.48), (3.51)

$\tau_f = 4.46$ N/mm^2, and for different flaw sizes:

a [mm]	τ_f [N/mm^2]
0.005	4.46
0.01	3.16
0.1	1.0
0.5	0.45
1.0	0.32
2.0	0.22
3.0	0.18
4.0	0.16

3.5.5.4.3. Double shear joint

For the double shear test, using equations (3.26) and (3.32), and for concrete and resin properties same as above, K is calculated as:

K = 1.06 N/mm$^{3/2}$

and for a joint with

d=40mm D=40mm,the following values can be obtained

a [mm]	Q_h	Q	τ_f [N/mm^2]
0.5	0.207	0.065	23.0
1.0	0.369	0.117	9.05
2.0	0.649	0.205	4.82
3.0	0.896	0.283	2.16
4.0	1.096	0.346	1.53
5.0	1.255	0.397	1.20

3.6. Concluding remarks

The possible mechanisms of adhesion involve:

- the mechanical interlocking
- the specific adhesion which is divided into:
    - the primary (or chemical) bonds which constitute the interatomic forces across an interface
    - the secondary (or physical) bonds which represent the intermolecular actions across an interface

The prerequisite for specific adhesion is that the two phases, the substrate and the adhesive, come into close contact so that the intermolecular forces become operative. Under certain circumstances, interatomic interactions may take place which result in chemical bonds.

The physical bonds involve:

- the dipole forces, which are the result of direct interaction of polar compounds across their interface
- the induced dipole forces between a polar and a non-polar phase
- the dispersion forces which exist at any interface

- the hydrogen bond, which is a special case of dipole interaction

The requirements of intimate contact between two phases and that of a large real contact surface between them can be fulfilled if one of the phases is liquid, so that it can fit into the irregularities of the other, and if it completely wets the solid phase. On the other hand, the wetting angle affects the reversible work of adhesion and hence the final adhesion strength.

In order to achieve the maximum adhesion, the surface tension of the liquid adhesive must be lower than the critical surface energy of the solid substrate. However, in order to take advantage of the capillary rise of the adhesive, its surface tension must be high enough to promote it.

In the case of the concrete epoxy-resin interfaces all the above mechanisms are mobilized.

The macroroughness initiated by the common drilling devices and the existence of the capillary and air pores, cause the mechanical interlocking to be established.

Due to the polar nature of many of the cement hydration products of the concrete gel and due to the polar components of the resins, permanent dipole forces are generated across a concrete-epoxy resin interface. At such an interface hydrogen bonds exist as well, formed between the hydroxyl containing amines and the calcium silicate hydrate of the cement matrix.

The low surface energy of resin in relation to the surface energy of concrete contributes to good wetting of concrete by the liquid epoxy-resin, as is confirmed by the existing data on the measurements of the respective

wetting angle.

In some instances, chemical bonds have been formed between concrete containing quartz aggregates and epoxy resins which enhance the bond strength.

Some mathematical expressions for the maximum value of the adhesive bond (ideal bond) as functions of the work of adhesion have been proposed. However important such expressions might be, the ideal bond strength is several times higher than the real (technical) bond strength, because the latter is reduced by the losses owing to:

- Inadequate contact between the molecules of the two phases.
- Incomplete wetting ($\cos\theta<1.0$) of the substrate by the adhesive.
- Shrinkage of the adhesive which induces internal stresses at the interface.
- Flaws within the adhesive and/or on the interface.

An estimation of the real adhesive strength can be based on the fracture mechanics analysis of the interface. Since the adhesive fracture can be handled in the same way as the cohesive one with only few differences, it is possible to obtain a relationship between the ultimate adhesive strength, the geometry and mechanical properties of the solid and adhesive parts of an adhesive joint using the energy or stress intensity approach of the fracture mechanics analysis.

In this way failure criteria for the tensile and shear adhesive joints can be derived and evaluated for the concrete-epoxy resin joints.

4. THE ADHESIVES IN USE

In this section the basic chemistry of the adhesives most widely used is given. In addition, aspects of their performance and suitability gained from professional personal experience, together with their physical and mechanical properties, are presented.

In chapter 3 the necessary properties of an adhesive were stated:

1. It must be fluid at an initial state and completely wet the substrate (Section 3.3.2).
2. It must have a surface tension almost equal to the critical surface tension of the substrate in order to achieve wetting and simultaneously high enough to be able to rise in the capillaries of the substrate (Section 3.4.2)
3. It must solidify without significant volume changes (Section 3.2.2.).
4. It must contain functional groups (adhesion promoters) in order to ensure the contribution of chemical forces to adhesion (Section 3.5.3.6).
5. After solidification it must possess high mechanical strength characteristics, in order to withstand the field of stresses induced by external loading and undergo minimal deformation.
6. It must also be durable during service life and, if possible, also contribute to the durability of the bolt in the case of chemical anchors.

For many reasons, but mainly because of their superior function regarding the criteria 1-4 above, polymers are the most widely used adhesives in chemical anchors. Nevertheless, cement based grouts, modified in order to

enhance their characteristics, are used under certain circumstances, for anchors with relatively long embedment lengths.

4.1. Polymer materials (Polymers)

Polymers are the materials which contain long chain molecules. The constitutive atoms of the chains can be either carbon (and in this case the material is called an organic polymer) or silicon. The small molecule which comprises the repeating unit is the monomer. In the case of more than one repeating units the polymers are called copolymers, terpolymers, etc.

Thermoplastics are the organic polymers consisting of long chain molecules attracted to one another only by secondary valence forces and physical entanglement, whereas in thermosetting materials (or resins), there are also secondary valence bonds between the chains of molecules (cross links, Arridge /41/), Fig.4.1.

This fact results in superior mechanical properties and thus in their applicability to structural repairs. Thermoplastics become, by heating, viscous liquids. By contrast, thermosetting materials, once set, will not soften.

The commonly used polymers as reported by Hennig and Knofel /42/ and Baoyu et al /47/are:

- **THERMOPLASTICS**

  Polymethylmethacrylate (PMMA) which is a product of polymerization:

  Initiator + Monomer + Heat -> Polymer + Heat

- **THERMOSETTING materials or DUROPLASTS**

- Epoxy resin (EP), a product of polyaddition:

  Monomer A + Monomer B + catalyst -> Polymer + Heat

- Unsaturated Polyester resin (UPR), a product of polycondensation

  Monomer A+ Monomer B+ Heat -> Polymer+Water + Heat

- Polyurethane resin (PU) - product of polyaddition.
- Vinylester resin (VE)

In the following, only the thermosetting materials are discussed because the thermoplastics in general are not suitable for structural application.

4.2. The chemistry of epoxy resins

Of all the thermosetting materials, the most widely used in structural applications are epoxy resins. They consist of a reactive resin and a hardener which partly deactivates the resin. The name of this group of resins is of greek origin ("epi"-meaning on the outside of, plus "oxygen"), and they have as constitutive grouping the epoxide groups as is shown in schematic illustration of Schutz /43/:

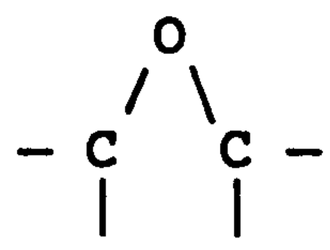

In addition to these epoxide groups (which are dipoles with positively charged carbon atoms and negatively charged oxygen atom), epoxy resins contain hydroxyl groups. The epoxide and hydroxyl groups are the highly reactive points of the epoxy reacting with various curing agents (hardeners). A curing agent acts as a link that joins the

epoxide groups, whereas a catalyst causes the groups to react with one another, Fig.4.2. Hence the idealization of EP resin, in non-chemical terms as a material with reactive "hooks" and the hardener as a material with reactive "eyes" which, mixed properly together in the pot, result in a three dimensional structure with the eyes engaged with the hooks, Shaw /44/, Fig.4.3.

Widely used hardeners are amine containing compounds. The chemical reaction which binds the groups together in three dimensions producing a solid system, once started cannot be stopped although it can be speeded up or slowed down.

Each of the aformentioned groups gives desirable properties to the epoxy resin (ultimate strength, bond to dry and damp substrates, rate of cure at different ambient temperatures, chemical resistance). Thus, the epoxide and hydroxyl groups give the inborn high polarity of the molecules which lead to excellent adhesion to different substrates, whereas there are other groups which control the rest of aformentioned properties. These, however, are also highly influenced by the additives introduced to the system when the components are mixed together. That is why correct proportioning and mixing is imperative for EP resins.

In addition to the practically infinite number of adhesives that can be produced by combining the action of resins with curing agents, there are several groups of modifiers that may be used to change certain properties of the system to best fit its use, Fig 4.4. Some of them are reactive, others are inert. Among them, as Charnecki and Puterman /32/ reported, are:

- **Adhesion promoters**

- **Diluents** (reactive or non-reactive) which lower the viscosity of the system (while simultaneously affecting the mechanical characteristics).

- **Thixotropic agents** to give the system predetermined non-sag properties.

- **Plasticizers**, to make the epoxy system more flexible in order to accommodate, for example, possible internal stresses due to differential shrinkage.

- **Fillers** that reduce the shrinkage and the creep rate of the system while also influencing the mechanical characteristics.

- **Flame retardants.**

- **Pigments** to modify the appearance of the system.

- **Accelerators and Retarders**

Of the many EP resins available the one made from epichlorohydrin with bisphenol A in the presence of caustic soda covers a very great percentage and is known as DGEBA (di glycidil ester of bisphenol A). Its composition as reported by Furr /45/ is shown in Fig.4.5.

The curing of the EPR systems is an exothermic reaction and the rate of cure is temperature dependent. Generally the rate of cure, as reported by Shaw /44/, doubles as the

temperature increases by 10°C and halves as the temperature drops by 10°C . Shaw /44/ further reported that most of the systems stop curing at 5°C, while, there are EP resins available specially formulated to cure down to 0°C.

It must be stressed that the heat evolved due to the exothermic nature of the reaction may not all be liberated and is certainly not all dissipated before the resin is set solid. Hence, there is a thermal contraction as the solid cools. However, for most epoxide systems this contraction and shrinkage is small. It can be ignored in specially formulated systems such as those for adhesive anchors.

In some cases chemical bonds between epoxy resins and concrete occur. Fiebrig /27/ reports the findings of Maier /33/ about the chemical bonds between epoxy resins and quartz aggregates, Fig 4.6, as a result of reaction between S_1O_2 groups of aggregates and NH_3R groups of the hardener of the resin across the interface. These bonds contribute to high adhesion between such aggregates and epoxy resin.

Polyester resin, UPR, is chemically much more simple than EP and the resin component contains both the "hooks" and the "eyes" in the right proportion as Shaw /44/ states. The hardener is a catalyst required to initiate the reaction throughout the mass of the resin, Fig.4.7. The reaction is also exothermic and unlike that with EP there is a change in volume between mixed uncured and the fully set system, which is not negligible.

4.3. Physical characteristics of adhesives

The most interesting and crucial physical properties of polymer materials are the ones which influence their bond to concrete, i.e surface tension and wetting angle. Apart from these, a set of properties mainly related to the specific application are of interest. Among them are:

- Specific gravity
- Viscosity
- Thermal expansion
- Curing shrinkage
- Water absorption
- Pot life
- Gel time and curing time
- Thermal conductivity

In addition, the influence of certain parameters on the above physical properties and on the mechanical characteristics of the final system are of importance e.g.:

- Effect of various mixing ratios of resin to curing agent.
- Effect of aggregates within the polymeric matrix.
- Influence of elevated ambient temperature.

In tables 4.1., 4.2. and figures 4.8.- 4.9. approximate representative values of the physical properties and the effect of the most important parameters are given.

TABLE 4.1: Physical properties of pure polymers

	EPOXY R	UNS.POLYEST.R	POLYURETH.R	PMMA	VINYLESTER R.
Density (g/cm^3)	1.1 - 1.25	1.0	1.0 - 1.5	1.0 - 1.2	1.0 - 1.3
Linear expansion coefficient (10^{-6})	25-30	25-30	45-75	30	15-30
Shrinkage rate (10^{-3})	1-5	15-25	1-5	30	410-1300
Maximum service temperature (^oC)	40-80	50-70	(-30)-(100)		
Water absorption 7 days at 25 ^oC (%)	0-1	0.2-0.5			
Rckwell hardness	60-70		60-70		
Lower curing temperature (^oC)**	10	15	10	-30	
Surface energies [mN/m^2]	42	50	44	41	
Fracture energy rate (J/m^2)	50-570				
Wetting angle to cement paste/low viscosity materials (^{o})	25-30			<25	

* Values partially reported by Shaw /44/, Baoyu /47/, Krausse /46/, Mouton /23/ and gained during the profesional practice of the author.

** Common, not specially formulated systems.

TABLE 4.2:Influence of inert fillers on thermal expansion coefficient and shrinkage rate of PMMA after Seidler /48/

	1:1	1:2	1:3	1:4	1:5	1:6	1:8	1:10	1:12	1:14
Th.exp.coe.	100%	97%	94%	69%	62%	62%	62%	62%	62%	62%
Shr.rate	100%	92%	25%	15%	15%	15%	15%	15%	15%	15%

4.4. Mechanical properties of adhesives

The mechanical characteristics of the most commonly used polymers in the cured state are shown in Table 4.3.

TABLE 4.3: Mechanical characteristics of pure adhesives for structural repairs. (*)

Property	EPR	UPR	PU	PMMA	VER
- Compressive strength (MPa)	40-120	40-110	50-80	60-120	60-120
- Tensile strength (MPa)	10-40	20-30	10-15	10-50	10-35
- Flexural strength (MPa)	10-50	25-30	15-50	5-50	10-30
- Modulus of elasticity (MPa)	1500-4000	1500-2500	1000-3000	1000-3000	1500-4000
- Elongation at break (%)	0.5-2	0.5-2	0.5-5	0-10	0.5-5
- Heat distortion temperature (θ^oC)	45-50	45-50	-	-	

* Values partially reported by Schutz /43/, Shaw /44/, Baoyu /47/, Krausse /46/ and gained from the professional experience of the author

The effect of added diluent to lower the viscosity of EP Resin in its fluid state is shown in Figure 4.8 whereas the change of viscosity of the fluid resin by increase in ambient temperature and the physical and chemical changes during the curing process are shown in Figures 4.9, 4.10.

From the design point of view the stress-strain diagrams for the cured resin are important. Diagrams of this kind for some specific types of resins are given in Fig.4.11.

Polymers can be mixed with aggregates of different types, usually silica sand, to modify their properties and to reduce their cost. The effect of mixing with aggregates is illustrated in Figures 4.12, 4.13. The grading of particles size depends on the type of application and the desired properties of the final mix.

A further two categories of parameters are interesting:

- The rate of gain of strength of the polymer material in use which is mainly dependent on the chemical composition of material and the ambient temperature as Furr /45/ reported, Fig.4.14.
- The effect of time and temperature on sustaining loading as are shown in Figures 4.15, 4.16, 4.17.

And finally, under certain circumstances it is useful to know whether an adhesive could bond on another existing adhesive. Table 4.4 shows information on this as given by Seidler /48/.

Table 4.4: Bonding properties between organic polymers after Seidler /48/

ADHESIVES

			PUR		EP	
Polymer substate	PMMA	UP	L	oL	L	oL
PMMA	+	-	(+)	-	-	-
UP	+	+	+	(+)	-	-
PUR L	+ (8-24)	+ (8-24)	+ (8-24)	(+) (4-12)	(+) (4-12)	-
PUR oL	+ (4-12)	(+) (4-12)	+ (8-24)	+ (4-12)	-	-
EP L	-	-	+ (8-24)	+ (4-12)	+ (8-24)	+ (8-24)
EP oL	-	-	+ (8-24)	+ (4-12)	(+) (4-12)	(+) (4-12)

+: very good — L: solvent containing
(+): good — oL: solvent free
(-): poor — (8-24): duration of loading in hours

4.5. Test methods

There are various methods which have been developed to test the bond of an adhesive to concrete. They vary from the direct tensile (bonding) test to the different forms of slant shear tests as can be seen from the following lists and include also dynamic tests for the cases of bond under reversing load. The direct shear test is chosen for this work as the most representative for the pull-out of anchors and one of the simpler tests of this range.

The relevant specifications for bonding tests, with the general specifications on epoxy adhesive tests most commonly used, are listed below.

4.6.1. RILEM TAC, 52 - RAC, /49/

4.6.1.1. Pull off test

4.6.1.2. Dynamic loading test

4.6.1.3. Slant shear test

4.6.1.4. Direct shear test

4.6.1.5. Cylinder tensile test

4.6.1.6. Thermal compatibility test I, II

4.6.1.7. Four point bending test

4.6.1.8. Injectability test

4.6.2. BRITISH STANDARDS INSTITUTION (1984)

4.6.2.1. Testing of resin compositions for use in construction. Method for measurement of bond strength (slant shear method), BS 6319:Part 4, London.

4.6.2.2. Testing of resin compositions for use in construction. Method for measurement of tensile strength, BS 6319: Part 7, London.

4.6.3.ASTM, AASHTO, AND ACI SPECIFICATIONS AND GUIDES

4.6.3.1. Epoxy resin based bonding systems for Concrete. /ASTM/ C 881-78(1983)

4.6.3.2. Bond strength of epoxy resin based bonding systems used with concrete. /ASTM/ C 882-78(1983).

4.6.3.3. Thermal compatibility between concrete and an epoxy resin overlay. /ASTM/ C 884-78(1983)

4.6.3.4. Use of epoxy compounds with concrete. /ACI/ 503R-80.

4.6.3.5. Bonding hardened concrete,steel, wood, brick, and other materials to hardened concrete with a multi-component epoxy adhesive. /ACI/503.1-79.

4.6.3.6. Bonding plastic concrete to hardened concrete with a multi-component epoxy adhesive. /ACI/ 503.2-79.

4.6.3.7. Repairing concrete with epoxy mortars. /ACI/ 503.4-79.

4.6.3.8. Epoxy adhesives for highway construction. /AASHTO/ M 234-76.

4.6.3.9. Epoxy resin adhesives. /AASHTO/ M 235-73.

4.6.4. DIN

4.6.4.1. Reaktionsharze, Reaktionsmittel und Reaktionsharzmassen, Pruefverfahren, DIN 16945 04.76

4.6.4.2. Harze. Begriffe, DIN 55958 E 09.85.

4.6.4.3. Kunsstoffe, Kurzzeichen fuer Homopolymere, Copolymere und Polymergemishe, DIN 7728/Teil 1 04.78

4.6.4.4. Kunsstoffe: Kurzzeichen fuer verstaerkte Kunstsoffe,Gemeinsame Begriffe,DIN 7728/teil 2 03.80

4.6.4.5. Deutcher Holz und Bauteushutz Verband. Arbeitskreis Geraete und Anwendunstechik. Merkblatt. Kraftschluessiges und abdichtendes Injizieren von Rissen und Fehlstellen an Beton-und Stahlbeton-bauwerken. B+B 1, 1984.

4.6.5. FIP. Proposal for a standard acceptance test and verification of epoxy bonding agents for segmental construction.

4.6. Concluding remarks

Polymers can fulfil the criteria for achieving high adhesion better than other available adhesives. Among polymers, the most important for use in structural applications and thus, in adhesive anchors are thermosetting materials or resins. The resins most widely used are epoxy resins (EP), whereas polyurethanes (PU), unsaturated polyester resins (UPR) and vinylester resins (VE) can also be applied for structural purposes.

The good adhesion characteristics of epoxy resins are attributed to their polar nature due to the epoxide and hydroxyl groups. As dipoles, EP resins, after coming in intimate contact with the substrate, mobilize permanent dipole-and induced dipole forces in addition to the

dispersion forces across the interface. Apart from these, chemical bonds of EP with quartz aggregates are reported, which enhance its adhesion to concrete containing such aggregates.

The properties of epoxy resins in both liquid and solid states can be modified by the addition of different agents. In this way, the physical and mechanical adhesion can be optimised by adjusting the surface energy and the viscosity of resin so that surface tension is kept below the critical surface energy of concrete but high enough to promote capillary rise and ensure higher mechanical interlocking across the interface. Characteristic values of physical and mechanical properties of different resins reported by several authors are given.

It is possible to test resins in order to evaluate their suitability in terms of their adhesion properties to concrete. For this reason a selection of existing codes, specifications and recommendations for testing the adhesion properties of resins is also given. From this set of specifications the direct shear test is chosen to represent the bonding properties of resins used in this work, because of the similarity of stress fields between adhesive anchors and the direct shear test and also its simplicity.

5. THEORETICAL ANALYSIS OF THE INDEPENDENT ANCHOR

5.1 The structural system.

The structural system of any anchor consists of, Fig 5.1.:

- the bolt, with a normal ratio of embedment length to diameter of 6-10
- the resin shell, with a normal ratio of height to thickness of 50-20
- the surrounding concrete

The external pull-out force applied results in:

a) shear forces across the steel-resin and resin-concrete interfaces

b) lateral forces across above interfaces due to macro-roughness of the anchor and to the micro-roughness of concrete boreface. There is also a contribution of shrinkage of both resin and concrete to the radial forces as will be seen later (Section 5.3).

The lateral forces are symmetrical and uniformly distributed along the perimeter of the steel and resin. Apart from causing radial compressive stresses, σ_r, they do not affect the compatibility and equilibrium conditions in resin and steel. They are, however, of importance for concrete stresses and strains.

5.2 Calculation of steel and resin strain and stress

The aim of this section is to obtain expressions for stresses and strains in each of the structural components of the anchoring system (the steel, resin and concrete) as mathematical functions of the geometry of the system and of

the applied load.

This can be achieved by examining the equilibrium and compatibility conditions between the structural components of the system. The mathematical strategy which follows involves three main steps.

Step 1. Determination of the distribution of the interfacial shear stress between concrete and resin.

Step 2. Determination of the steel strain distibution.

Step 3. Determination of the resin strain distibution.

The final step of calculating the strains in the concrete is then possible. This is carried out in Section 5.3.

The analysis of above steps 1 and 2 was based to a great extent on the work of Bresson /54/ for the analysis of the stress distribution of a steel plate glued to a concrete substrate.

In order to express mathematically the function of the local slip to the shear stress across the concrete-resin interface, which is necessary for the analytical solution, the constitutive law connecting the local slip measured in test series No 4 (Section 7.5.3) with the applied interfacial shear stress was used.

Before embarking on these steps the basic equilibrium and compatibility equations between the structural components of the system are examined.

Provided that all the materials involved are homogeneous and isotropic, the requirement for the equilibrium of the bottom part of the system, at a section with coordinate z,

is, Fig 5.2.:

$$P_s + P_r + P_c = 0 \quad \text{.....(5.1)}$$

Where:

P_s :the anchor steel axial force

P_r :the resin force distributed along the middle circumference of the resin shell

P_c :the resultant axial force applied to concrete

and the compatibility conditions among the displacements of steel and resin, and resin and concrete are:

$$w_s = w_r + \delta_{s,r} + \varphi t \quad \text{.....(5.2)}$$

$$w_r = w_c + \delta_{c,r} \quad \text{.....(5.3)}$$

where:

w_s : the displacement of steel

w_r : the displacement of resin assumed to be uniform across the resin thickness

w_c : the displacement of concrete across its contact surface with resin

$\delta_{s,r}$: the local slip between steel and resin

$\delta_{c,r}$: the local slip between concrete and resin

φ : the shear rotation of resin

t : the thickness of resin

and taking equations (5.2) and (5.3):

$$w_s = w_c + \delta_{c\,r} + \delta_{s\,r} + \varphi t \quad \text{.....(5.4)}$$

Ignoring the resin force, which as will be seen later is negligible in relation to the steel and concrete forces, means that:

$$d(\tau_{s,r}) = d_o(\tau_{c,r}) \quad \checkmark$$

and assuming that

$$\delta_{s\,r} = a(\tau_{s\,r}) \text{ , and } \delta_{c\,r} = a(\tau_{c\,r})$$

which is experimentally confirmed, Fig. 7.92-7.94, the

compatibility conditions, equations (5.2) and (5.3), become:

$$w_s - w_c = \delta_{cr} + \delta_{sr} + \varphi t = a(\tau_{cr}) + a(\tau_{sr}) + \varphi t =$$

$$= a(\tau_{cr}) + a[(d_o/d)\tau_{cr}] + \varphi t =$$

$$= a\tau_{cr}(1+(d_o/d)) + t(\tau_{cr}/G_a) =$$

$$= \tau[a(1+(d_o/d)) + (t/G_a)] = \mu\tau \quad .....(5.5)$$

where:

G_a : is the shear modulus of resin

a : coefficient of the local bond-local slip law: $\delta=a\tau$, [mm^3/N] for the anchor

$\mu = a(1+(d_o/d))+(t/G_a)$ .....(5.6)

$\tau_{c,r}=\tau$: the shear stress across the concrete-resin interface.

In Eq. (5.6) it was assumed that the resin shell is thin and therefore: $\varphi=\tau/Ga$

Differentiating (5.5) with respect to z, in order to express the shear gradient as a function of the concrete and steel strain, leads to:

$$\frac{d\tau}{dz} = \left[\left(\frac{dw_s}{dz} - \frac{dw_c}{dz}\right)\right] \frac{1}{\mu} \quad .....(5.7)$$

and because for elastic materials the strain is related to the rate of change of displacement by:

$$\varepsilon_s = \frac{dw_s}{dz} = \frac{P_s}{E_s A_s} = \frac{P_s}{\lambda_s}, \quad \varepsilon_c = \frac{dw_c}{dz} = \frac{P_c}{\lambda_c}, \quad \varepsilon_r = \frac{dw_r}{dz} = \frac{P_r}{\lambda_r} \quad .....(5.8)$$

where:

E_s, E_c, E_r: the moduli of elasticity for steel, concrete and resin, respectively

$$\frac{d\tau}{dz} = \left[\left(\frac{P_s}{\lambda_s} - \frac{P_c}{\lambda_c}\right)\right]\frac{1}{\mu} \quad .....(5.9)$$

Taking into account Eq.(5.8), equation (5.1) can be

written:

$$E_s A_s \frac{dw_s}{dz} + E_r A_r \frac{dw_r}{dz} + E_c A_c \frac{dw_c}{dz} = 0 \quad \text{.....(5.10)}$$

or

$$\frac{dw_s}{dz} + \frac{E_r A_r}{E_s A_s} \frac{dw_r}{dz} + \frac{E_c A_c}{E_s A_s} \frac{dw_c}{dz} = 0 \quad \text{.....(5.11)}$$

For common values of $E_c, E_r, E_s, A_s, A_r, A_c$ it can be shown that

$$\frac{E_r A_r}{E_s A_s} \approx 0$$

Thus, the second factor from Eq. (5.11) can be omitted

$$\frac{dw_s}{dz} + \frac{\lambda_c}{\lambda_s} \frac{dw_c}{dz} = 0 \quad \text{.....(5.12)}$$

or

$$P_s + P_c = 0 \quad \text{.....(5.13)}$$

Combining equations (5.13) and (5.9), the shear stress gradient is given by,

$$\frac{d\tau}{dz} = \frac{1}{\mu} \left(\frac{P_s}{\lambda_s} + \frac{P_s}{\lambda_c}\right) = \frac{1}{\mu} \left(\frac{1}{\lambda_s} + \frac{1}{\lambda_c}\right) P_s \quad \text{.....(5.14)}$$

or by differentiation with respect to dz, in order to obtain an equation for the differential changes in anchor tensile force P_s,

$$\frac{d^2\tau}{dz^2} = \frac{1}{\mu} \left(\frac{1}{\lambda_s} + \frac{1}{\lambda_c}\right) \frac{dP_s}{dz} \quad \text{.....(5.15)}$$

Examining the equilibrium of an elementary length of steel:

$$dP_s = (\tau_{s,R})(\pi d)dz = (\tau_{cr} \frac{d_o}{d})(\pi d)dz = \tau(\pi d_o)dz \quad (5.16)$$

and combining Eq.(5.15) and Eq.(5.16) :

$$\frac{d^2\tau}{dz^2} = \left[\frac{1}{\mu} \left(\frac{1}{\lambda_s} + \frac{1}{\lambda_c}\right) \pi d_o\right] \tau \quad \text{.....(5.17)}$$

The differential equation (5.17) has the form:

$$\frac{d^2\tau}{dz^2} - \varkappa^2 \tau = 0 \quad \text{.....(5.18)}$$

where: $$\varkappa = \sqrt{\left(\frac{1}{\mu}\left(\frac{1}{\lambda_s} + \frac{1}{\lambda_c}\right)\pi d_o\right)} \quad \text{.....(5.19)}$$

Step 1. Determination of the distribution of interfacial shear stresses between concrete and resin.

Equation (5.18) defines the distribution of shear stress across the resin-concrete interface.

According to Bresson /54/ this has the solution

$$\tau = A[\sinh(\varkappa z)] + B[\cosh(\varkappa z)] \quad \text{.....(5.20)}$$

The boundary conditions, are:

1 or L ?? $\varkappa = 1$

for $z=1 \rightarrow P_s = P$, and for $z=0 \rightarrow P_s = 0$ .....(5.21)

and because according to Eq. (5.14):

$$\frac{d\tau}{dz} = \frac{1}{\mu}\left(\frac{1}{\lambda_s} + \frac{1}{\lambda_c}\right) P_s \quad \text{.....(5.22)}$$

the above conditions become

$$z=0: \quad \frac{d\tau}{dz} = 0 \quad \text{.....(5.23)}$$

$$z=1: \quad \frac{d\tau}{dz} = \frac{1}{\mu}\left(\frac{1}{\lambda_s} + \frac{1}{\lambda_c}\right) P \quad \text{.....(5.24)}$$

Differentiating Eq. (5.20) with respect to z:

$$\frac{d\tau}{dz} = A\varkappa[\cosh(\varkappa z)] + B\varkappa[\sinh(\varkappa z)] \quad \text{.....(5.25)}$$

and hence equations (5.23) and (5.24) result in:

$$z=0, \quad (A\varkappa)(\cosh(0\varkappa) + (B\varkappa)(\sinh(0\varkappa) = 0$$

which means A=0, for z=0, and

$$\left.\frac{d\tau}{dz}\right|_{z=l} = B\varkappa(\sinh(\varkappa z)) = \frac{1}{\mu}\left(\frac{1}{\lambda_s} + \frac{1}{\lambda_c}\right)P \quad \ldots(5.26)$$

$$B\varkappa(\sinh(\varkappa l)) = \frac{1}{\mu}\left(\frac{1}{\lambda_s} + \frac{1}{\lambda_c}\right)P \quad \ldots\ldots\ldots\ldots\ldots(5.27)$$

where:

$$\lambda_s = (E_s)(A_s)$$

$$\lambda_c = (E_c)(A_c)$$ ← How is A_c defined ???

$$\mu = a(1+(d_o/d)) + (t/G_a)$$

$$\varkappa = \sqrt{\left(\frac{1}{\mu}\left(\frac{1}{\lambda_s} + \frac{1}{\lambda_c}\right)\pi d_o\right)}$$

or:

$$B = \left(\frac{1/\lambda_s + 1/\lambda_c}{\mu\varkappa[\sinh(\varkappa l)]}\right)P = \frac{\varkappa^2 P/\pi d_o}{\varkappa[\sinh(\varkappa l)]} =$$

$$= \frac{\varkappa P}{[\sinh(\varkappa l)]\pi d_o} \quad \ldots\ldots\ldots\ldots\ldots\ldots\ldots\ldots\ldots(5.28)$$

and therefore according to Eq. (5.20) the expression for interfacial shear stress between concrete and resin is given by,

$$\tau = B[\cosh(\varkappa z)] = \frac{\varkappa P}{[\sinh(\varkappa l)]}\left[\frac{\cosh(\varkappa z)}{\pi d_o}\right] \quad \ldots(5.29)$$

This distribution is illustrated in Fig 5.3.(a).

Step 2. Determination of the steel strain distribution

The steel strains can be calculated from the shear stress already determined by rearranging the equations relating the steel and concrete forces gradient to the shear stress, and the shear stress gradient to the steel and concrete displacements.

Considering equations (5.5) and (5.16):

$$\frac{dP_s}{dz} = (\pi d_o)\tau = \pi d_o\left[\frac{(w_s - w_c)}{\mu}\right] \qquad \text{.....(5.30)}$$

or according to Eq.(5.13)

$$\frac{dP_c}{dz} = -\frac{\pi d_o (w_s - w_c)}{\mu} \qquad \text{.....(5.31)}$$

$$\frac{d^2 P_c}{dz^2} = -\frac{\pi d_o}{\mu}\left(\frac{dw_s}{dz} - \frac{dw_c}{dz}\right) = -\frac{\pi d_o}{\mu}\left(\frac{P_s}{\lambda_s} - \frac{P_c}{\lambda_c}\right) =$$

$$= \frac{\pi d_o P_c}{\mu}\left(\frac{1}{\lambda_s} + \frac{1}{\lambda_c}\right) \qquad \text{.....(5.32)}$$

or,

$$\frac{d^2 P_c}{dz^2} - \frac{\pi d_o}{\mu}\left(\frac{1}{\lambda_s} + \frac{1}{\lambda_c}\right)P_c = 0 \qquad \text{.....(5.33)}$$

or,

$$\frac{d^2 P_c}{dz^2} - \varkappa^2 P_c = 0 \qquad \text{.....(5.34)}$$

where $\varkappa = \sqrt{\left(\frac{\pi d_o}{\mu}\left(\frac{1}{\lambda_s} + \frac{1}{\lambda_c}\right)\right)}$

The solution of Eq. (5.34) is :

$$P_c = C[\sinh(\varkappa z)] + D[\cosh(\varkappa z)] \qquad \text{.....(5.35)}$$

and the boundary conditions:

$z=0$, $P_s = P_c = 0$ which results in D=0

$z=l$, $P_s = -P_c = P$

and by consideration of above Eq.(5.35),

$$C = \left[\frac{-P}{\sinh(\varkappa l)}\right]$$

which leads to :

$$P_s = -P_c = \left[\frac{P}{\sinh(\varkappa l)}\right] \sinh(\varkappa z) \quad \text{.....(5.36)}$$

The distribution of the steel force along the anchor axis is shown in Fig 5.3.(b).

Then, the steel displacement can be calculated.

Because:

$$\frac{dw_s}{dz} = \varepsilon_s = \frac{P_s}{E_s A_s} ,$$

$$w_s = w_o + \frac{1}{E_s A_s}\int_0^l P_s\, d_z = w_o + \frac{P}{E_s A_s [\sinh(\varkappa l)]}\int_0^l \sinh(\varkappa z)dz$$

$$= w_o + \left[\frac{P}{E_s A_s \sinh(\varkappa l)}\right]\left[\frac{\cosh(\varkappa z)}{\varkappa}\Big|_0^l\right] =$$

$$= w_o + \frac{P(\cosh(\varkappa l)-1)}{\varkappa E_s A_s \sinh(\varkappa l)} \quad \text{.....(5.37)}$$

where:

$$w_o = w_r + \delta_{s,r} + \varphi t = w_r + (a(d_o/d) + t/G_a)(\tau_{z=l}) \text{...(5.38)}$$

w_o : the displacement of resin at the free surface

w_r : $\int \varepsilon_r\, dz$

$\tau_{z=l}$: the interfacial shear stress at the free end

Step 3. Determination of the resin strain distribution

In order to define the resin strain distribution a law connecting the local slip to the local shear stress is needed. In the following,the relationship obtained experimentally is used.

Ignoring the resin axial force as in Eq.(5.12), means that,

$$d(\tau_{s,r}) = d_o(\tau_{c,r})$$

Following Eq. (5.2) and assuming that the law $\delta=a.\tau$ is the same for both the concrete-resin and resin-steel interfaces, which is confirmed experimentally (Figures 7.147 and 7.149), the resin strain can be derived from Eq.(5.2):

$$w_r = w_s-(\delta_{s,r} + \varphi t) = w_s-(a\tau_{s,r} + (\tau_{c,r}\ \frac{t}{Ga}))$$

$$= w_s-(a\ \frac{d_o}{d} + \frac{t}{Ga})\tau = w_s-\rho_o\tau \quad \ldots\ldots\ldots\ldots\ldots(5.39)$$

$$\text{where } \rho_o = [a(\frac{d_o}{d}) + \frac{t}{Ga}] \quad \ldots\ldots\ldots\ldots\ldots\ldots(5.40)$$

or:

$$\frac{dw_r}{dz} = \frac{dw_s}{dz} - \rho_o\ \frac{d_\tau}{dz} = \varepsilon_s - \rho_o[\frac{d\tau}{dz}] =$$

$$= \frac{P_s}{E_s A_s} - \rho_o[\frac{d_\tau}{dz}] \quad \ldots\ldots\ldots\ldots\ldots\ldots\ldots\ldots(5.41)$$

and because in accordance with (5.29)

$$\frac{d\tau}{dz} = \frac{\varkappa P}{[\sinh(\varkappa l)]\pi d_o}\ \varkappa[\sinh(\varkappa z)] =$$

$$= \frac{\varkappa^2 P}{\pi d_o[\sinh(\varkappa l)]}\ [\sinh(\varkappa z)] \quad \ldots\ldots\ldots\ldots(5.42)$$

Eq.(5.41) becomes:

$$\frac{dw_r}{dz} = \frac{P_s}{E_s A_s} - \rho_o\ \frac{\varkappa^2 P}{\pi d_o[\sinh(\varkappa l)]}\ [\sinh(\varkappa z)] =$$

$$= \frac{P(\sinh(\varkappa z))}{\sinh(\varkappa l)} \frac{1}{E_s A_s} - \rho_o \frac{\varkappa^2 P}{\pi d_o (\sinh(\varkappa l))} \sinh(\varkappa z) =$$

$$= \frac{P}{\sinh(\varkappa l)} \left[\frac{1}{E_s A_s} - \rho_o \frac{\varkappa^2}{\pi d_o}\right] (\sinh(\varkappa z)) \qquad (5.43)$$

Generally, however: from where?

$$\varepsilon_r = \varepsilon_o - \frac{dw_r}{(r)\,dz} \qquad \ldots\ldots\ldots\ldots\ldots\ldots\ldots\ldots\ldots\ldots (5.44)$$

due to the existing bond link between concrete and resin at the bottom of the anchor.

where:

ε_o : the resin strain due to its adhesive tensile bond with concrete at the bottom of the hole.

Since:

for $z = l$, $\varepsilon_r = 0$ $\qquad \ldots\ldots\ldots\ldots\ldots\ldots\ldots (5.45)$

ε_o can be calculated by combining Eq.(5.43) and (5.44) at z=l as:

$$\varepsilon_o - \frac{P}{\sinh(\varkappa l)} \left[\frac{1}{E_s A_s} - \rho_o \frac{\varkappa^2}{\pi d_o}\right] \sinh(\varkappa l) = 0 \qquad (5.46)$$

or:

$$\varepsilon_o = P\left[\frac{1}{E_s A_s} - \rho_o \frac{\varkappa^2}{\pi d_o}\right] \approx P\left[\frac{1}{E_s A_s} - \frac{\rho_o}{\pi d_o} \left(\frac{\pi d_o}{\mu} \left(\frac{1}{E_s A_s}\right)\right)\right] \approx$$

$$\approx P\left[\frac{1}{E_s A_s} - \frac{\rho_o}{\mu} \left(\frac{1}{E_s A_s}\right)\right] \approx \frac{P}{E_s A_s} \left(1 - \frac{\rho_o}{\mu}\right) \qquad \ldots\ldots (5.47)$$

giving finally the distribution of resin strain as

$$\varepsilon_r = P\left[-\frac{\rho_o \varkappa^2}{\pi d_o} + \frac{1}{E_s A_s}\right]\left(1 - \frac{\sinh(\varkappa z)}{\sinh(\varkappa l)}\right) \qquad \ldots\ldots (5.48)$$

The distribution of resin strain along its z axis is illustrated in Fig 5.3.c.

5.3 Calculation of concrete stress (Step 4.)

There are two components of the concrete stress:

a) One arising from the shear forces transferred along the resin-concrete interface.

b) The second due to radial pressure applied at the bore face. These can originate from mechanical interlocking between steel and resin and resin and concrete, and also from shrinkage effects of resin and concrete.

The mechanical interlocking consists of:

- micro-interlocking owing to the microcracks, pores and capilliaries existing across the two interfaces as explained in sections 3.4.3. and 3.4.4. and
- possible macro-interlocking across the steel resin interface due to the surface of the steel rod (thread or ribs) and due to the roughness of boring across the concrete-resin interface, Fig.1.7, Section 3.4.3.

The shrinkage of concrete and resin causes lateral pressure on the steel-resin interface. At the resin-concrete interface the effect is complex since, due to shrinkage, the resin has a tendency to be disconnected from the concrete, applying in this way tensile stress to interface. The concrete shrinkage results in applied pressure to the resin across the interface. However, although

the shrinkage rates of resins are usually 3-5 times higher than that of concrete, the effect of shrinkage of resin is negligible in relation to that of concrete because it applies to resin thickness, whereas that of concrete to the specimen size, see Appendix C.1. The concrete shrinkage results in applied pressure to the resin across the interface. Besides, there is also the lateral contraction of steel rod under tension. This combined effect is examined by Takaku and Arridge /55/ for plain steel fibres embedded in epoxy resin, and by Laldji and Young /56/ on steel strands surrounded by cement grout. The effect of the lateral pressure including that of the radial deformation of steel bars embedded in concrete was examined by Robins and Standish /57/.

In the following a calculation of the concrete stress distribution is reported. It is based on the forces resulting from integration of shear stresses across the resin-concrete interface already defined, and those of the radial pressure due to mechanical interlocking and the combined shrinkage of concrete and resin. The proposal utilizes the Mindlin solution, /58/, for the problem of calculation of the stresses in a semi-infinite body with an internal concentrated load.

The Mindlin solution has two relevant forms:

- due to a single concentrated force perpendicular to the boundary of the semi-infinite body.
- due to a single concentrated load parallel to the boundary

The modelling process employed here is to represent:

(a) The radial stress distribution by sets of four concentrated forces at three levels, Fig.5.4.(a).

(b) The shear forces distribution by sets of three concentrated forces at the above levels, Fig.5.4.(a).

In the following the calculation of the values of the aforementioned concentrated shear and lateral forces applied to concrete are given.

The concentrated shear forces at the resin-concrete interface, derive by integration of the shear stresses. So, by taking 1/n as an integration interval, the uppermost concentrated shear force is:

$$T_1 = \pi d_o \int_0^{l/n} \tau dz = \pi d_o \int_0^{l/n} \frac{\varkappa}{\pi d_o} \frac{P\,[\cosh(\varkappa z)]}{\sinh(\varkappa l)}\, dz =$$

$$= \frac{\varkappa P}{[\sinh(\varkappa l)]} \int_0^{l/n} [\cosh(\varkappa z)]dz =$$

$$= \frac{\varkappa P}{\sinh(\varkappa l)]} \frac{1}{\varkappa} [\sinh(\frac{\varkappa l}{n})] =$$

$$= \frac{P\,[\sinh(\varkappa l/n)]}{[\sinh(\varkappa l)]} \quad \text{.....(5.49)}$$

T_2 is calculated by a similar process and the final force is given in general by:

$$T_n = \frac{P}{[\sinh(\varkappa l)]} [\sinh(\varkappa l) - \sinh((n-1)\varkappa l/n)] \quad (5.50)$$

In this case for the sake of simplicity n is set equal to 3.

Then, based on these forces it is possible to determine the stress distribution in the concrete, assuming that the concrete substrate is a semi-infinite solid. Mindlin /58/, for a semi-infinite body and for a global system x,y,z as illustrated in Fig. 5.4.(a), gave the stresses in any concrete point due a concentrated force T perpendicular to boundary. Based upon this, the stresses due to combined action of the homoaxial T_1 to T_n forces are:

$$\sigma_x = \sum_{i=1}^{n} \frac{T_i}{8\pi(1-\nu)} \left[\frac{(1-2\nu)(z-c)}{R_1^3} - \frac{3x^2(z-c)}{R_1^5}\right] +$$

$$+ \left[\frac{(1-2\nu)[3(z-c)-4\nu(z+c)]}{R_2^3} -\right.$$

$$- \left(\frac{3(3-4\nu)x^2(z-c)-6c(z+c)[(1-2\nu)z-2\nu c]}{R_2^5} \right) -$$

$$\left. - \frac{30cx^2 z(z+c)}{R_2^7} \right] -$$

$$-\left[\frac{4(1-\nu)(1-2\nu)}{R_2(R_2+z+c)}\left(1 - \frac{x^2}{R_2(R_2+z+c)} - \frac{x^2}{R_2^2}\right)\right] \quad (5.51)$$

$$\sigma_z = \sum_{i=1}^{n} \frac{T_i}{8\pi(1-\nu)} \left[- \frac{(1-2\nu)(z-c)}{R_1^3} +\right.$$

$$\left. + \frac{(1-2\nu)(z-c)}{R_2^3} - \frac{3(z-c)^3}{R_1^5} \right]-$$

$$- \left[\frac{3(3-4\nu)z(z+c)^2 - 3c(z+c)(5z-c)}{R_2^5} -\right.$$

$$- \frac{30cz(z+c)^3}{R_2^7} \Big] \quad \ldots\ldots\ldots\ldots\ldots\ldots\ldots\ldots\ldots\ldots (5.52)$$

$$\tau_{yz} = \sum_{i=1}^{n} \frac{T_i y}{8\pi(1-\nu)} \Big[- \Big\{ \frac{(1-2\nu)}{R_1^3} + \frac{3(z-c)^2}{R_1^5} \Big\} + \frac{(1-2\nu)}{R_2^3} -$$

$$- \frac{3(3-4\nu)z(z+c)-3c(3z+c)}{R_2^5} -$$

$$- \frac{30cz(z+c)^2}{R_2^7} \Big] \quad \ldots\ldots\ldots\ldots\ldots\ldots\ldots\ldots\ldots\ldots (5.53)$$

$$\sigma_y = \sum_{i=1}^{n} \frac{T_i}{8\pi(1-\nu)} \Big[\Big[\frac{(1-2\nu)(z-c)}{R_1^3} - \frac{3y^2(z-c)}{R_1^5} \Big] +$$

$$+ \Big[\frac{(1-2\nu)[3(z-c)-4\nu(z+c)]}{R_2^3} \Big] -$$

$$- \Big[\frac{3(3-4\nu)y^2(z-c)-6c(z+c)[(1-2\nu)z-2\nu c]}{R_2^5} \Big] -$$

$$- \Big[\frac{30cy^2 z(z+c)}{R_2^7} \Big] -$$

$$- \Big[\frac{4(1-\nu)(1-2\nu)}{R_2(R_2+z+c)} \Big(1 - \Big[\frac{y^2}{R_2(R_2+z+c)} \Big] - \Big[\frac{y^2}{R_2^2} \Big] \Big) \Big] \quad (5.54)$$

where:

T_i : the idealized vertical forces applied to different points along the anchor axis in concrete, regarded as a semi-infinite body. Forces Ti are calculated in accordance with equations (5.49), (5.50).

ν : the Poisson's ratio of concrete

x,y,z: the coordinates of the particular point of concrete

c : the z-coordinate of the point of z axis where the concentrated force is applied

$R_1 = \sqrt{(x^2+y^2+(z-c)^2}$

$R_2 = \sqrt{(x^2+y^2+(z+c)^2}$

The concrete stress due to radial forces is calculated from the value of the radial pressure acting across the resin-concrete interface due to combined mechanical interlocking, shrinkage and lateral contraction of the steel.

The radial pressure due to mechanical interlocking can be expressed in the form of

$$\sigma_i = n\,\tau \qquad \text{.....(5.55)}$$

where:

σ_i : the radial pressure

τ : the concrete-resin interfacial shear stress

n : coefficient taking into account the possible identation of steel and the roughness of concrete

As far as the combined shrinkage of resin and concrete is concerned, Takaku and Arridge /55/, derived the following relationship from radial pressure, σ_i

$$\sigma_i = \left[\frac{\varepsilon_0 E_s}{\nu_s}(1+\nu_r)\right]\left[1-\exp\left[-\frac{2(E_r)(\nu_r)(\mu x)}{(E_s)(r_s)(1+\nu_r)}\right]\right] \qquad \text{..(5.56)}$$

where:

E_s, E_r : elastic modulus for steel and resin respectively

ν_s, ν_r : Poisson's ratio of steel and resin

ε_0 : original lateral strain in resin

ε_o : original lateral strain in resin

μ : coefficient of friction between wire and resin

r_s : radius of steel fibre

x : the embedment length

Laldji and Young /56/ for the case of high values of grout specimen size to steel diameter gave the relationship:

$$\sigma_i = [(E_s)\varepsilon-(\nu_s)(\sigma_s)+2m(\sigma_o)]/K \quad \text{.....(5.57)}$$

where:

$K = (1-\nu_s)+m(1+\nu_g)$

σ_s : the tensile stress of steel strand

ν_s, E_s : Poisson's ratio and modulus of elasticity of steel

ν_g, E_g : Poisson's ratio and modulus of elasticity of the grout

$m = E_s/E_g$

σ_o : the lateral pressure possibly applied to the specimen

Using the above expressions it is possible to calculate the concentrated radial forces, Fig.5.4.(a), by integration of σ_i over the same particular lengths of integration as for the shear forces. Then the concrete stress can be calculated in a way similar to above, Eq.(5.51)-Eq.(5.54), using the following relationships of Mindlin /58/, for the concrete stresses due to a concentrated force parallel to the boundary of a semi-infinite body, Eq.(5.58)-Eq.(5.61).

$$\sigma_x = \sum_{i=1}^{n} \frac{Hx}{8\pi(1-\nu)} \left[- \frac{(1-2\nu)}{R_1^3} + \frac{(1-2\nu)(5-4\nu)}{R_2^3} - \right.$$

$$- \frac{3x^2}{R_2^5} - \frac{3(3-4\nu)x^2}{R_2^5} -$$

$$- \frac{4(1-\nu)(1-2\nu)}{R_2(R_2+z+c)^2} \frac{(3-x^2(3R_2+z+c))}{R_2^2(R_2+z+c)} +$$

$$+ \frac{6c}{R_2^5}(3c-(3-2\nu)(z+c)+\frac{5x^2z}{R_2^2})] \quad \ldots\ldots\ldots(5.58)$$

$$\sigma_y = \sum_{i=1}^{n} \frac{Hx}{8\pi(1-\nu)} [(\frac{1-2\nu}{R_1^3}) + \frac{(1-2\nu)(3-4\nu)}{R_2^3} -$$

$$- \frac{3y^2}{R_1^5} - \frac{3(3-4\nu)y^2}{R_2^5} -$$

$$- \frac{4(1-\nu)(1-2\nu)}{R_2^2(R_2+z+c)}(1- \frac{y^2(3R_2+z+c)}{R_2^2(R_2+z+c)^2}) +$$

$$+ \frac{6c}{R_2^5}(c - (1-2\nu)(z+c) + \frac{5y^2z}{R_2^2})] \quad \ldots\ldots\ldots(5.59)$$

$$\sigma_z = \sum_{i=1}^{n} \frac{Hx}{8\pi(1-\nu)} [(\frac{1-2\nu}{R_1^3})-(\frac{1-2\nu}{R_2^3}) -$$

$$- \frac{3(z-c)^2}{R_1^5} - \frac{3(3-4\nu)(z+c)^2}{R_2^5} +$$

$$+ \frac{6c}{R_2^5}(c+(1-2\nu)(z+c) + \frac{5z(z+c)^2}{R_2^2})] \quad \ldots\ldots(5.60)$$

$$\tau_{yz} = \sum_{i=1}^{n} \frac{Hxy}{8\pi(1-\nu)}[- \frac{3(z-c)}{R_1^5} - \frac{3(3-4\nu)(z+c)}{R_2^5} +$$

$$+ \frac{6c}{R_2^5}\left(1-2\nu + \frac{5z(z+c)}{R_2^2}\right)\Big] \quad \text{.....(5.61)}$$

where :

H_i : the ideal lateral forces calculated as above

ν : the Poisson's ratio of concrete

x,y,z: the coordinates of the particular point of concrete

c : the z-coordinate of the point of z axis where the concentrated force is applied

$R_1 = \sqrt{(x^2+y^2+(z-c)^2}$

$R_2 = \sqrt{(x^2+y^2+(z+c)^2}$

A general representation of the concrete stress or corresponding strain distribution in the same way as for interfacial shear stress and for steel and resin strain is not possible.

Therefore, calculations of concrete stresses and strains for a particular case are carried out in Appendix A.4 and the resulting distributions compared graphically with experimental and finite element results in Chapter 8.

5.4 Concluding remarks

With the assumption that all the materials involved in an adhesive anchor system are homogeneous and behave elastically, it is possible to determine the stress and strain in each component.

Thus, by examining the equilibrium and compatibility of the components of the system, the following expressions for the internal forces and strains of the system are gained:

The concrete-resin interfacial shear stress (τ) distribution due to applied load (P) is:

$$\tau = \frac{\varkappa P}{\pi d_o [\sinh(\varkappa l)} [\cosh(\varkappa z)] \quad \ldots\ldots\ldots\ldots\ldots(5.29)$$

It is illustrated in Fig 5.3.(a).

The steel tensile force is:

$$P_s = - P_c = \frac{P}{[\sinh(\varkappa l)]} [\sinh(\varkappa z)] \quad \ldots\ldots\ldots(5.36)$$

P_s is illustrated in Fig 5.3.(b).

The steel displacement is:

$$w_s = w_o + \frac{1}{\varkappa} \frac{P[\cosh(\varkappa l)-1]}{E_s A_s [\sinh(\varkappa l)]} \quad \ldots\ldots\ldots\ldots\ldots\ldots\ldots(5.37)$$

Finally the resin strain,illustrated in Fig 5.3.(c),is :

$$\varepsilon_r = [\frac{1}{E_s A_s} - \frac{\rho_o \varkappa^2}{\pi d_o}] [1 - \frac{\sinh(\varkappa z)}{\sinh(\varkappa l)}] \quad \ldots\ldots\ldots\ldots\ldots(5.48)$$

where:

$$\varkappa = \sqrt{(\frac{\pi d_o}{\mu} (\frac{1}{E_s A_s} + \frac{1}{E_c A_s}))} \quad \ldots\ldots\ldots\ldots\ldots\ldots(5.19)$$

$$\mu = a(1+(d_o/d))+(t/Ga) \quad \ldots\ldots\ldots\ldots\ldots\ldots\ldots(5.6)$$

$$\rho_o = a(d_o/d)+(t/Ga) \quad \ldots\ldots\ldots\ldots\ldots\ldots\ldots\ldots(5.40)$$

$$w_o = w_r + \rho_o \tau_{z=1} \quad \ldots\ldots\ldots\ldots\ldots\ldots\ldots\ldots(5.38)$$

w_r : the displacement of resin at the free surface.

The stresses in the concrete in any particular point can be calculated using superposition of a number of equations of Mindlin /58/ for single concentrated shear

forces T_i and concentrated radial forces H_i applied along the z axis to concrete, Eq. (5.51),(5.52), (5.53), (5.54), (5.58), (5.59), (5.60), (5.61).

To conclude this section a brief description of the theoretical prediction of effects of changes in the principal parameters associated with the anchorage problem is now given.

From the above equations it can be seen that:

- An increase in embedment length l causes:
  - a decrease in τ in accordance with the hyperbolic function of $\sinh(\varkappa l)$, Eq.(5.29), and therefore a similar decrease in the radial pressure σ_i and the idealized forces T and, as a result, the same decrease in the stresses σ_x, σ_z, τ_{xy} and σ_y induced in concrete, Eq. (5.51), (5.52), (5.53), (5.54), (5.58), (5.59), (5.60), (5.61).
  - a lower anchor displacement, since both the factors resulting in the displacement decrease, i.e. the resin displacement almost as above (change in τ) and the elastic anchor displacement in accordance with the function $\frac{\sinh(\varkappa l)-1}{\sinh(\varkappa l)}$, Eq.(5.37).
  - A change in the distribution of the resin strain along the axis in accordance with the quantity $1 - \frac{\sinh(\varkappa z)}{\sinh(\varkappa l)}$, Eq.(5.48).

- An increase in the diameter of anchor with constant value of resin thickness causes:

- a decrease in τ approximately in accordance with the factor $(\sqrt{d_o})(\sinh(\sqrt{d_o}Cl))$, Eq.(5.29), (5.19).
- a decrease in w_s, dependent on the shear stress τ which decreases as above and on the elastic anchor displacement decreasing by the value of $\sinh((\sqrt{dC})l)$, since the quantity $(\cosh(\varkappa l)-1)$ varies little because of the normally low values of $(\varkappa l)$, Eq.(5.37).

- a sharp decrease in resin strain since the quantity $\frac{1}{E_s A_s}$ decreases sharply, Eq.(5.48).

- an increase in the stresses induced in concrete, especially in the vicinity of the hole, related to the change in coordinate system in order to utilise the Mindlin solution in the presence of the hole, Fig.5.4.(b). Simultaneously it causes increase in the radial forces H applied at the boreface, $H=(\sigma_i)d$. (Although internal pressure decrease with τ because $\sigma_i = n\tau + \sigma_{i\,shr}$, the product $(\sigma_i)_d$ increases). As a result, the concrete stresses, σ_x, σ_y, increase. Thus, the splitting failure mode becomes more likely.

- Increase in the resin thickness, t, results in:
  - a linear increase, in μ and ρ_o, Eq.(5.19), Eq.(5.6), which in turn cause a change of τ in relation to the function

$$\left(\frac{1}{\sqrt{(c+Dt)}} \quad \frac{\cosh(B/\sqrt{(c+Dt)})}{\sinh(A/\sqrt{(c+Dt)})} \right), \text{ Eq.(5.29).}$$

This tends to slight decrease in τ at relatively higher values of t.

- an increase in ε_r, approximately in a linear variation with

$$\left(\frac{1}{A} - \frac{c+t}{(c+t)}\right), \quad \text{Eq.(5.48), Eq.(5.19),}$$

- Better adhesive bond, which is expressed by lower values of the coefficient a, causes the opposite effect to an increase in resin thickness as can be seen from Eq.(5.19),Eq. (5.6).

- Higher values of E_c, if they were isolated from any other changes, would cause a negligible decrease in the quantity $\varkappa$ and therefore in τ, dependent on the factor

$$\left(\frac{\varkappa}{\sinh(\varkappa l)}\right) \cosh(\varkappa z), \quad \text{Eq.(5.29).}$$

However, it must be noted that the increase in E_c values means higher concrete strength and therefore better adhesive behaviour of the resin - concrete interface. The values of μ and ρ_o are lower and therefore give rise to higher values of $\varkappa$, which in turn causes lower anchor displacements. This displacement, however, in reality is further reduced due to the improved original concrete tensile strength which results in an extended pre-cracked elastic stage.

From the closed form mathematical expressions obtained it is possible to design an anchoring system by defining:

- the displacement of the anchor, Eq. (5.37) and (5.38)
- the shear stress distribution along the concrete-resin interface, Eq. (5.29), Fig 5.3.(a)
- the steel force distribution, Eq. (5.36), Fig 5.3.(b)
- the resin strain distribution, Eq.(5.48), Fig 5.3.(c)

The calculation of the concrete strains at different points is laborious. It demands firstly integration of the shear stress along the concrete-resin interface at defined intervals, and, secondly calculation of the radial forces using Eq. (5.55) and Eq. (5.56) or Eq (5.57). Then, the concrete stresses at any point can be calculated as the sum of the stresses due to axial forces and the ones due to radial forces. Eq. (5.51) - Eq. (5.54) can be used for the calculation of stresses due to forces perpendicular to the surface and Eq. (5.58) - Eq. (5.61) for the stresses due to radial ones. Using very simple commercially available spreadsheet programmes this work can be done very easily and quickly (see Appendix A.4).

The results from this section can be used for the prediction of the displacement of the anchor at any load and for calculation of concrete stress distribution upon the assumption that the behaviour of the system remains linearly elastic up to failure. This assumption is not far from reality as can be seen from Figures 7.58 - 7.91 as far as the whole system is regarded and Figures 7.92 - 7.94 for the local slip-local bond relationship. All these are later discussed in comparison with finite element analysis and the experimental results.

6. FINITE ELEMENT ANALYSIS OF THE INDEPENDENT ANCHOR

The finite element analysis of a model simulating the actual specimen used in the majority of the tests is a limited study because it utilized linearly elastic stress-strain laws for all materials involved (steel, resin, concrete). Thus, the post-cracking inelastic behaviour of concrete and the non-linear constitutive law of local interfacial slip to local interfacial bond could not be taken into account.

However, there were two reasons for selecting it for study:

- It was thought that the initial stage of linear behaviour would be relatively extended, because the combined failure (which is the mode most likely to occur for the majority of systems commonly used, as will be seen later in the experimental results) is controlled by the tensile strength of concrete and resin and by the concrete-resin interfacial shear strength, Fig. 1.2.(e). The first two mechanisms behave elastically almost up to failure whereas the interfacial local bond-local slip law does not deviate too much from linearity for small resin thickness and low viscosity resins, as will be seen later in Section 7.14.1.
- It would be possible to simulate easily the interfacial local slip-local bond constitutive law using linear slip elements. The stiffness of these elements could be calculated from the real interfacial constitutive law obtained experimentally. This was essential because as is shown in

Section 5.2, Eq. (5.38), the steel displacement depends on the resin slip a great deal. Under these circumstances it would be worthwhile to use a method of analysis which is readily available in practice without demanding high capabilities of hardware and too expensive software.

This analysis is limited to that stage of loading at which either the concrete enters a generalized cracking state or the interfacial shear stress starts to deviate from linearity (at almost 9.00 N/mm² for low viscosity resins, Fig 7.92-7.94).

Nevertheless, there was some useful information obtainable:

- First of all it was easy to obtain concrete strain distributions at any section. This might be of importance in examining the effect of the different parameters of the problem, especially as a supplement to the strain distributions obtained experimentally (which, as a matter of fact, were limited in extent).
- Given that the values of critical strains of concrete and resin and that of interfacial shear stress are known, the results of such analysis for a unit applied load will be used for the prediction of failure mechanisms.
- The stress and strain distributions obtained from finite element analysis could be compared with those of theoretical analysis, which readily gives the elastic steel-and resin strain and interfacial shear stress distribution.

The analysis was made by means of a commercially available programme (SAP 90) using linear slip elements to simulate the interfacial constitutive law of local slip-local bond. Linear slip elements were also used to simulate the steel-resin and resin-concrete interfaces at the bottom of the anchor. The contribution of the present thesis to such analysis was the combination of the slip elements with the interfacial constitutive relationship obtained from the direct shear tests.

The model analysed here simulated the specimen used in test series No 3, Fig 7.8. For the modelling of the specimen its symmetry about x and y axis (coplanar with the 600mm x 600mmm plane) and about its diagonals was taken into consideration. Thus, only 1/8 of the specimen was analysed, Fig 6.1.(a), (b).

The analysis carried out was linearly elastic. The element used was a three-dimensional solid element with 8-nodes based upon an isoparametric formulation including nine optional incompatible bending modes in the SAP 90 library. For the slip elements linear elements were used. All stress values were calculated at the element joints in the global coordinate system. In order to examine the effect of the different variables five different models were studied:

- The standard model.
- The model with resin thickness of 4mm.
- The model with reduced anchor diameter (d=8mm)
- The model with a fully developed crack, inclined at 39° to the vertical axis and starting at a point (0.21) deep from the external face,

Fig 6.1,(e).

- The model with a partially developed (stabilized) crack starting at the same depth with the same inclination and only 14mm long, Fig 6.1,(f).

6.1. Characteristics of geometry, materials and loads.

The first mesh included:

- thirty elements for steel extending 1mm and 2mm radially, Fig 6.1(b),(d)
- ten elements for resin extending 2 mm radially and four elements of 2mm thickness below the bolt, Fig 6.1(c),(d)
- 1388 elements for concrete extending 2-4-8-16-32 and 64mm radially from the axis, Fig 6.1(b),(c).

In order to take into account the slip across the concrete-resin and resin-steel interface, elastic diagonal elements connecting the nodes across the two interfaces and accommodating the actual slip were used. Their stiffness characteristics were calculated on the basis of the local slip expressed as function of the corresponding local shear stress derived from experimental results described in Section 6.2. The stiffness of the tensile slip elements was calculated in the same way assuming that the coefficient of the tensile constitutive relationship is double that of the shear relationship.

The boundary conditions imposed on the model (1/8 of the whole specimen) were:

- restraint against translation in both the radial and tangential directions of all the nodes along the diagonal (section 5) and y axes, Fig

6.1.

- restraint against translation in all directions for the nodes of the half perimeter of the support H_1 (where in the real specimen the reaction P/4 is applied).

The stabilized crack was formed by disconnecting four elements at their common nodes, Fig 6.1,(f).

The model with the fully developed inclined crack starting at a distance of (0.2)1 from the top was formed by omitting the corresponding elements involved in the cracked zone, Fig 6.1,(e).

The mechanical properties of the materials involved were taken as:

E_c = 30,000 N/mm^2 $\quad$ ν_c = 0.20

E_r = 2,200 N/mm^2 $\quad$ ν_r = 0.30

E_s = 210,000 N/mm^2 $\quad$ ν_s = 0.29

Apart from the modulus of elasticity of resin, which was found experimentally in test series No 5, all the remaining values are representative of those given by the most codes in use.

Linear constitutive relationships were used for all materials, hence, no post-cracking concrete behaviour was taken into account.

The loads applied were:

- a tensile axial force of 10kN uniformly distributed to the steel elements
- a radial compressive force distributed on the nodes of resin-concrete interface to simulate the mechanical interlocking and combined shrinkage

effect of resin and concrete. The mechanical interlocking component was calculated from the corresponding values of the interfacial shear forces obtained from the first analysis, taking into consideration a threaded anchor similar to that used in tests, Appendix C.1. The combined shrinkage effect was calculated from equation (5.57) for the concrete shrinkage developed in the real specimen up to the time of the pull-out of the anchor (t=28 days).

6.2. Calculation of the stiffness characteristics of slip elements

In this section the formulation of a relationship connecting the stiffness properties of the diagonal slip elements simulating the two interfaces with the local slip-local bond law obtained experimentally for these interfaces is sought.

Assuming that the law of $\delta=\delta(\tau)$ is a linear function for both the concrete-resin and resin-steel interfaces (which does not deviate too much from the real law as is later proved experimentally, Fig.7.147, 7.149),

$$\delta = a\ \tau \qquad (6.1)$$

In order to make use of the possibilities of SAP 90 programme library, as Probst did in his work /59/, the above interfaces were simulated using linear slip elements as is illustrated in Fig. 6.2.

For two diagonal elements D_1, D_2 connecting nodes across the interface the following relationships are valid.

The shear force at each node is equal to:

$$T = (\tau_{s,r})\ (\frac{1}{2}\ b) = (\tau)(\frac{1}{2}\ b) \quad \ldots\ldots\ldots\ldots(6.2)$$

$$S_1 = -S_2 = (\tau)(\frac{1}{2}\ b)\ \frac{1}{\cos\varphi} = (\frac{\delta}{a})(\frac{bl}{2})\ \frac{1}{\cos\varphi} \quad \ldots\ldots(6.3)$$

The length of the diagonals is $l_1 = l/\cos\varphi$ and their elongation due to slip of δ:

$$\Delta l_1 = -\Delta l_2 = \delta\ (\cos\varphi) \quad \ldots\ldots\ldots\ldots\ldots\ldots(6.4)$$

Simultaneously Δl_1, Δl_2 are the elastic displacements of the diagonals due to their axial forces S_1, S_2. Thus:

$$S_1 = -S_2 = \frac{E_1 A_1}{l_1}\ \Delta l_1 = \frac{E_1 A_1}{l_1}\ \delta(\cos\varphi) \quad \ldots\ldots(6.5)$$

where:

E_1, A_1 the modulus of elasticity and the cross sectional area of the diagonal elements.

Equating the expressions for S_1, S_2 from Eq. (6.3), Eq.(6.5)

$$(\frac{\delta}{a})(\frac{bl}{2})\ \frac{1}{\cos\varphi} = \frac{E_1 A_1}{l_1}\ \delta(\cos\varphi) =$$

$$= \frac{E_1 A_1}{1/\cos\varphi}\ \delta(\cos\varphi) = \frac{E_1 A_1}{1}\ \cos^2\varphi \quad \ldots\ldots\ldots\ldots(6.6)$$

giving the effective elastic modulus of the slip element as:

$$E_1 = \frac{bl^2}{2a\ A_1\ (\cos^3\varphi)} \quad \ldots\ldots\ldots\ldots\ldots\ldots\ldots\ldots(6.7)$$

where:

b :the width of the resin element

a :the factor of the law $\delta = a.\tau^m$ in accordance with Fig. 7.147, Fig 7.149. For sake of simplicity

this factor was taken as α=0142[mm^3/N] for both the concrete-resin (Fig 7.147) and resin-steel (Fig. 7.149) interfaces.

l :the height of the elements

A_1 :the cross section of the element.

φ_r :arctan (r/l)

r :$\sqrt{(b^2 + t^2)}$

In the same way the corresponding stiffness of the tensile slip elements at the bottom was found to be:

$$E_2 A_2 = (btl/2a_t) \quad \text{.....(6.8)}$$

where:

b,t :the dimensions of anchor element at the bottom, on a plane perpendicular to anchor axis

E_2 ,A_2 :the modulus of elasticity and the cross section of the slip element

a_t :the factor of the relationship $\delta=(a_t)\sigma$ for the tensile steel-resin and the resin-concrete interfaces at the bottom of the anchor assumed to be: a_t=2a, where a the corresponding factor for the shear interfacial law.

6.3. Results from the linearly elastic finite element analysis

The results gave stresses at the centre of each face of the elements. For later comparison of these data with those gained from theoretical analysis and the experimental work, the strains of all components of the system related

to the value of external pull-out load of P=10 kN were calculated. In addition, the interfacial shear stress distribution was also drawn.

Since the finite element analysis was linearly elastic the diagrams of distribution of strain and shear stress at the interface were drawn only for the load level P=10 kN. The relative values at any other load level are proportional to these.

The distribution of strains in the steel, resin and concrete at a section extending 18 mm from the anchor axis, and the distribution of the shear stress along the concrete-resin interface are shown in Fig 6.3 - Fig 6.6 for the parameters investigated.

A comparison shows that:

- The increase in resin thickness from 2mm to 4mm caused:
  - an increase in resin strain between 34% at the top and 540% at the bottom. However, the maximum value of resin strain (857 με at P=10 kN) was far below the ultimate value (6000με for C1380-5334 με for LV, Fig 7.150, 7.151).
  - an increase in concrete radial strain at a section extending 18 mm from anchor axis of 20% at top and 150% at bottom.
  - an increase in the value of concrete vertical strain of 50% at the top of the same concrete section, and a decrease of 64% at the bottom of the section
  - a decrease of 50% in the concrete tangential strain, at the bottom in this

section (18 mm far from the anchor axis) and a decrease of 10% at the top.

- a decrease in interfacial shear stress, varying between 38% at the top and 43% at the bottom.

- The decreased anchor diameter 8 mm instead of 12 mm of the standard model caused:
  - an increase in the resin strain in the lower part of the anchor with a maximum of 1069% at the bottom. The maximum value of resin strain (1567 με at P=10kN) was however, far below its critical value at tensile failure
  - a decrease in the radial concrete strain, ε_{yy}, of 114% at the top and an increase of 75% at the bottom
  - a decrease of 50% in concrete vertical strain at bottom
  - a decrease of 14% at the top and 33% at the bottom in the concrete tangential strain. This implies that by smaller diameter the splitting mode of failure tends to become unlikely
  - an increase of 26% at the top and a decrease of 13% at bottom in the interfacial shear stress

- The full depth crack inclined at 39° to vertical axis caused:
  - a great increase in resin strain with a maximum of 1220% at the start of the crack
  - an increase of 325% at a depth of 0.21, in the concrete radial strain at a section

extending 18 mm from axis

- a change of the sign of the vertical strain of concrete in the upper part of the above section whereas this strain remained unchanged at the bottom of this section
- an increase of 9% in the maximum value of the concrete tagential strain at a section 18 mm from anchor axis (and only 1 mm from the crack face), which makes splitting of concrete more likely
- an increase in the interfacial shear stress between 134% at the top and 7% at the bottom

- The partially developed (stabilized) crack starting at a point 0.2 l deep caused at a section extending 18 mm from anchor axis:
  - the tangential ε_{xx} values of concrete strain to decrease by 18% maximum, at the top
  - the concrete radial strain to increase by 30% at the top
  - the concrete vertical strain to increase by 77% in the upper part, in relation to those of the standard homogeneous model

The range of anchor displacements calculated in the different models analysed, is illustrated in Fig 6.3 and shows that:

- An increase in resin thickness from 2mm to 4mm results in a decrease of 10% in anchor displacement.
- A decrease in the anchor diameter from 12 mm to

8 mm leads to an increase of 30% in the steel displacement.

- The partially developed (stabilized) crack does not affect the steel displacement.
- The fully developed crack starting at a depth of 0.20l and inclined at 39° to the vertical axis causes an increase of 9% in anchor slip.

6.4. Concluding remarks

A finite element elastic analysis was carried out. It was based on the mechanical properties of the resin materials measured in the tests (Section 7.15). Linear elastic slip elements were used to model the slip across the steel-resin and resin-concrete interfaces. The stiffness of the slip elements was calculated on the basis of the relationship $\delta=\alpha\tau^m$, derived from tests, Section 7.14.2, Figures 7.147-7.149, with the assumption that m=1, and that for the tensile interface at the bottom $a_t=2a$.

The general effects of the parameters involved as indicated by the finite element analysis have been summarized in Section 6.3.

The results of finite element analysis can be used for the prediction of the anchor displacement and the failure mechanism provided that the system behaves linearly elastically, which is not far from reality, Fig.7.58-7.91. This is stated in Chapter 8, where a comparison is also made between these results and the corresponding values derived from theoretical analysis or obtained experimentally.

7. EXPERIMENTAL WORK

The aims of the experimental work were to examine:

- The modes of failure of the adhesive anchors.
- The mechanical behaviour in terms of load-slip relationship.
- The stress and strains of all the structural components of the system (steel anchor-resin-concrete).
- The effect of the different parameters.

The parameters affecting the behaviour of the anchors, Fig.7.1. are:

- The concrete strength.
- The embedment length of the anchor.
- The thickness of resin (i.e. the gap between hole and anchor).
- The diameter of the anchor.
- The type of the anchor surface (threaded-ribbed-plain bar).
- The type of resin.
- The method of drilling the hole (percussive-rotary-diamond drilling).
- The amount of reinforcement in concrete.
- The size of the specimen.
- The method of installing the resin (pouring-injecting-coating the anchor).

The structure of this Chapter is:

- Outline of experimental work (Section 7.1).

- Description of the five test series (Sections 7.2 -7.6).
- Test materials (Section 7.7).
- Test equipment (Section 7.8).
- Specimen preparation (Section 7.9).
- Results (Section 7.10).
- Discussion (Sections 7.11 - 7.15).
- Sequence of failure in the combined mode (Section 7.16).

In order to keep the text consistent with the above structure, in the early sections only those results and findings are reported which are necessary to proceed to next section.

7.1 Outline of experimental work

The data sought from the test work were:

- The load - displacement (slip) relationship for quasi static loading, i.e. the values of slip at any loading level.
- The strains in all components of the anchor system, i.e. in the surrounding concrete, the shell of resin and the steel anchor.
- The ultimate load of the system.

In order to obtain the above data a set up for test loading the anchor was designed and also the configuration for the necessary measuring and recording devices, Plates 1-5.

7.1.1 Scope

Five series of tests were conducted, Fig 1.3. Three of them comprised pull-out tests, the fourth involved the

direct shear tests and pull-out of partially bonded anchors and the fifth consisted of the resin tensile tests.

In the first (non-gauged) series only 2 tests were carried out. The purpose of these tests was to examine the initial choice of a 910X910X190mm concrete specimen and the initial idea of measuring the strains at predetermined places in concrete mass by using precast mortar cubes accurately preplaced in the formwork Fig.7.2. These cubes would carry the strain gauges, in the later test series. The conclusion of these tests, Section 7.2.3, was that the precast mortar cubes of 40 X 40 X 40mm suspended triaxially by nylon threads in the steel form are a proper means to install accurately the strain gauges in the concrete mass in respect to simplicity and reliability of this device. The preplaced mortar prisms resting at the bottom of the steel form, which were also tested, caused problems in positioning during casting and compaction the concrete, because they tended to overturn during the process. The results of these tests are discussed fully in Sections 7.2.2. and 7.2.3.

In the second test series, Table 7.1, the load applied and the displacement of the anchor were measured by means of a data acquisition and recording system which is described in Sections 7.3.c and 7.8.7..

The aim of this series of tests was to examine a smaller specimen of 600X600X200 mm, to identify the influence of the parameters listed below and to check the function of the data acquisition and recording system.

The parameters examined were:

a) the embedment length of concrete

b) the diameter of the anchor

c) the thickness of resin

d) the type of anchor surface

e) the type of resin

They were chosen because they were not found enough pieces of information on the way they affected the anchor behaviour.

Table 7.1. Test series No.2 - Partially gauged tests

Specimen	Enbedment Length [mm]	Type of anchor	Diamer of anchor d	Gap/Hole diameter	Epoxy resin	Method of insertion of resin	Concrete grade	Load and strain measurements
2.01	120	Thread.	12	2/16	C1380	Pour.	C25	L-D
2.02	60	Thread.	12	2/16	C1380	Pour.	C25	L-D
2.03	80	Thread.	16	3/22	C1380	Pour.	C25	L-D
2.04	improperly	mixed resin					C25	
2.05	120	Plain bar	12	2/16	C1380	Pour.	C25	L-D
2.06	120	Thread.	12	2/16	LV	Pour.	C25	L-D
2.07	100	Thread.	16	3/22	C1380	Pour.	C25	L-D

L: Load

D: Displacement

The influence of the parameters examined in this series is shown in Fig.7.3., and the results of this test series are discussed fully in Section 7.3.2.

The measuring devices and the data acquisition and recording system were found to be operating satisfactorily, therefore, no change was necessary.

The gauged test series No.3 consisted of 34 tests, Table 7.2. (The variable examined in each test are underlined).

Table 7.2: Test series No.3

Specimen	Embed. Length (mm)	Type of Anchor	Anch Dia (mm)	Cap/hole diam (mm)	Adhesive	Method of drill.	Method of ins. of resin	Concr. grade	Specim. dimens. (mm)	Group of anchors	Edge Effect	Str. meas.
3.01	100= 8.3d	Thr.	12	2/16	C1380	Perc.	Pour.	C25	600	-	-	L-D-S-C-R
3.02	84= 7d	Thr.	12	2/16	C1380	Perc.	Pour.	C25	600	-	-	L-D-S-C-R
3.03	60= 5d	Thr.	12	2/16	C1380	Perc.	Pour.	C25	600	-	-	L-D-S-C-R
3.04	100	Pln.	12	2/16	C1380	Perc.	Pour.	C25	600	-	-	L-D-S-C-R
3.05	100	Rib.	12	2/16	C1380	Perc.	Pour.	C25	600	-	-	L-D-S-R
3.06	83= 8.3d	Thr.	10	2/14	C1380	Perc.	Pour.	C25	600	-	-	L-D
3.07	66= 8.3d	Thr.	8	2/12	C1380	Perc.	Pour.	C25	600	-	-	L-D
3.08	100	Thr.	12	4/20	C1380	Perc.	Pour.	C25	600	-	-	L-D-R
3.09	100	Thr.	12	2/16	LV	Perc.	Pour.	C25	600	-	-	L-D-R
3.10	100	Thr.	12	2/16	GEL	Perc.	Coat.	C25	600	-	-	L-D-R
3.11	100	Thr.	12	4/20	C1380	Perc.	Pour+Ecc.	C25	600	-	-	L-D-R
3.12	95= 7.9d	Thr.	12	2/16	C1380	Perc.	Pour.	C25	600	-	-	L-D
3.13	90= 7.5d	Thr.	12	2/16	C1380	Perc.	Pour.	C30	600	-	-	L-D-C
3.14	100	Thr.	12	2/16	C1380	Perc.	Pour.	C50	600	-	-	L-D-C
3.15	100= 8.3	Thr.	12	2/16	C1380	Perc.	Inj.	C25	600	-	-	L-D-S-R
3.16	100	Thr.	12	4/20	Cem.gr	Perc.	Pour.	C25	600	-	-	L-D
3.17	100	Thr.	12	4/20	N.Shr.Gr.	Perc.	Pour.	C25	600	-	-	L-D-C
3.18	100	Thr.	12	4/20	Pol.Conc.	Perc.	Pour.	C25	600	-	-	L-D
3.19	100	Thr.	12	4/20	R.C.Gr	Perc.	Pour.	C25	600	-	-	L-D
3.20[1]	100	Thr.	12	2/16	C1380	Perc.	Pour.	C25	600	-	-	L-D
3.21[2]	100	Thr.	12	2/16	C1380	Perc.	Pour.	C25	600	-	-	L-D
3.22	90=11.2d	Thr.	8	2/12	C1380	Perc.	Pour.	C25	600	-	-	L-D
3.23	100	Thr.	12	2/16	LV	Perc.	Pour.	C25	600	-	-	L-D
3.24	100	Rib.	12	2/16	C1380	Perc.	Pour.	C25	600	-	-	L-D
3.25	100	Thr.	12	4/20	C1380	Diam.Dr.	Pour.	C25	600	-	-	L-D
3.26	100	Thr.	12	2/16	C1380	Perc.	Pour.	C25	300	-	-	L-D
3.27	100	Thr.	12	4/20	C1380	Perc.	Pour.	C25	300	-	-	L-D
3.28	100	Pln.	12	2/16	C1380	Perc.	Pour.	C25	600	-	-	L-D
3.29	100	Thr.	12	2/16	LV	Perc.	Pour.	C25	600	-	-	L-D
3.30	100	Thr.	12	2/16	C1380	Perc.	Pour.	C25	600	4Anch.	-	L-D
3.31	100	Thr.	12	2/16	C1380	Perc.	Pour.	C25	600	-	Y	L-D
3.32	100	Thr.	12	2/16	C1380	Perc.	Pour.	C60	-	-	-	L-D
3.33	100	Thr.	12	8/28	C1380	Perc.	Pour.	C25	600	-	-	L-D
3.34	100	Thr.	12	10/32	C1380	Perc.	Pour.	C25	600	-	-	L-D
3.35	Calibration of tension transfer system											

1= Reinf./ratio: $\mu x=\mu\psi=1\%, \mu z=0,7\%$

2= Reinf./ratio: $\mu x=\mu\psi=2\%, \mu z=1,4\%$

L= Measurement of Load - D= Measurement of slip - S= Measurement of steel strain

C= Measurement of concrete strain - R= Measurement of resin strain

Underlining: Variable examined in each test.

R.C.Gr:Reinforced cement grout

Thr. : Threaded

Pln. : Plain

Rib. : Ribbed

Ecc. : Eccentricity of the anchor in relation to the hole axis.

The anchor slip was measured in all the tests and in thirteen tests the strains of the structural components were measured as well. The experimental set up is shown in Fig.7.4. and Fig.7.5. The slip was measured continuously via a Linear Displacement Transducer, LDT, mounted at the top of the anchor, Fig.7.6. The anchor strains were measured by means of 3 special bolt strain gauges inserted in a 5mm hole drilled axially along the anchor. The resin strain gauges were initially glued together on a thin resin shell which was then glued by means of the same resin at the perimeter of the anchor accurately at its predetermined place, Fig 7.7. There were three rosette type strain gauges glued on the lateral surfaces of the precast mortar cubes which were suspended in the steel form of the concrete specimen by means of nylon threads in three dimensions Fig.7.8. The concrete specimens were fixed at the top of the steel frame of the loading machine, Fig 7.4, Fig 7.9. The pull-out load was applied to the anchor by means of a steel frame, Fig 7.10, which converted the upward movement of the piston to tension. Finally, the load was measured with the pressure transducer incorporated in the testing machine.

Among the thirty four tests, one test (Test No 3.30) was carried out on a group of four equal anchors symmetrically placed in the specimen, Fig 7.11. In another test (No 3.31) the edge effect was studied, Fig 7.12, in two tests (Nos 3.20 and 3.21) the effect of reinforcement of concrete and in two other tests (No 3.26, 3.27) the effect of reduced specimen size were examined. In all tests the same formwork, Fig 7.13, and the same method of fixing the precast mortar cubes carrying the concrete strain gauges, were used, Fig

7.8, Fig 7.13.

Apart from pull-out tests, two other series of tests were carried out. They were the direct shear (Fig.7.14, Fig.7.15), and the resin tensile (Fig.7.16, Fig.7.17) tests. Both series gave results for the identification and characterization of resins used in the pull-out tests. The direct double shear tests, in addition, provided very important data for the theoretical analysis, Section 5.2, on the local bond - local slip law. The same law was used as the basis for the calculation of the stiffness of the slip elements across the concrete-resin and resin-steel interfaces, Section 6.2.

7.1.2. Lay-out of measuring devices

The load - displacement relationship was obtained by monitoring continuously the load and slip values, the first directly from the loading machine and the second from an electronic measuring device, a linear displacement transducer (L.D.T). This was installed in order to monitor the movements of the free part of the anchor, Fig.7.6., and fixed as near as possible to the concrete surface in order to nullify the effect of possible non-verticality in the transfer of the pull-out load on the anchor, (since the eccentricity, e, of the LDT needle in combination with the anchor free length, l_a, and a possible under angle, φ, inclined pull-out load P could cause a fictitious reverse slip $\Delta\delta$, Fig.7.18).

For strain measurements in the surrounding concrete, after the experience of series No.1 and 2 it was decided to use 30X30X30mm cement mortar cubes preplaced in the concrete mass, with, as nearly as possible, the same mechanical

characteristics as the concrete. Strain gauges were glued accurately onto the surface of the mortar cubes in predetermined positions, so that the data obtained could be referred to definite points in the concrete mass and to definite directions, Fig.7.8. Evidence that the mortar blocks and interfaces remained intact during testing is shown in Plates 6 and 7.

Regarding the measurement of the resin (adhesive) strains three methods were examined. The first one was the accurate gluing of the resin strain gauges into a thin resin cylindrical shell cast from the same resin, which then would be positioned in the middle of the annular gap between the anchor and the hole before insertion of resin. This idea proved unrealistic since the total thickness (thin shell and strain gauges) could not be less than 1.5 mm, and the space left in most specimens for each of the inner and outer ring of resin was only 0.25mm. This gap, could not be filled without incorporating voids. The second method consisted of gluing the strain gauges together with their leads so that two semi cylindrical shells were formed which then would be placed in the annulus between anchor and hole where the fresh resin should already have been cast. This procedure however did not ensure the accurate placement of the films at the predermined position radially. The final method, Fig 7.7, was to glue all the strain gauges together so that a thin film of resin, was formed. This film carrying the strain gauges was then glued onto the lateral surface of the anchor before inserting it into the hole where the same adhesive had already been poured. Thus the problem of accurate positioning was solved.

The first idea for the steel strain measurement was to

cut the anchor along its axis and place the gauges into a groove on the one half. Then the two halves could be glued together with an adhesive. However practical and well known this technique is, it proved in Test series No.1 difficult and complicated especially in fixing the two halves with a uniform adhesive thickness so that deformity of the external surface was avoided. Instead, the use of special newly developed strain gauges for bolt strain measurement was much simpler and more accurate. The gauges were of Type BTM-6C and were placed into a hole of 5mm diameter drilled exactly on the anchor axis. They were glued in their final positions after having been put into place with leads attached, by injecting the appropriate adhesive, a low viscosity epoxy resin, from the bottom to the top of the hole by using a special needle, Fig.7.7.

The data acquisition and recording system, consisted of,

Fig 7.19:

- the strain gauges
- a linear displacement transducer
- the pressure transducer of the loading machine
- an amplifier receiving all the signals
- a portable IBM computer

7.2. Test series No.1 (Non gauged tests)

The main purpose of the test series No 1 was:

a) to examine the initial choice of 910X910X190 mm concrete specimen and the possibility of the reduction of the specimen dimensions,

b) to check the performance of the precast, preplaced mortar cubes as carriers of the concrete strain

gauges and the way they were temporarily fixed into the steel form. The mortar cubes were cast with a three dimensional wire cross at their center with loops at the edges protruding from the mortar surface, Fig.7.8. Onto these loops, nylon threads were tied which were anchored at their other end onto the steel form (into which the concrete was to cast), and onto a steel shape specially constructed for this purpose at the top of the steel form, Fig.7.13. In this way the positions of the cubes were stabilized and were not affected by the concrete casting and compaction.

c) to examine the possibility of using, as an alternative to (b), a preplaced mortar prism resting at the bottom of the steel form carrying the strain gauges and having a height equal to the specimen height (190mm), Fig.7.2. Although this was an alternative solution for the exact positioning of concrete strain gauges, it was thought that it might cause difficulties in casting the concrete in these areas.

d) To examine the possibility of using normal strain gauges fixed into an axial groove cut in one half of the anchor, the two halves subsequently being glued together.

7.2.1. Description of test series No.1

Two tests only were carried out in this series. The concrete specimen used was 910X910X190mm. Its dimensions were calculated in order to fulfil the requirements of BS

5080 / Part 1-1974 for anchor diameters up to 18 mm, Appendix B. The concrete mix was a typical C30 grade mix with plasticizer. Before casting the concrete a suspended cube and a prism resting at the bottom were fixed onto the steel form by means of nylon threads. The holes with a diameter of 14mm in the first test and 18mm in the second were drilled by a rotary percussive drilling machine. The anchors with a diameter of 10mm in the first test and 14mm in the second were threaded bars. They were cut in two halves, into which grooves were machined and two strain gauges for measurement of steel strain were glued. Then the two halves were glued together by an epoxy resin. The adhesive of the anchor (an epoxy resin of type C 1380) was poured into the gap between hole and anchor and left to set for 7 days.

The specimens were tested on the hydraulically driven TONI TECHNIK MODEL 1515 TONIPAKT 3000 Machine at a loading rate of 0.10 kN/s. The machine was a 600 kN compressive loading machine which had a four column loading frame. In order to be able to apply tensile loads the system was supplemented by an additional frame as is illustrated in Fig.7.4. The load was measured by the readings in the monitor of the testing machine.

7.2.2. Description of findings

The first specimen exhibited adhesive failure whereas the second showed concrete cone failure.

It was observed that no differential slip of cubes and prisms had taken place. In order to check this observation fully, the specimen with cubes was cut through by diamond sawing and the positioning of cubes found to be intact. The

concrete failure cone was remote from the specimen edges, at a distance of 250-350 mm in every direction.

7.2.3. Conclusions

From this test series it was concluded that:

a) The dimensions of the concrete specimen could be reduced in relation to the anchor diameter as prescribed by the specifications. Thus, the maximum steel bar diameter selected was 12 mm, which covers the types of anchors most broadly used in practice. The corresponding size of specimen was determined to be 600x600x200 mm, Appendix B.

b) The precast mortar cubes proved to be a suitable and simple means of placing accurately the concrete strain gauges, and they showed no sign of differential movement in relation to the surrounding concrete. This performance was emphasized also by the fact that the failure cone surface passed through the mortar cube without any change in the tangential plane or any disturbance of the failure surface at the edges of the cube, Plates 6 and 7. Conversely, the mortar prisms proved very difficult to handle and they had a tendency to overturn during casting and compacting the concrete. So, the preplaced prisms were abandoned and the mortar cubes adopted as the final solution.

c) It was very difficult to handle the anchor cut in two halves with the steel strain gauges glued into grooves. Thus, it was decided to use the special bolt strain gauges which would be inserted in a small diameter hole drilled axially along the anchor.

7.3. Test series No.2 (Partially gauged tests)

The aims of this series of tests were:

a) To confirm the suitability of the new smaller concrete specimen of 600x600x200 mm for anchor diameter up to 12 mm.

b) To identify the influence of the different parameters under consideration, i.e.:

b.1) The embedment length.

b.2) The anchor diameter.

b.3) The size of the gap between borehole and anchor.

b.4) The concrete strength.

b.5) The type of the anchor (threaded - ribbed - plain surface).

b.6) The type of the adhesive.

b.7) The method of installation of the adhesive (by pouring, injecting or coating in the case of gel).

b.8) The method of drilling the hole (percussive or diamond drilling).

The concrete strength, the method of installing the adhesive and the method of drilling the hole were not

investigated in test series No. 2, because their influence could be, at least quantitatively, forecast before the final tests.

c) To check the function of the data acquisition and recording system. This system is shown in Fig. 7.19 and consisted of:

- The strain gauges for concrete, resin and anchor strain measurements.
- A linear displacement transducer for measuring the slip of the anchor head.
- A pressure transducer incorporated into the loading machine.
- An amplifier collecting the signals from the strain gauges, the LDT and the machine, amplifying, converting and transferring them to a computer. The unit was designed to be capable of being programmed to collect the data within a predetermined time interval, to combine them with time indication, to label the data of the different sources, to show them in the monitor, to print and to send them to its own storage unit and to the computer.
- An IBM Portable Computer, with a 20 MB hard disc, which received the signals from the amplifier, stored them and processed according to a programme written for this purpose, so that the data could be presented in tables or graphs in terms of load, strains and stress.

During this test series, 7 tests were carried out.

7.3.1. Description of tests

This series consisted of 7 Tests shown in Table 7.1. The concrete mix was a typical C25 concrete mix consisting ofthe following quantities per cubic metre:

Cement II/35	: 350 kg
Coarse gravel	: 580 kg
Fine gravel	: 310 kg
Sand	: 965 kg
Water	: 210 kg

with a slump of 160mm.

In one of the tests, namely Test No 2.04, the two components of resin were improperly mixed and this led to a highly plastic behaviour of the system as can be seen in Fig.7.3. The test was repeated as Test 2.06.

In test 2.01 the embedment length was set at l=10d. In test 2.02 it was l=5d. In test 2.03 the influence of the anchor diameter was examined by embedment length l=5d. In test 2.05 the anchor used was a plain bar. In test 2.06 a type of resin with slightly higher modulus of elasticity and the same surface energy and contact angle to concrete as that in the other tests in this series, was used. In 2.07 the embedment length was changed to l= 6.25d.

The same loading machine was used to load the specimens at a rate of 0.20kN/s.

For the measurement of the slip of the anchor the lay-out described in Section 7.1.2. was used. Strains in the concrete, resin and steel were not measured. Nevertheless, the function of measuring system was checked with only two channels used (one each for the machine pressure transducer and the L.D.T.).

In all the tests the mechanical behaviour of precast

mortar cubes was controlled visually, in order to pinpoint possible differential slip of the cube in relation to the surrounding concrete. In one test (specimen 2.01) the mortar cube was coated with an epoxy bonding agent applied before casting the concrete. The positioning of all the cubes was found to be intact after failure, Plates 6,7.

7.3.2. Results of the test series No.2

The results obtained are illustrated in Table 7.3. for each test and also in Fig.7.3. where the curves of P-δ relationship are drawn.

Table 7.3. Test series No.2 - Summary of pull-out data

SPEC.	f_{cc} [MPa]	Pult [KN]	Mode of failure	δ5 [μm]	δ10 [μm]	δ20 [μm]	δ30 [μm]	δ40 [μm]	δy [μm]
2.01	28.0	39.0	I+C+R	180	330	540	880	-	1089
2.02	30.2	30.0	I+C+R	-	-	-	-	-	-
2.03	27.5	47.6	Split	-	51	100	190	320	880
2.04	28.5	improperly mixed resin							
2.05	28.5	34.4	I+R	50	99	157	637	-	1957
2.06	26.0	41.3	C+R+I	-	100	390	1040		
2.07	31.0	53.0	Split	-	80	240	490	760	

δ5, 10, 20, 30, 40: displacements at load levels of 5, 10, 20, 30, 40 kN respectively.
δy: displacement at failure load.

The modes of failure of each specimen are shown in Fig.7.20. and 7.21.

The specimens in which concrete failure was exhibited showed a combined mode involving the concrete cone failure, concrete-resin interface failure below the concrete cone and resin failure at the lowest part of the anchor, Plates 8 and 9.

The splitting mode of failure consisted of a multicrack network on meridian sections of the specimen, Fig 7.20, 7.21.

The combined mode of failure was exhibited by specimens 2.01 (standard test of the series), 2.02 (with the shorter embedment length), partially by 2.05 (plain bar) and 2.06 (with a type of resin of higher elastic modulus). The splitting failure mode was exhibited by specimens 2.03 (anchor d=16, l=5d) and 2.07 (anchor d=16, l=6.25d). The related values of C/l (concrete cone height to embedment length) varied between 0.29 for specimen 2.06 to 0.66 for specimen 2.01. The ultimate pull-out loads varied for the combined mode specimens between 30.00 kN (specimen 2.02) to 41.3 kN (specimen 2.06). The respective ultimate loads for the splitting mode were rather higher: 47.6 kN for specimen 2.03-53.0 kN for specimen 2.07. It must be pointed out here that the concrete strength of the different specimens was slightly different (26.0-31.0 MPa).

7.3.3. Conclusions

The conclusions from this series were:

a) That the new smaller specimen, which of course was much more easier to handle, did not influence the failure mechanism, as the concrete failure cone was still far from reaching the supports for anchor diameters not more than 12mm.

b) Taking into consideration the influence of the different variables shown in Fig.7.3 in terms of the pull-out load and slip relationship, it is clear that, as expected:

- Shorter embedment length caused lower ultimate pull-out load and greater displacements.
- plain bars undergo the same effect, above a

certain load level

- an increase in anchor diameter causes an increase in ultimate pull-out load and a decrease in displacement
- the type of resin influences the overall mechanical behaviour of the anchor, by changing the stiffness of the anchor at the different loading levels as can be seen from the comparison of curves 2.01 and 2.06, Fig 7.3.

c) That the measuring system was functioning perfectly and handling the rather large number of data. (Under a loading rate of 0.20kN/s, and for scanning intervals of 1.0s, approximately 200-250 data per parameter per test were stored and handled. In the test series 3, for three strain gauges for concrete (rosettes consisting of 3 strain gauges each), three strain gauges for the resin, three strain gauges for the anchor, one LDT and the pressure transducer of the machine, there were seventeen sources for collection of data, with approximately 250 data per source which leads to handling approximately 4,250 items of data per test).

Thus, the initial variables were retained in the final test series, the concrete specimen dimensions confirmed and the measuring and recording system accepted without change.

7.4. Test series No.3

The test series No.3 (gauged test series) consisted of the tests shown in Table 7.2.

The diameter of the anchor, which affects the size of the specimen, Appendix B, was chosen to be not more than 12mm, which was set as the standard value of anchor diameter. In some tests this was varied to 8mm (specimens 3.07-3.22) and 10mm (specimen 3.06).

The embedment length varied between 5.d (Specimen 3.03) to (11.25)d (Specimen 3.22). Three tests were carried out with l=(7.0-7.9)d in order to examine the influence of l in this range. For practical purposes the standard value of the embedment length was chosen as 100mm which is equal to (8.3)d for a diameter of 12mm.

Apart from threaded bolts, ribbed and plain reinforcing bars were used as anchors. The ribbed bar was a normal cold worked grade 460 steel bar in accordance to BS 4449. The thickness of the resin layer surrounding the bar was chosen as 2mm for the major part of the test series and changed to 4mm (tests 3.08, 3.11, 3.25, 3.27), 8mm (Test 3.33) and 10 mm (Test 3.34).

The concrete compressive strength was designed to have a standard value around 25 MPa, which resulted in values between 19.56 MPa (specimen 3.01) to 31.67 MPa (specimen 3.09). As variations, the values of 30, 50 and 60 MPa were designed which resulted in 37.90 MPa (specimen 3.13), 51.78 MPa (specimen 3.14) and 62.45 MPa (specimen 3.32).

Apart from specimen 3.25, which was drilled using a rotary diamond drilling machine with water as the cooling medium at the drilling bit, all the specimens were drilled with an electrically driven percussive hand-held drilling

machine.

The standard method of inserting the resin was by pouring into the gap between the pre-placed and centered anchor and the hole. However, in specimen 3.15 the resin was injected into the gap, after sealing its external surface, by means of an automatic injection machine and forced into penetrating the hole surface for 1 minute at a pressure of 3 bars. In specimen 3.10, the resin, which was a gel type resin, was inserted by means of a simple handgun after the bolt had been placed in position.

Two tests were carried out on normally (1%) and heavily (2%) reinforced specimens (Tests 3.20-3.21) and two other tests on unreinforced concrete specimens 300X300X200mm (Tests 3.26-3.27) in order to examine the effect of the amount of reinforcement and smaller size of specimens.

In one test (3.30) the mechanical behaviour of a group of four anchors spaced relatively close to each other (at a distance of 150mm (12.5d)) was examined.

Finally, the edge effect was studied in test 3.31, in which two anchors (in order to keep the symmetry of the set up about x axis, Fig 7.12, and avoid rotation of the loading frame) were placed near to the edge of concrete specimen at a distance of 75mm (6.25d) from it.

The tests were carried out under monotonically incremental quasi static loading. The rate of loading was 0.20 kN/s. From every concrete batch, samples were taken and compressive and tensile splitting tests carried out the same day as the concrete specimen was pulled out, so that every test could be related to the actual concrete compressive and tensile strength.

The anchor steel was grade 8.8. for bolts and 5.8 for

plain bars.

High yield cold worked grade 460 steel according to BS 4449 was used for ribbed bars.

The different types of resin were tested in direct shear to determine their adhesion properties to the concrete of the specimens (Test series No.4). The tensile properties of two types of low viscosity resin used as adhesive were tested in accordance with ASTM D638 M-876 (test series No.5). The properties of the rest of materials when needed were taken as given by the manufacturers.

7.4.1. The experimental set up

The experimental set up for the pull-out tests, is illustrated generally and in details in Figs 7.4., 7.5., 7.6., 7.9., 7.10., 7.11., 7.12. and discussed in sections 7.7.(materials),7.8.(equipment), 7.9.(specimen preparation).

The set up for the direct shear tests is shown in Fig.7.14., 7.15. and the set up for resin tensile tests is illustrated in Fig.7.16., 7.17. A detailed description of the experimental set up follows.

7.4.2. Materials used, testing and measuring equipment

The grade of concrete varied between C25 and C60 in the third test series. As adhesives, two different types of low viscosity epoxy resin, a gel type epoxy resin, a PMMA polymer grout and four different types of Portland cement grouts were used. Threaded bolts, high yield reinforcing bars and plain bars were used as anchors. An analytical presentation of all the materials used is given in section 7.7.

7.5. Test series No.4 - Direct shear tests

The tests were carried out in order to study the mechanical behaviour of the different resins used in terms of local bond - local slip relationship.

The direct shear tests divided into:

- Direct double shear tests carried out on 40mm concrete cubes, Fig.7.15.
- Direct double shear tests of the concrete-resin-steel interface on appropriate specimens, Fig.7.15.
- Local bond - local slip tests, carried out on anchors partially bonded in the hole. The length of adherence along the anchor axis, was 10mm only, Fig.7.4. - Detail A.

The local bond - local slip relationship was a necessary feedback for the theoretical analysis and for the calculation of data of slip elements in finite element analysis, Chapter 6.

7.5.1. Scope

The first aim was to determine the mathematical function $\tau=\tau(\delta)$, where τ is the local shear stress at the interface and δ is the slip of the steel in relation to concrete. In order to define this law it was necessary to work with a specimen with a limited adhesive length so that the interface could be regarded as infinitesimal and therefore the slip measured as local and not as total slip from the one to the other end of the interface. Set ups for tests of this kind have been used in order to determine the related $\tau= \tau(\delta)$ relationship for reinforcing bars embedded in concrete, Rehm /60/.

The second aim was to determine the local bond-local slip relationships of the concrete-resin, and resin-steel interfaces.

7.5.2. The experimental set up

The initially designed test, which was based on the RILEM Draft Recommendation 52-RAC-24, Fiebrig /49/, is shown in Fig.7.23.a. In accordance with this, cores with a diameter of 80mm were taken from each concrete specimen. The cores were cut into two halves which were then bonded together by the resin along the core axis over a length of 10mm.

The problem which arose by testing these specimens was that it was very difficult to achieve a coincidence of the two opposite loads at the top and the bottom in the same vertical plane. As a result, the two halves of the specimen tended to rotate under loading resulting, first, in a stress distribution in the adhesive joint involving normal stresses in addition to shear stresses and secondly, in test termination by failure of the highly compressed edges of the specimens.

After this experience another specimen was designed, Fig.7.23.b, which could also be used to determine the $\tau=\tau(\delta)$ law. But the rotation of the specimen, although reduced in relation to the previous specimens, still affected the stress situation of the interface, where normal stresses were also caused by rotation of the two halves. It also caused premature failure of the specimen at the compressed edges.

As a result it was decided to abandon the single shear stress set up and to design a direct double shear stress

adhesive joint, which is shown in Fig.7.14.

The possible eccentricity of applied load did not affect the stress situation of the adhesive joint because the gaps between the concrete cubes were filled up by teflon pieces, Fig 7.15, which prevented the differential rotation of the cubes without transferring any shear, as the coefficient of friction at the interface teflon-concrete is nearly zero.

In order to obtain the $\tau=\tau(\delta)$ function for both the concrete to concrete and steel to concrete joints, three different specimens were designed, Fig.7.15. In the concrete to concrete specimens, cubes cut from cores taken from the pull-out specimens were glued together with the resins used in test series No.3.

In the steel to concrete specimens purposely grooved steel plates were used. They were plane plates with horizontal grooves matching the thread of the bolts. Finally, a series of direct shear tests was carried out to study the steel to steel behaviour, Fig.7.15.

The overall series of tests is shown in Tables 7.4., 7.5., 7.6. Variables were the resin thickness, the resin type and the concrete strength.

Table 7.4. Test series No.4. Direct double shear tests. Concrete-Resin-Concrete.

Test	Concrete grade	Concr. spec.	Resin	t [mm]
4.09	C.25	3.12	C.1380	2
4.10	C.25	3.12	C.1380	8
4.11	C.30	3.09	C.1380	2
4.12	C.25	3.12	LV	2
4.13	C.25	3.12	GEL	2

Table 7.5. Test series No.4. Direct double shear tests. Concrete - Resin - Steel.

Test	Concrete grade	Concrete specimen	Resin	Anchor	t [mm]
4.14	C.25	3.12	C.1380	Grooved pl.	2
4.15	C.25	3.12	C.1380	"	3.5
4.19	C.25	3.12	GEL	"	2

Table 7.6. Test series No.4. Direct double shear tests. Steel-Resin-Steel.

Test	Steel Plate A	Steel Plate B	Resin	t [mm]
4.20	Grooved	Grooved	C.1380	2

7.5.3. The tests of partially bonded anchors

In order to cross-check the results of the direct shear tests, a series of tests involving partially bonded anchors was carried out. In these tests the same specimens as in test series No.3 were used. After the pull-out of series No.3, they were drilled at the bottom side and then anchors were bonded onto a length of only 10mm on the whole. The gap underneath the bonding length was filled with plasticine before insertion of the resin, Fig.7.4 detail A. Intact (non-cracked) concrete specimens were used only. The variables of this test series were the concrete strength, the type of the anchor, the type of the resin and its thickness. These are shown in Table 7.7. underlined.

Table 7.7. Test series No.4. Partially bonded anchors

Test	Bonding length [mm]	Type of anchor	Anchor diam.	Gap diam. of hole	Adhesive	Method of drilling	Method of insert of resin	compressiv str.(MPa)	tensile str.(MPa)	Concrete Specimen
4.01	10	Threaded	12	2/16	C.1380	Perc.Dr.	Pour	19.56	2.63	3.01
4.02	10	Threaded	12	2/16	C.1380	Perc.Dr.	Pour	51.78	3.69	3.14
4.03	10	Threaded	12	2/16	LV	Perc.Dr.	Pour	21.29	2.64	3.03
4.04	10	Plain	12	2/16	C.1380	Perc.Dr.	Pour	20.66	2.25	3.22
4.05	10	Threaded	12	2/16	GEL	Perc.Dr.	Pour	22.25	2.25	3.25
4.07	10	Threaded	12	8/28	C.1380	Perc.Dr.	Pour	23.11	2.71	3.06

7.5.4. The results of direct shear tests

The results obtained from this series of tests are illustrated in Fig.7.92, 7.93, 7.94, 7.147, 7.148, 7.149 and in Table 7.19. as $P=P(\delta)$ and $\tau=\tau(\delta)$ relationship. They are discussed in detail in section 7.14.

7.6. Test series No.5 (Resin tensile tests)

From test series No.2 it was already proven that the type of resin affects the overall behaviour of the system. In order to check the data given by the formulators for the resins and grouts used, a test series involving tensile stress and strain measurement was carried out as shown in Table 7.8.

Table 7.8. Test series No.5. Resin tensile tests.

Test	Resin
5.01	C.1380
5.02	LV

7.6.1. The test set up

The tests were designed to comply with ASTM D638M-876, and the set up is illustrated in Fig 7.16, 7.17. The specimens were tested at 7 days. They were tested in a electrically driven tensile loading machine of type SOILTEST - 20 kN with a rate of straining of 15 με/s. They carried two strain gauges of type TML PL-60. The load measurements were taken via a load cell properly calibrated. The same data acquisition and recording system as in test series No.3 was used.

7.6.2. Results

The results in the form of P=P(ε) relationship are shown in Figures 7.150 and 7.151. From these curves the tensile modulus of elasticity can be obtained for each type of resin used.

7.7. Materials used in test series No.3

The concrete mix was designed to match that of common structures in which anchors are usually installed. The steel, resins and grouts were of the type of materials broadly used in practical applications of adhesive anchors.

7.7.1. Concrete

For most of the tests concrete C25 was used. In order to investigate the influence of the concrete strength, concrete C30, C50 and C60 was used for some specimens. The respective mixes are shown in Table 7.9.

Table 7.9.: Mixes for the concrete used

Materials in kg	C 25	C 30	C50	C60
Cement II/35	310	385	500	-
Cement I/45	-	-	-	500
Course gravel	676	570	658	658
Fine gravel	256	305	345	345
Sand	895	935	735	735
Water	207	185	170	170
Plasticizer CONPLAST 211	1.10	-	-	-
Superplastizer CONPLAST 430	-	3.50	10	10

The aggregates were crushed limestone aggregates from Athens with the grading shown in Fig. 7.22.

The cement was Portland Cement of strength class 35 (P.F.A. or other pozzolanic admixtures up to 20%) or ordinary Portland Cement of strength class 45.

The characteristics of plasticizer Conplast 211 and superplasticizer Conplast 430 manufactured by FOSROC Ltd are shown in Appendix D. The mortar for the preplaced cubes was made of the following mix: Fine sand 7.0 kg - Cement 10 kg - water 3.8 kg - superplacicizer CONPLAST 430 0.16 kg, resulting in 28 days compressive strength of mortar at about 35 MPa.

7.7.2 Steel of the anchor

The steel of the bolts was high yield steel grade 8.8 with yield strength 640 N/mm² and failure strength 800 N/mm² according to DIN 267, zinc electro-plated.

The ribbed bars were cold worked high yield steel 460 bars according to BS 4449. The bars were threaded at their free end in order to enable them to be fixed in the loading bridge.

The plain bars were high yield steel grade 5.8 bars.

7.7.3 Resins

The following adhesives were used:

7.7.3.1. An epoxy resin of DGEBA type of very low viscosity, under the commercial name CONCRESSIVE 1380, with surface tension of 45 mN/m² and physical and mechanical properties as shown in Appendix D, manufactured by ADHESIVE ENGINEERING Co, was used as the standard adhesive in most tests.

7.7.3.2 As a variation, a low viscosity epoxy resin was also used with the same value of surface energy and contact angle on concrete, but with mechanical strength lower and modulus of elasticity slightly higher than those of CONCRESSIVE 1380, manufactured by DURAL INC under the commercial name DURAL LV. Its properties are shown in Appendix D.

7.7.3.3 As thixotropic adhesive, an epoxy resin with gel consistency under the commercial name DURAL GEL manufactured by DURAL INC. with the properties shown in Appendix D was used in order to investigate the consequences of incomplete wetting.

7.7.3.4 Polymer mortar

A polymer mortar (which is also referred to as polymer concrete) was used also in one test. It concerns a PMMA mortar containing inorganic fine filler with the properties shown in Appendix D.

7.7.4. Grouts

7.7.4.1. Non shrink grout.

As cementitious based adhesive a nonshrink grout with the properties shown in Appendix D, (tradename CONBEXTRA HF manufactured by FOSROC Ltd.) mixed with water according to the instruction of the manufacturer was used.

Its average 28 day strength was 66.00 N/mm² measured on 50 mm cubes.

7.7.4.2. Cement grout

Finally, a mix commonly used for cement grouting was used. The mix consisted of:

- Cement 10.0 kg
- Fine sand (Zone 4) 10.0 kg
- Water 4.4 kg
- Microsilica 1.8 kg
- Superplasticizer 2% x Cement

Its average 28 day strength was about 25 N/mm² measured on 50 mm cubes.

The main properties of the material used are summarized in the Table 7.10 below.

TABLE 7.10. Properties of resins and polymer grouts used

	C 1380	DURALLV	DURAL GEL	DURALCRYL
Surface energy (γ_A)	45 mN/m²	38mN/m²	(GEL)	(mortar)
Contact angle(θ_A)	40° "	11°	>90°	(mortar)
Compressive str.	115.6 MPa	56.0 MPa	56.0 MPa	87.5 MPa
Tensile str.	63.6 MPa	28.0 MPa	28.0 MPa	13.0 MPa
Emodul/tensile	2157 MPa	2340 MPa	1750 MPa	7000 MPa
Bond str. to concrete (slant shear test)	34.5 MPa	10.5 MPa	10.5 MPa	-
Viscosity (cps) at 25 C	352	150 - 250	Gel	Grout

7.8 Testing equipment

The whole series of tests comprised

- Pull-out tests
- Direct shear tests
- Resin tensile tests
- Common compressive and splitting tests, which were conducted in an independent laboratory.

The testing equipment used consisted of:

- Two loading machines, one hydraulically and the other electrically driven.
- Strain gauges.
- Two different types of linear displacement transducers.
- The data acquisition and recording system.

7.8.1 Pull-out tests

For the preliminary and the final series of pull-out tests, an automatic loading machine was used. The machine was TONI TECHNIK MODEL 1515 TONIPACT 3000, Plate 4, with loading capability up to 600kN and loading rates from 0.01 kN/s to 10.00 kN/s. The machine was hydraulically driven and offered the option of two modes of setting the load limit, either to increase the load until failure, which was used in these tests, or to a certain preset limit. The load level was continuously indicated digitally. Simultaneously the pressure transducer incorporated in the machine was connected to the digital converter, thus giving continuous information which was processed by the data acquisition and recording system.

A steel frame was designed to convert the upward movement of the piston to tension (pull-out load) of the anchor (Fig.7.4, 7.5, 7.10, Plates 1, 2, 4).

7.8.2 Direct shear tests

For the direct shear tests the same machine was used, without the steel frame. Fig.7.14.

7.8.3. Resin tensile tests

For the resin tensile tests an electrically driven machine of type SOILTEST 20 kN was used. The rate of straining was 15 με/s. In order to have continuous indication of the loading level an external load cell was used, which was connected to the recording and processing unit.

7.8.4 Compressive and splitting tests of concrete

These tests were carried out in an independent, registered laboratory and for each group of tests a certificate was issued.

7.8.5. Slip measurements

A displacement transducer TML CDP-25 was mounted at the top of the bolt using a steel angle fixed at the top of one of the machine columns, completely independent of the specimen, to allow measurement of the slip of the anchor, Fig.7.6.

For the measurement of slip in the direct shear test a displacement transducer of type TM-8FLP10A was used, mounted in the machine frame.

7.8.6. Strain measurement

The strains in the concrete, resin and bolt had to be measured.

For the bolt axial strain a special strain gauge BTM-6C, of 1 mm width and 6 mm length was used, placed in an axially drilled hole of 5 mm diameter. The gauge was glued using a low viscosity epoxy adhesive injected in the hole by a special needle Fig.7.7.

For the adhesive strain measurement, the strain gauges

of type PL 5-11 were glued together at their correct positions by the same resin with their leads already attached, so that a thin film of resin was formed. Then this film was glued onto the lateral surface of the anchor by using the same resin, Fig.7.7. Finally, the anchor with the glued film was inserted into the hole into which the resin had already been poured. In this way accurate positioning of the resin strain gauges was ensured.

Strain gauge rosettes of type TML-PR-20-11 were glued accurately at the corners of the lateral surface of the precast cement mortar cubes described in sections 7.1.1., 7.2.3, Fig. 7.8).

7.8.7. The data acquisition and recording system.

The system consisted of:

- The different strain gauges placed in the anchor, the resin and concrete.
- The linear displacement transducer.
- The pressure transducer of the testing machine.
- The analogue to digital converter.
- The amplifier.
- An IBM computer.

This was described in Section 7.3.c. It was operating in accordance with two programmes written for this purpose. The first handled the collection of data at predetermined time intervals, the labelling of them, their display on the monitor and their acquisition by printing or storing in the computer. The second handled their interpretation to physical quantities (loads, strains, displacements) according to the calibration of testing equipment and recorded them in the form of tables or graphs.

7.8.8. Calibration of testing and measuring components.

The whole configuration comprising the load cell of the machine, each component of the measuring system and the analogue to digital converter was calibrated. This calibration was carried out twice at the beginning and repeated throughout the course of experimental work, as described in Appendix E.

7.8.8.1. The calibration of tension transfer system

The tension transfer system, i.e. the system which transferred the loading of the machine to the anchor had also to be calibrated. The system involved the loading bridge A at the top of the loading frame B and its bearings C, (Figures 7.10, 7.24), the coupling devices D at the end links of the chain, and the chain itself (Fig 7.24). The set-up designed for the calibration comprised all these components and a concrete specimen 600X600X200mm similar to the specimens used in the test series No.3. The specimen was drilled through at its axis and an M26 bolt was fixed at the bottom side by means of a washer 8mm thick (Fig 7.24).

The settlement, Δ, of the system due to compression of the bearings and the seating of the links of the chain is shown in Fig.7.24. The elastic deformation of the bolt for tensile load of 10 kN was calculated at 0.0197mm and omitted as negligible. The deformation of the concrete slab fixed at its corners and loaded with a concentrated load of 10.0 kN at its centre was calculated and found to be 0.003mm (Appendix F) and therefore omitted in the calculations.

7.9. Manufacture of test specimens

7.9.1. Processing of materials and procedures

The concrete was mixed in a vertical axis concrete mixer, compacted by means of a rod and left to cure indoors with a polyethylene sheet over the top of the specimen. The indoor temperature was approximately 25 to 27 °C.

The required quantities of the two components of the resin were measured separately and mixed thoroughly according to the instructions of the manufacturers. The low viscosity resin was poured in the hole and then the bolt was inserted and accurately positioned by means of small steel wedges mounted at the top, which were removed when the resin became very viscous. The adhesive with gel consistency was inserted into the hole by means of a handgun and then the bolt placed into its position in the same way. Since by this procedure the filling of the gap by resin was not ensured, this method of inserting the gel type resin was rather a kind of internal coating than a type of injection. So, it is referred to as "coating" in the text following.

The mortar cubes were cast in steel moulds, left to cure for 7 days and then the strain gauge rosettes were accurately glued at the corners by means of an epoxy adhesive which was nonsensitive to the damp interface.

The cubes were placed in position by means of thin nylon thread tensioned against the walls of steel formwork and a bridge at the top of the formwork, Fig. 7.8, 7.13.

When the concrete was 21 days old the concrete specimen was drilled by percussive or diamond drilling equipment respectively, the resin inserted and the bolt installed. The resin was left to cure for 7 days.

Before placing the bolt in position the thin shell of

resin containing the PL type strain gauges was placed using the same resin on the lateral threaded surface of the bolt, Section 7.1.2.

7.9.2. Details of specimens

7.9.2.1. Pull-out specimens

According to BS 5080, Part 1-1974, the minimum dimensions for the single specimen are based on the characteristic dimension A of the anchor, which is the maximum of the hole diameter or 1/4 of the embedment length. So, for the extreme case of this experimental work:

$$A = \max[\ d=12\ mm,\ 1/4x100=25\ mm\ ] = 25\ mm$$

Then the dimensions of the specimen should be such that the minimum depth below the hole is 4A=100mm, and there shall be a minimum of 12A=12x25=300mm between the centre of the anchor and a free edge. So, the dimensions of the specimen were determined to be 600x600x200mm.

The holes for fixing the specimen onto the machine were formed by placing four plastic tubes with 30mm diameter at the corners.

7.9.2.2. Direct shear specimens

In the final series of direct shear tests the following different specimens were used each for the respective test sub-series.

- Partially bonded anchors, Fig.7.4. - Detail A.
- Double direct shear specimens for concrete to concrete bonding behaviour, Fig.7.14, 7.15.
- Double direct shear specimens for steel to concrete bonding behaviour, Fig.7.15.
- Double direct shear specimens for steel bonding

behaviour, Fig 7.15.

As specimens for the partially bonded anchors, the uncracked, intact specimens of test series No.3 were used. They were drilled at the bottom size (in relation to the series No.3 tests) in the same way. The anchors were coated with a bond breaking material (plasticine) at their lower part. Then the resin was inserted in the inverted specimen so that a bonding length of 10mm only was achieved, in order to fulfil the requirements of limited bonding length required to obtain local bond - local slip values.

The 40mm concrete cubes for the concrete - to concrete tests were cut from cores taken from the pull-out specimens using diamond cutting equipment. For the application of resin and its curing and the loading procedure as well the provisions of RILEM TC-52 RAC Draft recommendations were followed.

For the concrete to steel tests, steel plates purposely grooved to match the threading of the bolts as described in section 7.5.2 were bonded to concrete cubes cut from the pull-out concrete specimens as described above. The steel grade was C60.

For the steel to steel tests, the aformentioned grooved steel plates were bonded together by means of the resin used in test series No.3.

In all the tests the bonding length was limited to 10mm. The resin was poured into the gap at the interface with the specimen lying horizontally. The gap was sealed at the top and bottom by means of a bond breaking temporary sealing material. The rest of the joint was filled with teflon sheet which prevented differential rotation of the adjacent pieces of specimens by means of compression without any

friction.

7.9.2.3. Concrete tensile splitting tests

These tests were carried out according to BS 1881:Part 117:1983, on 150/300 cylinders.

7.9.2.4. Resin tensile specimens

These were cast and loaded according to ASTM D638M-876 and are illustrated in Fig.7.17.

7.10 Interpretation of the results

The most important parameter of the mechanical behaviour of the anchor from the point of view of designing such systems is the load-slip relationship. So, the results of all tests, including the non-gauged ones, were presented in this way.

A computer programme was designed to collect the data from the analogue to digital converter, to process them according to calibration carried out beforehand and to plot the results in P-δ or P-ε curves for the structural components of the anchor (steel-resin-concrete). The programme for processing and plotting was based on a commercially available spread sheet programme.

7.10.1 General remarks

In almost all graphs of P=P(δ) the region 0 - 8.0 KN was an area where the curves exhibit an inflexion point. A careful investigation of the problem has shown that it is caused by the following:

Firstly, there was a compression of the bearings of

the loading bridge on the steel frame (Fig. 7.10)) which took place at the level between 2.5 to 10.0 kN.

Secondly, there was a possible settlement due to the varying relative position of each link of the loading chain before they attained their final position, i.e. initial seating of the chain. Both caused the anchor to retract accordingly. In order to take this effect into account the calibration of the tension transfer system was conducted (section 7.8.8.1) and the relevant data were taken as input in the data processing system.

Apart from these two factors there was a different calibration factor for the loading levels up to 7.20 kN, Table E.1 Appendix E, deviating from the typical calibration factor for the test of load cell by almost 3% up to 3.20 kN and approximately 1.5% up to 7.20 kN.

7.10.2 Repeatability of the tests

The purpose of the tests was to examine the influence of the main parameters (see introduction of Section 7) on the mechanical behaviour of the anchors (i.e. on the mode of failure, the load-slip and load-strain relationship).

It was intended that only one specimen under a certain combination of the parameters to be investigated should be tested, in order to keep the number of tests at a realistic level.

This fact was always borne in mind during the whole range of tests and necessitated the repetition of some tests, in those cases in which there was any suspicion about the deviation from the standard conditions. The testing also of all the materials involved which could have a possible influence on the mechanical behaviour of the

anchor was a necessity for verification of this behaviour. In addition, for each of the critical parameters more than one test was conducted with corresponding values of the parameters.

Thus, as can be seen in Table 7.2, for the embedment length of the anchor five tests, with values ranging from 5d to 11.25d, were carried out in order first to identify its influence on the final behaviour and secondly to be able to identify any suspect results. In this way test 3.22 was carried out to cover the uncertainty about the embedment length of the anchor in test 3.07. This anchor exhibited a relatively high slip and it was thought that the reason was the small embedment length. Test 3.22 was designed and conducted in order to cross-check the results of test 3.07. There were also three tests with concrete strength above the level of 30 MPa whereas the concrete strength was designed to be close to 25 MPa for the rest of tests. In six tests the gap between the hole and the anchor was greater than 2mm, which was the standard dimension for this series of tests. In three tests the anchor diameter was varied. The shape of the anchor varied from the threaded anchor which was the standard type in four tests, and the type of adhesive in eight tests. Only one test was conducted with a method of insertion of the low viscosity resin other than pouring and also only one test with a method of drilling other than percussive drilling of the hole. The effect of the reinforcement, with varying ratio of reinforcement was tested on two specimens and the group and edge affects on one specimen each. Finally, the effect of the size of the specimen was examined in two tests on one of which the influence of a greater gap was also tested. In

some cases additional tests were decided upon as a result of an unexpected event. More precisely:

- Because of a relatively high slip of anchor d=8mm (Test 3.07) Test 3.22 was also conducted for confirmation [but see below *]
- Because of the initially stiff behaviour of the anchor with resin of type LV (Test 3.09), another test (3.23) was carried out to check it. But in the latter, the mode of failure changed to the splitting mode which is generally associated with greater displacements, Section 7.11. So, another test (3.29) was carried out which confirmed the original result.
- The influence of the larger gap in the P=P(δ) relationship of specimen 3.08 caused the conducting of tests 3.33 and 3.34, each with different a dimension of the gap.
- The unexpectedly stiff behaviour of the anchors fixed in relatively high strength concrete (tests 3.13,3.14) was the background to the decision to run also test 3.32, where a very high concrete strength was used.
- * Due to a mistake in the preparatory work the anchor of test 3.22 initially designed to be 66mm (8.3d) long was fixed with a length 90 mm (11.25d) as measured after pull-out. Thus, the effect of the ratio of embedment length of anchor to diameter with so high a value was examined, although not originally planned.
- Because of a mistake in boring, the hole of

specimen 3.12 was found to have a an enlarged diameter of 20mm at the bottom. The hole diameter was reduced towards the free surface of the specimen where it was 16 mm. This fact, which contributed to stronger wedging action during pull-out was borne in mind in discussing the splitting mode, Section 7.11.2.10.

- Finally, due to eccentric placement of the loading frame, the measurements of the anchor displacements in tests 3.24 and 3.28 were regarded as unreliable because the differential settlement of the contact point of the LDT affected to a high degree the measurement of the anchor displacement, Fig. 7.18.b. These tests were not taken into account in any further discussion.

The results of tests series No3 dictated the scope of test series No4 (Partially bonded anchors) in the sense that the significant parameters (concrete strength, type of anchor, type of resins, gap) were also examined in this test series.

7.10.3 Brief presentation of the results

The data obtained from the tests were:

Test series No 3

- The type of failure of each specimen.
- The P=P(δ) relationship in the form of ordered number pairs (Pi,δi) and in P-δ curves.
- The concrete resin and steel strains at each

loading level (numerical pairs P, ε_c, ε_r, ε_s).

Test series No 4

- The P = P(d) relationship for the partially bonded anchors.
- The $\tau=\tau(\delta)$ relationship for concrete-resin, concrete-resin-steel and steel-resin double shear interfaces in the form of ordered (τ_i, δ_i) number pairs.

Test series No 5

- The resin strains at each loading level.

In order to present an overview of the experimental work of test series No 3 the most from the data obtained from each test are illustrated in figures 7.58 - 7.91. In these figures, the plan and sectional elevations of the failure surfaces, details of the failed part and the relative P=P(δ) curve are illustrated. The embedment length, the anchor diameter, the gap, the adhesive used, the method of drilling the hole and of the insertion of the resin, the concrete strength, the concrete splitting tensile strength, the mode of failure and the slip measured at different loading stages are also given. The mechanical properties of concrete, the mode of failure observed and the slip measured are also given in Table 7.11., for the test series No3. In a similar way, for the test series No4 - partially bonded anchors, the aformentioned characteristics are presented, in figures 7.92 - 7.94.

Table 7.11. Summary of pull-out data. Test series No.3

Test	fcc (Mpa)	√fc	ft,s (Mpa)	Failure load (kN)	Mode of failure	δ10 [µm]	δ20 [µm]	δ30 [µm]	δymax [µm]	PY [kN]
3.01	19.56	4.42	2.63	33.3	I+C+R	267	599	940	1210	33.30
3.02	20.38	4.51	2.96	28.90	I+C+R+Spl	397	668	-	968	28.90
3.03	21.29	4.61	2.64	20.10	I+C+R	148	687	-	688	20.10
3.04	26.39	5.14	2.55	22.5	I	202	359	-	395	22.50
3.05	23.20	4.82	3.13	38.1	I+C+R	145	193	772	1100	38.10
3.06	23.11	4.81	2.71	27.7	I+C+R	299	480	-	550	27.70
3.07	29.48	5.43	3.68	23.2	S	920	1620	-	2370	23.20
3.08	28.76	5.36	3.05	53.40	I+C+R	0/144	260	518	2230	53.40
3.09	31.67	5.62	2.76	34.9	I+C+R	165	418	558	618	34.90
3.10	25.30	5.03	2.61	30.2	I	361	921	2350	2830	30.20
3.11	28.48	5.34	2.51	34.50	I+C+R	139	506	531	1160	34.50
3.12	21.93	4.68	2.58	40.00	Spl+ R	861	1610	2150	3450	39.70
3.13	37.90	6.16	3.17	35.90	I+C+R	268	265	334	759	35.90
3.14	51.78	7.20	3.69	50.00	I+C+R	178	330	440	662	50.00
3.15	21.48	4.63	2.37	46.30	I+C+R	149	398	672	1550	46.30
3.16	24.93	4.99	3.05	6.30	I	-	-	-	506	6.28
3.17	21.66	4.65	2.88	17.80	I+R	1690	-	-	5640	17.80
3.18	21.66	4.65	2.88	17.20	I+R	3950	-	-	8440	17.20
3.19	21.66	4.65	2.88	9.05	I	-	-	-	951	9.05
3.20	26.07	5.11	2.65	42.90	I+C+R+Spl	533	1140	1620	4880	42.90
3.21	20.93	4.57	2.30	32.60	I+C+R	169	292	576	835	32.60
3.22	20.66	4.55	2.25	16.60	S	725	-	-	3200	16.60
3.23	18.97	4.36	2.15	45.00	I+C+Spl+R	312	589		2000	45.00
3.24	24.89	4.99	2.65	40.70	I+C+R					40.70
3.25	22.25	4.72	2.25	47.30	I+C+R	656	916	1370	4830	47.30
3.26	20.02	4.47	2.15	18.00	I+C+R+Spl	385	-	-	536	18.00
3.27	20.61	4.54	2.40	36.2	I+C+R+Spl	205	447	744	1130	36.20
3.28	22.84	4.78	2.65	27.15	I+C+R					27.15
3.29	24.25	4.92	2.60	45.30	I+C+R	202	493	682	1860	45.30
3.30	20.61	4.53	2.70	20.40	Spl+I+C+R	1510	2770		2860	20.40=81.50/4
3.31	24.89	4.99	2.55	33.15	Spl.	291	918	1470	1620	33.15=66.3/2
3.32	62.45	7.90	3.59	49.50	I+R	179	151	151	911	49.50
3.33	27.61	5.25	2.67*	47.60	I+C+R+Spl.	41	43	488	1860	47.60
3.34	26.55	5.15	3.25**	48.20	I+C+R	542	870	1040	1720	48.20

I: Interface failure.
C: Cconcrete cone.
Sp:Splitting of concrete

S: Steel failure.
R: Resin failure.

* : The same specimen as 3.04 tested later (core taking for determination of f_{cc}) $f_{ct33} = (f_{ct4}).(f_{cc33})/(f_{cc4})$.

** : The same specimen as 3.16 tested later. (core taking for determination of f_{cc}) $f_{ct34} = (f_{ct16}).(f_{cc34})/(f_{cc16})$.

δ10, 20, 30: anchor displacements at the levels of 10,0kN, 20,0kN, 30,0kN.

Py: failure pull-out load.
δ_{ymax}:maximum anchor displacement measured.

fcc: compressive strength of concrete at 28 days on 200mm cubes.
ft,s: splitting strength of concrete at 28 days on 150X300mm cylinders

Each aspect of the results is considered in detail in the following section, where quantitative considerations are made, and initial, general conclusions from these data are given here:

- Interfacial failure, Plate 18, occurs if a combination of variables leading to poor adhesion are present (plain bar or gel type of adhesive). It is associated with low ultimate load and large slip of the anchor.
- Resin failure at the bottom, Plates 26, 27, 28, 29, 30, 31, took place in almost all the types of failure.
- The splitting mode, Plate 13, is associated with large displacements.
- Shorter embedment length results in a decrease in the ultimate pull-out load.
- A smaller diameter causes an increase in displacement and a decrease in the pull-out load.
- An increase in the gap causes an increase in the pull-out load and a decrease in displacement up to a certain limit.
- Higher concrete strength results in stiffer behaviour of the anchor and increase in pull-out load.
- Injection of the resin improves the overall behaviour of the anchor (increase in the pull-out load and decrease in the anchor displacement).
- The reinforcement of the substrate contributes to improved overall anchor behaviour.

- The reduction of specimen size causes reduction of the ultimate load.
- Closely placed anchors in a group or those near to edge, exhibit larger displacements and lower ultimate load.

A detailed presentation and discussion of the results of test series No 3 follows in sections 7.11 (modes of failure), 7.12 (load-displacement relationship) and 7.13 (stress and strain distributions).

The discussion of the results of test series No 4 and No 5 is stated in Section 7.14 and Section 7.15 respectively.

7.11 Presentation and discussion of results relating to the mode of failure

As can be seen from Table 7.11, all the possible modes of failure, i.e concrete cone, splitting of concrete, interfacial adhesive failure, across either to the concrete -resin or resin-steel interface, resin failure and steel failure were exhibited in test series No 3, Plates 8-37. The most frequent mode, however, was the combined mode usually involving interfacial adhesive failure, resin and concrete failure, generally in the form of a double cone.

7.11.1. Discussion of the results

Steel failure took place only in specimens 3.07 and 3.22 (d=8mm, d_o=12, l=66mm, threaded bolt). The maximum load was 23.2kN for test 3.07 and 16.6 kN for test 3.22. The average bond stress at the concrete-resin interface at that time was τ_{ac}=9.32 N/mm² for 3.07 (6.67 N/mm² for 3.22) and

the maximum slip 2370 μm for 3.07 and, 3200, μm for test 3.22 whereas the maximum steel stress at the free part of the anchor (As=31.9mm² at root of thread) σ_s=727.3 N/mm² for specimen 3.07 and 520.4 N/mm² for the specimen 3.22. Of all the specimens with epoxy resin as adhesive, two, namely 3.04 and 3.10 exhibited an adhesive failure, the first along the resin-steel interface and the second along the conrete -resin interface.

Specimen 3.04 (d=12mm, d_o=16mm, l=100mm, plain bar made of grade 5.8 steel) failed at 22.50 kN at which level the average bond stress at the resin-steel interface was τ_{as}=5.97 N/mm² and the slip 395 μm. The average bond stress at concrete-resin interface was τ_{ac}=4.48 N/mm², whereas the steel stress at the free edge section at the root of thread was σ_s=298 N/mm², far from yield point (640 N/mm²). The concrete principal strain at point C1 was 24 με and the maximum resin tensile strain 2340 με.

For specimen 3.10 (d=12, d_o=16, l=100, threaded bolt, GEL type resin) the relative figures were P=30.2 KN, τ_{as}=8.01 N/mm² (at the resin-steel interface) and τ_{ac}=6.00 N/mm²). However, by taking into consideration the augmentation of the extended lateral surface of the threaded bolt in relation to a plain bar of the same diameter ω=1.096 (Appendix G) τ_{as} is equal to 7.31 N/mm².

Although average (shear) bond stress cannot be used as a failure criterion, it is indicative that in Specimen 3.07 (d=8mm, threaded bolt, standard resin) the shear stress at the concrete-resin interface, τ_{ac}, reached 9.32 N/mm², while in Specimen 3.10 (d=12, threaded bolt, GEL type resin) it failed at 6.00 N/mm², which is significantly lower than that of specimen 3.07 and illustrates the lower

effectiveness of resins with lower wetting properties.

Examination of the steel-resin interface shows that, although Specimen 3.07 did not exhibit any sign of failure at τ_{as}=13.99 N/mm², Specimen 3.04 (plain bar) failed at τ_{as}=5.97 N/mm² with a slip of 1/6 of the relative of Specimen 3.07.

This fact confirms the contribution of the macro interlocking effect of the threading of bolt (or of ribs of the ribbed bars) on the bond strength which, however, seems to take place after the failure of specific adhesive bond, associated with low displacements (see Test 3.04).

It must also be noted that at the bottom of the hole of specimen 3.10 (GEL type adhesive) no adhesion was found between bolt and adhesive at all.

Apart from specimens 3.04 and 3.10 the use of adhesives with very low strength led to pure adhesive failure along the concrete-grout interface as in the case of specimen 3.16 (the extreme case with low strength cement grout as adhesive) and specimen 3.18 (adhesive of low strength polymer mortar).

Specimen 3.17, where a high strength non-shrink grout was used as adhesive, showed a mixed mode of failure involving cohesive failure of the grout close to the steel-grout interface, failure in the concrete-grout interface at the top and a grout failure connecting the two failed interfaces, Fig.7.74.

The rest of the specimens exhibited a combined mode of failure which generally involved resin failure, adhesive failure at the concrete-resin interface commonly at the lower part of the anchor and concrete failure (cone failure or splitting). From the analysis of measured strains in

the resin and concrete it can be concluded that the order of failure is: concrete cracking - interfacial failure - resin fracture, usually at the bottom (Section 7.16).

The resin failure with a tensile failure occurred in the lower part of the specimen near the bottom (specimens 3.01, 3.02, 3.08, 3.12, 3.13, 3.14, 3.15, 3.17, 3.18, 3.21, 3.23, 3.24, 3.25, 3.26, 3.27, 3.28, 3.29, 3.30, 3.32, 3.34). Thus, it seems that the resin failure is associated with:

- high bond strengths at the concrete - resin interface,
- long embedement lengths,
- larger anchor diameters,
- larger gap dimensions,
- high tensile bond strength at the concrete-resin interface at bottom,
- generally, all the factors contributing to high interfacial bond strengths (like high concrete strength and insertion of resin by injection).

Resin failure did not take place in the cases of:

- plain bar,
- ribbed bar (which failed at the resin-steel interface at the bottom),
- lower anchor diameter d8, d10,
- using as adhesive the GEL type of resin and cement grout

The adhesive failure was not literally an "adhesive" failure, in the real meaning of the term. It involved almost invariably fine concrete particles of the interface, thus, it was more than 90% concrete failure at the interface (Specimens 3.01, 3.02, 3.03, 3.06, 3.08, 3.09, 3.11, 3.12, 3.13, 3.14, 3.15, 3.20, 3.21, 3.23, 3.24, 3.25, 3.26, 3.27,

3.28, 3.29, 3.30, 3.31, 3.32, 3.33, 3.34). Only in the case of low adhesive strength (GEL type resin) the above percentage was reduced to 50%, the rest being an adhesive failure. This means that the lower adhesive strength in the case of GEL type resins (which have a very much greater contact angle on concrete surfaces than the low viscosity resins) can be attributed not only to the lower physical bond strength but also to the lower penetration of concrete at the borehole, resulting in a lower interlocking effect which affects the final (shear) bond strength.

The concrete cone in general exhibited the form of double cone (Specimens 3.01, 3.02, 3.03, 3.05, 3.06, 3.08, 3.09, 3.11, 3.13, 3.14, 3.15, 3.20, 3.21, 3.23, 3.27, 3.29, 3.33, 3.34). The geometrical data obtained are shown in the Table 7.12 below.

Table 7.12. Geometrical data of the concrete failure surface. Test series No 3

Specimen	C_1 mm	C_2 mm	$\frac{C_1+C_2}{2}$	$Cr=\frac{C_1+C_2}{2\,1}$	a_1 [o]	a_2 [o]	a_3 [o]	a_4 [o]	dx	dy	$\frac{dx+dy}{2}$	$dr=\frac{dx+dy}{21}$	Remarks
1	57	40	48.5	0.485	50	39	45	18	310	310	310	3.10	
2	35	25	30.0	0.353	20	22	55	-	225	180	202.5	2.38	
3	40	42	41.0	0.683	70	45	60	52	390	350	370	6.17	
4	-	-	-	-	-	-	-	-	-	-	-	-	Interfacial failure
5	30	42	36	0.360	16	-	-	-	250	260	255	2.55	
6	61	43	52	0.626	56	25	17	37	285	310	298	3.58	
7	-	-	-	-	-	-	-	-	-	-	-	-	Steel failure
8	60	50	55.0	0.550	45	22	55	27	260	240	250	2.50	
9	45	35	40.0	0.40	24	15	30	20	230	140	185	1.85	
10	-	-	-	-	-	-	-	-	-	-	-	-	Interfacial failure
11	22	30	26	0.26	30	30	45	25	110	84	97	0.97	
12	70	75	72.5	0.763	30	20	26	-	510	300	405	4.26	Splitting of concrete
13	22	30	26	0.289	40	-	60	-	110	190	150	1.67	
14	32	40	36	0.36	55	45	45	-	220	210	215	2.15	
15	20	35	27.5	0.275	-	-	42	14	165	110	137.5	1.375	
16	-	-	-	-	-	-	-	-	-	-	-	-	Interfacial failure
17	-	-	-	-	-	-	-	-	-	-	-	-	Interfacial failure
18	-	-	-	-	-	-	-	-	-	-	-	-	Interfacial failure
19	-	-	-	-	-	-	-	-	-	-	-	-	Interfacial failure
20	30	30	30	0.,30	15	13	-	-	350	300	325	3.25	μ_X= 1%
21	40	32	36	0.36	41.5	-	51.5	-	190	170	180	1.80	μ_X= 2%.
22	-	-	-	-	-	-	-	-	-	-	-	-	Steel failure
23	48	52	50	0.50	-	-	-	-	170	255	212.5	2.125	Mode of fail: I+C+R+Spl.
24	25	25	25	0.25	53	53	45	45	70	140	105	1.05	
25	25	25	25.0	0.250	36	36	14	14	70	140	105	1.05	
26	10	15	12.5	0.125	19	19	17	17	90	67	78.5	0.785	
27	35	35	35	0.35	37	-	54	-	210	175	192.5	1.925	small specimen
28	30	30	30	0.30	54	54	52	52	120	70	95	0.95	t=4
29	60	60	60	0.60	-	-	-	-	390	390	390	3.90	
30	-	-	-	-	-	-	-	-	-	-	-	-	splitting of concrete
31	-	-	-	-	-	-	-	-	-	-	-	-	splitting of concrete
32	-	-	-	-	-	-	-	-	-	-	-	-	Interfacial failure
33	55	38	46.50	0.465	-	-	-	-	200	270	235	2.35	mode: I+C+R+Spl.
34	35	48	41.50	0.415	-	-	-	-	325	320	322.5	3.225	

C_1, C_2: maximum and minimum values of heigth of the double cone (Figures 7.58 - 7.91)
1: embedment length (Figures 7.58 - 7.91)
d_x, d_y: dimensions of the base of the concrete cone (Figures 7.58 - 7.91)
a_1, a_2: inclination angles of the double cone surface, right side (Figures 7.58 - 7.91)
a_3, a_4: inclination angles of the double cone surface, left side (Figures 7.58 - 7.91)
C_r: $(C_1+C_2)/21$ average value of C normalized with respect to the embedment length
S_{Cr}: Standard deviation of C normalized with respect to the embedment length
d_r:average cone base normalized with respect to embedment length

Although there were differences between individual specimens which led to differences in behaviour, an overall indication can be seen from the average values of Cr, a_1, a_2, a_3, a_4 and the corresponding standard deviations. These were:

$c_r = 0.40$ $\quad Sc_r = 0.16$

$a_1 = 38°$ $\quad Sa_1 = 15.99$

$a_2 = 31°$ $\quad Sa_2 = 13.98$

$a_3 = 42°$ $\quad Sa_3 = 15.29$

$a_4 = 28°$ $\quad Sa_4 = 15.82$

$a_{1,3} = 40°$ $\quad Sa_{1,3} = 16.43$

$a_{2,4} = 30°$ $\quad Sa_{2,4} = 14.23$

$d_r = 2.40$ $\quad Sd_r = 1.32$

By taking all the anchors which were installed in plain 600x600x200mm concrete block and had embedment length 100mm, diameter 12mm, low viscosity adhesive, 2mm gap and exhibiting a combined mode of failure (specimens 3.01, 3.05, 3.09, 3.14, 3.15, 3.23, 3.24, 3.29 which form the reference group A), these values became:

$C_r = (C_1 + C_2)/2l = 0.403$, $Sc = 0.12$

$a_{1,3} = 37°$, $\quad Sa_{1,3} = 16.94°$

$a_{2,4} = 33°$, $\quad Sa_{2,4} = 15.59°$

$d_r = 2.26$, $\quad Sd_r = 0.92$

By calculation of these values for the group of specimens with gap $t \geq 4$mm and the rest properties the same as the above group of selected specimens (specimens 3.08, 3.11, 3.33, 3.34) it was found that:

$c_r = 0.37$

$a_{1,3} = 44°$

$a_{2,4} = 26°$

$d_r = 2.260$

It seems however, that although specimen 3.11 was an anchor with t=4mm, the eccentricity of the anchor in relation to hole axis changed the overall behaviour of the anchor. Its ultimate pull-out load was Pult=34.5 kN compared with 53.40 kN for specimen 3.08 and 47.60 kN and 48.20 for specimen 3.33 and 3.34 respectively). By disregarding the corresponding values of specimen 3.11, the average values for this group of specimens became:

$c_r = 0.48$

$a_{1,3} = 50°$

$a_{2,4} = 24°$

$d_r = 2.7$

7.11.2 Influence of the different parameters

7.11.2.1 The embedment length

The influence of the embedment length is shown by comparing the geometric data of specimens of group A(l=8.3d) with those of specimens 3.02 (l=7d) and 3.03 (l=5d).

	Group A (l=8.3d)	Sp. 3.02 (l=7d)	Sp. 3.03 (l=5d)
C_r	0.40	0.35	0.68
$a_{1,3}$ [°]	37	37	65
$a_{2,4}$ [°]	33	22	48.50
d_r	2.26	2.38	6.17

This means that with a small reduction in embedment length (l=7d) the above factors remain practically invariable, whereas, a large decrease in embedment length

causes increase in the value C_r which is the cone height normalized with respect to the embedment length and increase in the base and the concrete slopes as well.

7.11.2.2 The anchor diameter

The influence of the anchor diameter is shown by comparing the above data of collected specimens of group A with those of specimen 3.06 (d=10).

	Group A (d=12mm)	Sp. 3.06 (d=10mm))
C_r	0.40	0.62
$a_{1,3}$ [°]	37	36.5
$a_{2,4}$ [°]	33	21
d_r	2.26	3.58

which indicates that a relatively greater depth and base of cone with almost the same inclination of the lateral surface of the first cone and reduced inclination of the second cone accompanies a decrease in the anchor diameter.

7.11.2.3 The resin thickness

By increasing the resin thickness (annulus) and keeping the remaining bonding properties constant - (Specimens 3.08, 3.33, 3.34) the following differences arise:

	Reference specimen Group A	Specimens 3.08, 3.33 and 3.34 (Average values)
C_r	0.40	0.47
$a_{1,3}$ [°]	37	50
$a_{2,4}$ [°]	33	24
d_r	2.26	2.70

As a result, by increasing the annulus an increase in the cone depth and in the cone base, an increase in the

angle of the first cone, and a decrease in the slope of the truncated lower cone are expected.

7.11.2.4 The strength of concrete

The high concrete strength (specimens 3.13-3.14) leads to the situation illustrated below:

	Refer.specimen Group A	Spec. 3.13 (f_{cc}=37.9MPa)	Spec.3.14 (f_{cc}=51.78MPa)
C_r	0.41	0.29	0.36
$a_{1,3}$ [°]	37	50	50
$a_{2,4}$ [°]	29	———	45
d_r	2.28	1.67	2.15

which means that the cone becomes shallower and steeper and that the double cone tends to a single cone (In the above values of C_r, $a_{1,3}$, $a_{2,4}$, d_r of reference specimen the corresponding values of specimens 3.13, 3.14 were not considered in order to bring out the relative differences).

7.11.2.5. The type of resin

The use of a resin with higher modulus of elasticity leads to cones with greater height and base (specimens 3.09, 3.23, 3.29).

	Reference Spec. Group A	Spec. 3.09-3.23-3.29 (Average values)
C_r	0.40	0.50
$a_{1,3}$ [°]	37	27
$a_{2,4}$ [°]	33	17
d_r	2.26	2.62

7.11.2.6 The effect of injection

The effect of the resin placed by injection with the same wetting and consequently adhesive properties is shown by taking specimen 3.15 and comparing it with the reference specimen.

	Reference Spe.	Spec. 3.15
c_r	0.40	0.27
$a_{1,3}$ [°]	37	42
$a_{2,4}$ [°]	33	14
d_r	2.26	1.38

This shows that injection affects the height and the base of concrete cone in a way similar to that of higher concrete strength.

7.11.2.7 The type of the anchor

The influence of the ribbed bar is shown below:

	Reference Spec.	Spec. 3.05-3.24 (Average values)
c_r	0.40	0.30
$a_{1,3}$ [°]	37	32
$a_{2,4}$ [°]	33	———
d_r	2.26	80

This shows that the use of ribbed bars instead of threaded ones, leads to shallower concrete cones.

7.11.2.8. The effect of the reinforcement

The presence and amount of reinforcement in the substrate, as can be seen from the table below, causes a considerable shallowness in the concrete cone and an accompanying decrease in the inclination of its lateral surface. From the failed specimen it can be seen that the

inclination of the cone surface in particular is regulated by the spacing and cover of the reinforcement on planes perpendicular to the anchor, since the failure planes are significantly directed in the top by the presence of reinforcing bars.

	Refer.Specimen Group A	Spec. 3.20 ($\mu_x = \mu_z = 1.0\%$)	Spec. 3.21 ($\mu_x = \mu_y = 2\%$)
C_r	0.40	0.30	0.36
$a_{1,3}$ [°]	37	15	46
$a_{2,4}$ [°]	33	13	———
d_r	2.26	3.25	1.80

7.11.2.9 The effect of the size of specimens

The decrease of the dimensions of the substrate (specimens 3.26, 3.27) causes both a considerable reduction in cone depth and base and the inclination of lateral surface as well. The correlation between the data of specimens 3.26 (t=2mm) and 3.27 (t=4mm) demonstrates the contribution of larger gaps to the high increase in cone depth in the presence of a compressive stress field caused by the supports which existed close to the anchor.

	Refer.Spec.	Spec.3.26	Spec.3.27	Spec.3.08
C_r	0.40	0.12	0.35	0.55
$a_{1,3}$ [°]	37	18	45	50
$a_{2,4}$ [°]	33	18	———	25
d_r	2.26	0.78	1.92	2.50

7.11.2.10 The splitting of concrete

Seven normal size specimens exhibited splitting of the concrete. Namely 3.02 (at which the cracking appeared just at the pull-out level) 3.12, 3.20 (where the crater after the detachment of the concrete cone was found cracked, but no generalized cracking was observed), 3.23 (where the same

phenomenon occurred), 3.30, 3.31 and 3.33. Specimens 3.06, 3.09, 3.14, 3.26, 3.27 were found slightly cracked with fine cracks (W<0.15mm). It must be recalled that in specimen 3.12 there was a stronger wedging action due to pull-out, because of the larger hole diameter at bottom, Section 7.10.2.

Apart from specimens 3.30 (group of anchors) and 3.31 (edge effect), what all the split specimens exhibited in common was one or two cracks starting at a distance of about (0.20)l to (0.25)l from the upper specimen's free surface and going upwards at about 30° - 45°(Fig.7.59 - D2, 7.69/I-I, 7.77/I-I, 7.80/I-I, 7.90/I-I). The important thing is that cracks of this form were not found in the rest of the specimens.

In addition, it was found (Test series No 2-Test 2.03) that increased diameters lead to a splitting mode. This fact combined with the splitting of small specimens (tests 3.26, 3.27) may allow the conclusion that the ratio of hole diameter to the size of specimen could be the parameter controlling the splitting mode. This concept is also emphasized by the fact that by increasing diameter an increase in the radial and tangential stresses at any point in concrete is expected, Section 5.4. As a result, the development of splitting is controlled by the ratio of the area of sections coplanar with the axis to cross sectional area perpendicular to this.

Thus, the development of a full depth conical crack firstly changes this ratio towards lower cross section of planes involving the pull out axis and secondly causes reduction in embedment length which results in higher

interfacial shear stress and this, in turn, in higher radial pressure. Thus, concrete splitting becomes more likely.

In order to have the stress distribution in the components of an anchor, a finite element analysis was carried out for the typical specimen with a crack starting from a point 0.20l lower than the free surface and inclined at 39% to the vertical axis. The analysis showed that in this case an increase of 9% in the upper part tangential tensile strains occurred in relation to the values of this strain in the uncracked specimen (Appendix C.4. Fig 6.6). Simultaneously, the inplane vertical normal stresses were compressive along the upper part of the anchor. Thus, the critical strain in this case changed to be the tangential tensile strain rather than the inplane vertical strain which was the situation in the rest of specimens (apart from 3.02 which splitted just at failure).

Another feature of the split specimens was that they exhibited excessive anchor displacement in relation to similar specimens with concrete cone failure.

Thus:

- Specimen 3.12 exhibited anchor displacement more than two times greater than 3.01 at any level.
- Specimen 3.20 (reinforced specimen) showed the same behaviour in relation to 3.21 which was also reinforced but with higher reinforcement ratio.
- Specimen 3.23 which was similar to 3.09, underwent almost two times greater displacement at the level of the failure load of 3.09, Fig 7.80, 7.66 than this.
- Specimen 3.33 exhibited a sharp reduction in

slope in the P-δ curve after the level of 30 kN. This reduction is about double that which occurs for specimen 3.34 at the same load level, Fig 7.90, 7.91.

The same behaviour in terms of large anchor displacements was exhibited by specimens 3.30 (group of 4 anchors in distance of 150mm from each other) and 3.31 (anchors placed near the edge), when compared with their homologue 3.01. The anchors of 3.30 underwent displacements 5.65 times greater than the corresponding values of 3.01 at 10.0 kN and 4.62 times at 20.0 kN, whereas those of 3.31, were 1.09 times greater at 10.0 kN, 1.53 times at 20.0 kN and 1.56 times at 30.0 kN level, than the corresponding ones of specimen 3.01.

The mechanism of splitting of 3.31 was similar to the described above, whereas the splitting of 3.30 can be attributed to superposition of the radial tensile stresses caused by each anchor in the area in between.

Related data reported in the existing literature are shown below.

Reference	c_r	Single cone $a_{1,3}$	Double cone $a_{1,3}$	Double cone $a_{2,4}$	Characteristics of the tests
Lee et al /9/	0.250	/	+	+	d16-Polyester resin- l/d=(4.7-7.8) —
P.Wachtsmuth et al /11/	0.70	35°-40°			state of the art report
R.Eligehausen- et al /14/	0.600-0.750				state of the art report

The shallow cone height of the tests of Lee et al /9/ can be attributed to the relatively higher anchor diameter used, which, according to Section 7.11.2.2, might have led to low C_r ratios. The most probable reason for high values of c given in references /11/ and /14/ might be connected with the low values of the embedment length or of the type of resin used, which, most commonly, was unsaturated polyester resin with aggregates (because they made reference to commercially available anchors, which are common UPR anchors with relatively low ratio of embedment length to diameter, or anchors with diameter lower than 12mm).

7.12. Overall discussion of the load-displacement relationship

The results obtained are presented and discussed generally and then the influence of particular variables is examined.

The anchors with low adhesive characteristics (gel type of resins - cementitious grouts), which failed by interfacial failure, exhibited much greater displacements than those with better adhesion properties of the adhesive.

Large displacements were observed in the case of an anchor diameter of 8mm which showed a steel failure, whereas, this was not the case with 10mm diameter of the anchor. All the split specimens except specimen 3.02, which cracked just at failure, showed excessive slip of the anchor.

Most of the specimens which failed by a combined mode involving resin, interfacial adhesive and concrete cone failure exhibited nearly linear behaviour up to failure.

In order to examine the behaviour of each combination of variables, the best fit curve to each set of P-δ data was calculated by means of power regression.

Table 7.13. defines the characteristics of these curves.

Table: 7.13. Fit curves of each test. Test series No 3.

Specimen	ft[MPa]	P_{ult} [kN]	Mode of failure	Curve fitting model: $\delta = b.P^m$, δ[μm], P[kN]	correlation coefficient r	Variable
3.01	2.63	33.3	I+C+R	$\delta = (26.9).P^{1.0472}$	.9923	Reference test
3.02	2.96	28.9	I+C+R+Spl.	$\delta = (17.7).P^{1.218}$	.9759	l= 7d
3.03	2.64	20.1	I+C+R	$\delta = (2.1).P^{1.9006}$	.9953	l= 5d
3.04	2.55	22.5	I	$\delta = (11.7).P^{1.1795}$	.9659	Plain bar
3.05	3.13	38.1	I+C+R	$\delta = (12.7).P^{1.1296}$	.8865	Ribbed bar
3.06	2.71	27.7	I+C+R	$\delta = (97.2).P^{0.5242}$	.9814	d= 10
3.07	3.68	23.2	S	$\delta = (3.99).P^{2.03}$	.999	d= 8
3.08	3.05	53.4	I+C+R	$\delta = (3.64).P^{1.551}$	.9619	t= 4
3.09	2.76	34.0	I+C+R	$\delta = (17.3).P^{1.0286}$	.9833	LV
3.10	2.61	30.2	I	$\delta = (3.5).P^{1.8832}$	.9526	GEL
3.11	2.51	34.5	I+C+R	$\delta = (6.4).P^{1.402}$	.9368	Eccentricity of Anchor t=4
3.12	2.58	40.0	Spl.+R	$\delta = (106.2).P^{0.9066}$	.9874	Split
3.13	3.17	35.9	I+C+R	$\delta = (37.7).P.^{0.699}$	.8637	C30
3.14	3.69	50.0	I+C+R	$\delta = (32.3).P.^{0.7715}$	.9947	C50
3.15	2.37	46.3	I+C+R	$\delta = (5.6).P^{1.438}$	.9913	Injection
3.16	3.05	6.3	I	$\delta = (80.6).P$	1.000	Cem.gr.
3.17	2.88	17.8	I+R	$\delta = (63.7).P^{1.5255}$	.9573	N.Shr.gr.
3.18	2.88	17.2	I+R	$\delta = (77.0).P^{1.6669}$	.9927	Pol.concr.
3.19	2.88	9.05	I	$\delta = (105.).P$	1.000	R.cem.gr.
3.20	2.65	42.9	I+C+R+Spl.	$\delta = (21.0).P^{1.3477}$	.9555	Reinf.sp.μ= 1%
3.21	2.30	32.6	I+C+R	$\delta = (10.2).P^{1.1936}$	.9512	Reinf.sp.μ.=2%
3.22	2.25	16.6	S	$\delta = (10.5).P^{1.8991}$	.9820	d= 8
3.23	2.15	40.7	I+C+R+Spl.	$\delta = (34.2)\ P^{0.9792}$	.8677	LV
3.24	2.65	40.7	I+C+R	-		
3.25	2.25	47.3	I+C+R	$\delta = (29.7)\ P^{1.24}$	.967	diam.drilling
3.26	2.15	18.0	I+C+R+Spl.	$\delta = (49)\ P^{0.910}$	.962	Small spec.
3.27	2.40	36.2	I+C+R+Spl.	$\delta = (12.5)\ P^{1.2091}$	.9962	Small spec/t=4
3.28	2.65	27.15	I+C+R			Plain bar
3.29	2.60	45.3	I+C+R	$\delta = (14.4)\ P^{1.182}$	.9654	LV
3.30	2.70	20.4	I+C+R+Spl.	$\delta = (167.9)\ P^{0.940}$	.9989	Group of anchors
3.31	2.55	33.15	Spl.	$\delta = (36.6)\ P^{1.08}$	1000	Edge effect
3.32	3.59	49.5	I+R	$\delta = (17.8)\ P^{0.7841}$	.6899	C60
3.33	2.67	47.6	I+C+R+Spl.	$\delta = (2.88)\ P^{1.64}$	.908	t=8
3.34	3.25	48.2	I+C+R	$\delta = (2.66)\ P^{1.722}$	.857	t=10

P[kN]
δ[μm]

I, C, S, Sp, R: stand for Interfacial, Concrete, Steel, Splitting and Resin modes of failure

7.12.1. Mechanical behaviour of anchors in terms of P=P(δ) relationship

As can be seen from Table 7.13., Anchor 3.01. showed a nearly linear relationship up to failure i.e.

$$\delta = (26.9)\ p^{1.047},\ \text{(Fig.7.58)}.$$

The use of a low viscosity epoxy resin with the same wetting characteristics (γ, θ) did not change the character of this function significantly (Fig.7.95). The relevant curves for the tests 3.09, 3.23, 3.29 in which the adhesive was an epoxy resin of type LV, (with different modulus of elasticity in relation to that of the standard type used in most tests), were found to be:

$$\text{Test 3.09: } \delta = (17.3)\ p^{1.0286}$$

$$\text{Test 3.23: } \delta = (34.2)\ p^{0.9792}$$

$$\text{Test 3.29: } \delta = (14.4)\ p^{1.182}$$

The stiffness of the anchor ($\Delta Pi/\Delta \delta i$) is different in each test, but the fact that anchors with the same specific adhesion properties behave almost linearly was considered important.

The use of resin with the same modulus of elasticity but with lower specific adhesion properties (gel type) resulted in a curve significantly flatter with continuously decreasing anchor stiffness. This was the case of Test 3.10 in which the adhesive used had the same elastic modulus as the low viscosity epoxy resin of type LV used in tests 3.09-3.23-3.29. The curve is described by the function:

$$\delta = (3.5)p^{1.883}$$

The decrease in embedment length caused the function P= P(δ) to deviate from the almost linear to a flatter branch

towards the δ axis (Fig.7.96).

This is demonstrated by the comparison below.

Test	l	P = P(δ)
3.01	l=(8.3)d	$\delta = (26.9).\ P^{1.0472}$
3.02	l=(7.0)d	$\delta = (17.7).\ P^{1.218}$
3.03	l=(5.0)d	$\delta = (2.1).\ P^{1.9006}$

The curve P=P(δ) also remained almost linear in the case where ribbed bar was used instead of threaded one, whereas, it deviated little from the linearity in the case a plain bar was used as anchor (Fig. 7.97).

Threaded bar: $\delta=(26.9)P^{1.0472}$

Ribbed bar : $\delta=(12.7)P^{1.1296}$ (Test 3.05)

Plain bar : $\delta=(11.7)P^{1.1795}$ (Test 3.04)

The ultimate pull-out load was significantly lower in the latter than in the former type.

The decrease in the anchor diameter led to steeper curves, with the centre of curvature towards the P axis, provided the same mode of concrete failure is kept (Fig. 7.98).

Refer test 3.01 (d=12) : $\delta=(26.9).\ P^{1.0472}$

test 3.06 (d=10) : $\delta=(97.2).\ P^{0.5242}$

Should the combined mode of failure change to steel failure due to a large reduction of anchor diameter, then a flat curve would be expected as tests 3.07 and 3.22 demonstrate:

test 3.07/d=8 : $\delta=(3.99).P^{2.03}$

test 3.22/d=8 : $\delta=(10.5).P^{1.8991}$

Increase in the strength of the concrete results in a steeper curve, as can be seen from the mathematical expression following and from Fig. 7.99 and Fig. 7.70 - 7.71 - 7.89.

Ref.test 3.01(f_c=19.56 MPa, f_t=2.63 MPa):$\delta=(26.9).P^{1.0472}$

Ref.test 3.13(f_c=37.90 MPa, f_t=3.17 MPa):$\delta=(37.7).P^{0.699}$

Ref.test 3.14(f_c=51.78 MPa, f_t=3.69 MPa):$\delta=(32.3).P^{0.7716}$

Ref.test 3.32(f_c=62.45 MPa, f_t=3.59 MPa):$\delta=(17.8).P^{0.7841}$

The anchor, which was fixed by means of the resin injection (Test 3.15 - Fig.7.72 - 7.100), behaved in a quite different manner. The relevant expression for the P=P(δ) relationship was found to be:

$$\delta=(5.6).P^{1.438}$$

which indicates a more ductile behaviour of the system. This was expected because the low viscosity resin penetrates the pores of concrete and alters the mechanical behaviour of concrete in this vicinity by blunting the peak of the stresses.

The effect of increased thickness of resin was found to be similar (tests 3.08, 3.33, 3.34), and Fig.7.101, 7.65, 7.90, 7.91 correspondingly). The relevant functions were:

Test 3.08/t=4 :

$\delta=(3.64)\ P^{1.5512}$ Pult= 53.4 kN, δ_y=2230μm

Test 3.33/t=8 :

$\delta = (2.88)\ P^{1.640}$ Pult= 47.6 kN, δ_y=1860μm

Test 3.34/t=10:

$\delta = (2.66)\ P^{1.722}$ Pult= 48.2 kN, δ_y=1720μm

and they are characterized by the continuously falling stiffness of the anchor.

The eccentricity of the anchor in relation to the hole axis caused the curve to take on double curvature with significant stiffness at the penultimate stage, Fig.7.102 - Test 3.11. The best fit single curvature relationship, is:

$$\delta = (6.4)P^{1.402}$$

The diamond drilling of the hole (Test 3.25), which produced a substantially smoother adhesive - concrete interface, resulted in remarkably larger displacements at any load level. It shows a double curvature form where the second branch shows continuously falling stiffness of the anchor, Fig 7.82.

The influence of the specimen size is evident from comparison of Tests 3.26 and 3.27 with Tests 3.01, and 3.08 and 3.25 respectively. Tests 3.26 and 3.27 were carried out with smaller specimen size (300x300x200 mm instead of 600x600x200 mm which was the normal size). It can be seen that these had a stiffer behaviour in terms of the P=P(δ) law, due to the proximity of supports.

t=2 mm

Specimen 3.01 (normal specimen): $\delta=(26.9)P^{1.0472}$

Specimen 3.26 (small specimen): $\delta=(49.0)P^{0.940}$

t=4 mm

Specimen 3.08 (normal specimen): $\delta=(3.64)P^{1.551}$

Specimen 3.25 (normal specimen): $\delta=(29.7)P^{1.24}$

Specimen 3.27 (small specimen): $\delta=(12.5)P^{1.2091}$

The amount of reinforcement did not greatly affect the anchor behaviour since the P= P(δ) relationship remained close to linearity:

Test 3.21 μ=2% $\delta=(10.2).P^{1.1936}$,

Fig.7.105 (Fig.7.78). This evidence proved consistent with the fact that the concrete failure of this anchor took place within the space of two adjacent reinforcing bars (Fig.7.78), thus, the presence of reinforcing bars must have affected the overall mechanical behaviour of the anchor only to a small extent. However, in the case of splitting mode, the reinforcing effect became more evident (Test 3.20, Fig 7.77 which exhibited greater anchor displacement and a more uniform ductile response in comparison with 3.12).

The splitting mode showed a more ductile behaviour, Fig.7.106, than the brittle concrete cone failure, which is attributed to the progressive cracking of the concrete surrounding the anchor (Tests 3.12, 3.20, 3.23 and Fig. 7.69, 7.77, 7.80).

The group of anchors and the edge effect can be regarded as a case of the splitting mode since the mechanism of failure of the specimen was the cracking of concrete. The p= P(δ) relationships obtained for the relevant tests

(3.30-3.31) are shown in Fig.7.87, 7.88. The comparison with the reference test of the independent anchor is illustrated in Fig.7.107. The mathematical expressions for the best fit curves were found:

$$\text{Test 3.30} \quad \delta=(167.9)p^{0.940}$$

$$\text{Test 3.31} \quad \delta=(36.6)p^{1.08}$$

7.12.2. Discussion of the effect of the particular variables on the overall behaviour of the anchor system

Since the results obtained relate to a set of characteristics (Geometry of failure, P= P(δ) relationship, P_{ult}, strain of the materials involved in the overall system) which were measured on a wide range of different anchors, attempts have been made to select a common parameter to which all the data might be related.

If that were possible then the critical differences among the systems would be identified in a clearer way.

The variable which had different values in almost all tests was the concrete strength. If its effect could be identified, the comparison of the results of each test to the others will be more reliable.

7.12.3. The concrete strength

Since the concrete strength had different values in almost all the tests a suitable parameter was sought which could incorporate this variation and against which all the other parameters investigated in this work should be examined. Various ratios of the P_{ult} to different

expressions of tensile strength of concrete were examined.

In Fig.7.108 the measured ultimate pull-out loads of specimens 3.01, 3.14, 3.32, which represent the extremes of concrete strength in this series of tests, were normalized with respect to the different criteria for the tensile strength of concrete and plotted against the concrete compressive strength of each specimen. The expressions used to relate the concrete compressive strength to its tensile strength were:

$$f_{ct} = k[(f_{cc})^{1/2}]$$

$$f_{ct} = k[(f_{cc})^{2/3}]$$

The tensile splitting strength (with value taken as average of the measured values of two cylinders for each test), was also used as common parameter.

The specimens examined (3.01, 3.14, 3.32) had the same values of all the variables except that of concrete strength. The graphs drawn shown that the examined normalized values of $P_u/\sqrt{(f_{cc})}$, $P_u/[(f_{cc})^{2/3}]$, P_u/f_t exhibited a slight inclination against the f_{cc} axis and therefore could be considered almost independent of the concrete compressive strength. The values P_u/f_t, exhibited a slight increase by increasing concrete strength, whereas the inclination of the $P_u/\sqrt{(f_{cc})}$ line was almost the same, but in the opposite direction (decrease of $P_u/\sqrt{f_{cc}}$ values with increasing f_{cc}). The $P_u/(f_{cc}{}^{2/3})$ line had a somewhat greater scope with values also decreasing with increasing f_{cc}.

If the slight inclination of the P_u/f_t and $P_u/(f_{cc})^{1/2}$ lines is assumed to be 0, this would mean that the above

quantities were independent of the strength of concrete substrate.

In order to identify the effect of concrete strength on the anchor displacement, an attempt was made to connect the measured displacement with the functions describing the dependence of the elastic modulus of concrete on its compressive strength. The most commonly used expressions are:

$$E_c = 9.1 \quad (f_{cc})^{0.33}$$

$E_c = 18000\ [(f_{ccyl})^{1/2}] = \omega.(f_{cc})^{1/2}$ (where ω is an appropriate factor).

Since the anchor slip is the sum of the following integrals, Eq.(5.4):

$$\delta = \int_0^1 \varepsilon_{zc}\ dz + 2\int_0^1 \delta\ dz + \int_0^1 \varphi\ t\ dz =$$

$$= 2\int_0^1 \frac{\tau}{a}\ dz + \frac{1}{E_c}\ \left(\int_0^1 \frac{t\tau}{\psi}\ dz + \int_0^1 \sigma_{zc}\ dz\right) =$$

$$= \frac{2}{E_c}\int_0^1 \frac{(\tau E_c)}{a}\ dz + \frac{1}{E_c}\ \left(\int_0^1 \frac{t\tau}{\psi}\ dz + \int_0^1 \sigma_{zc}\ dz\right) =$$

$$= \frac{1}{E_c}\ \left(\int_0^1 \frac{(2\tau E_c)}{a}\ dz + \int_0^1 \frac{t\tau dz}{\psi} + \int_0^1 \sigma_{zc}\ dz\right)$$

or

$$[E_c.\delta] = \int_0^1 \frac{(2\tau Ec)}{a}\ dz + \int_0^1 \frac{t\tau dz}{\lambda} + \int_0^1 \sigma_{zc}\ dz$$

where:

δ : the slip of the adhesive - concret interface

τ : the local shear stress of the adhesive

a : the factor gained from the relationship $\delta=a\tau$, Fig 7.147, 7.149

$\varepsilon_{z\,c}, \sigma_{z,c}$: strain and corresponding stress of concrete in the direction of the anchor axis

ψ : E_c/G_a

E_c : modulus of elasticity of concrete

G_a : shear modulus of the adhesive,

it seemed reasonable to examine the variation of the quantity $(\delta.E_c)$ instead of δ in relation to the varying concrete strength. Commonly used expressions for the modulus of elasticity involve relationships of the form $E_c=\omega(f_{c\,c})^m$ with m=1/2, 2/3.

Thus, instead of the absolute values of slip at the load levels of 10 kN, 20 kN and 30 kN (δ_{10}, δ_{20}, δ_{30}) the values $\delta_{10}.\sqrt{f_{c\,c}}$, $\delta_{20}.\sqrt{f_{c\,c}}$, $\delta_{30}.\sqrt{f_{c\,c}}$, and the $\delta_{10}.(f_{c\,c})^{2/3}$, $\delta_{20}.(f_{c\,c})^{2/3}$, $\delta_{30}.(f_{c\,c})^{2/3}$ were plotted against the $f_{c\,c}$ values as is illustrated in Fig.7.109. At higher loads the effect of concrete strength in reducing displacements is more pronounced. The relationship at all levels found to be almost linear. The displacements at failure have not been examined, since their values depend on the final mode of failure, which for specimen 3.32 was different from that of specimens 3.01 and 3.14.

Because the effect of concrete strength will be an essential factor to take into consideration before analysing the effects of the rest of variables, the mathematical

expression for that would be helpful. So, in accordance with Fig.7.109 for a given concrete strength, f_{c1}, the relevant factors λ_{10}, λ_{20}, λ_{30} by which the quantities $\delta.\sqrt{fc}$ must be divided in order to be normalized with respect to the concrete quality of specimen 3.01 (f_{cc}=19,56 MPa), are:

$$\lambda_{10} = \delta_{10i}/\delta_{10in1}$$

$$\lambda_{20} = \delta_{20i}/\delta_{20in1}$$

$$\lambda_{30} = \delta_{30i}/\delta_{30in1}$$

where:

δ_{10i}, δ_{20i}, $\delta_{30,i}$:
the quantities $\delta_{10}(\sqrt{f_{cc}})$, $\delta_{20}(\sqrt{f_{cc}})$, $(\delta_{30}\sqrt{f_{cc}})$ for a specimen with concrete strength f_{c1}

δ_{10in1}, δ_{20in1}, δ_{30in1}:
the quantities δ_{10i}, δ_{20i}, δ_{30i} normalized with respect to an idealized specimen with the concrete strength 19.56 MPa, which was the concrete strength of specimen 3.01.

$\delta_{10,20,30}$
or
δ_{10i}, δ_{20i}, δ_{30i} :
the relevant anchor displacement at the load levels of 10.0-20.0-30.0 KN.

Thus, according to Fig.7.109.c and table, λ_{10}, λ_{20}, λ_{30} can be calculated as follows:

$$\lambda_{10} = \delta_{10i}/\delta_{10in1} = 1$$

$$\lambda_{20} = \delta_{20i}/\delta_{20in1} = [2647-(f_{ci}-19.56)29.2]/2647 =$$

$$= 1-[(f_{ci}-19.56)/90.65].$$

because for the line $\delta_{20}(\sqrt{f_{cc}})$:

$$\text{tana} = (2647-1192)/(19.56-69.45) = -29.2$$

where α the slope of the $\delta_{20}(\sqrt{f_{cc}})$ line to the f_{cc} axis, and therefore:

$$\delta_{20}(\sqrt{f_{ci}}) = 2647-(f_{ci}-19.56)29.2$$

Further:

$$\lambda_{30} = \delta_{30i}/\delta_{30in1} = [4154-(f_{ci}-19.56)59.37]/4154 =$$

$$= 1-[(f_{ci}-19.56)/70]$$

because for the corresponding line $\delta_{30}(\sqrt{f_{cc}})$:

$$\text{tana} = [4154-1192]/[19.56-69.45] = -59.37$$

and therefore:

$$\delta_{30}(\sqrt{f_{ci0}}) = 4154-[f_{ci}-19.56]59.37$$

7.12.4. The embedment length

Since it has been shown that the quantity $(P_u/\sqrt{f_{cc}})$ is almost independent of the concrete strength the effect of embedment length can be identified by examining the $[P_u/\sqrt{f_{cc}}]$-δ relationship.

In Fig. 7.110 the relevant values of $P_{cc}/\sqrt{f_{cc}}$ for tests 3.01 (l=8.3d), 3.02 (l=7.0d), 3.03 (l=5.0d), 3.13 (l= 7.5d)

are plotted against the values of the ratio of embedment length to the anchor diameter. The graph indicates that, for l/d values greater than about 8, the embedment length has no influence on the ultimate pull-out load, which retains its maximum value. Below this limit it seems that the values of $[P_u/\sqrt{f_{cc}}]$ decrease according to a second order relationship with decreasing values of l/d.

In order to examine the effect of embedment length on the anchor displacement, first the quantities were normalized with respect to the reference concrete strength of specimen 3.01 (Appendix H) and then the resulting values were plotted against the l/d values of the specimens 3.01 - 3.02 - 3.03 - 3.13 Fig.7.111. Only the values $\delta_{10}\sqrt{f_{cc}}$ and $\delta_{20}\sqrt{f_{cc}}$ were considered since δ_{30} in most cases is not realized because the failure of the anchor occurred at load levels lower than 30.0 kN. The value of 148 μm for δ_{10} of the specimen 3.03 (l= 5d) (surprisingly low in relation to the characteristics of the specific anchoring system on the particular concrete specimen), was disregarded as not relevant to the rest of the δ_{10} values.

7.12.5. The effect of the anchor diameter

The diameter of the anchor varied in 3 tests. Namely 3.06 (d=10mm), 3.07 (d=8mm) and 3.22 (d=8mm). In tests 3.07 and 3.22 the anchor failed by steel fracture. Hence, the pull-out data of these tests could not be taken into consideration. Thus, the comparison of P_{ult} values was only made between Tests 3.01 (d=12mm) and 3.06 (d=10mm) of the test series No.3 and test 2.07 of test series No.2. This last test, however, was conducted with embedment length

l=(6.25)d and therefore the relevant value $P_u/\sqrt{f_{cc}}$ had to be corrected in accordance with Fig.7.110. The relationship of $[P_{ult}/\sqrt{f_{cc}}]=f(d)$ was found to be linear (Fig.7.112) in the range d=8-16mm but it changes to a power curve at lower diameters, becoming zero at zero diameter. The influence of the anchor diameter on the displacement of the anchor is also illustrated in Fig.7.112 in terms of the $[(\delta_{10in1})\sqrt{f_{cc}}-d$, and $[(\delta_{20in1})\sqrt{f_{cc}}]-d$ relationships (after the calculation of the normalized values δ_{10in1}, δ_{20in1} according to Section 7.12.3)

The relevant curves exhibit a sharp increase in displacement at diameters less than 10mm.

7.12.6. The thickness of resin

The tests conducted with variation in thickness of resin only were 3.08 (t=4mm), 3.33 (t=8mm) and 3.34 (t=10mm), apart from those tests in which another parameter was also varying (Test 3.11 - eccentricity of the anchor instead of symmetrical fixing, Test 3.25. - diamond drilling instead of percussive rotary drilling, Test 3.27 - small specimen in place of normal specimen, Tests 3.16 - 3.19. - cementitious grouts instead of epoxy resin as adhesive). To verify the influence of the thickness of resin on the overall behaviour the first three only were taken into account after the necessary normalization with respect to concrete strength (Appendix H) according to Section 7.12.3.

The comparison in terms of $[P_u/\sqrt{f_{cc}}]$-t or $[P_u/\sqrt{f_{cc}}]$-(t/d) is shown in Fig. 7.113. It demonstrates that for the normal specimens of 600x600mm the curve tends to be stabilized above the value of t/d=0.40. Exceeding this value has no influence on the ultimate pull-out load.

The results in terms of $[\delta\sqrt{f_{cc}}]$-(t/d), relationship indicate that there is an initial decrease in $[\delta\sqrt{f_{cc}}]$ with increasing thickness, which, after reaching a critical value of t/d at about 0.50-0.60, changes to give increase in $\delta\sqrt{f_{cc}}$ with further increase in t/d. This behaviour can be attributed to the beneficial effect of increasing thickness on the more uniform distribution of shear stresses on the concrete-resin interface, which results in less concrete deformation. This effect, however is offset by the increasing shear displacements associated with increasing thickness over a certain value, since the shear modulus of resin is substantially lower than that of concrete.

7.12.7. The type of anchor

In this instance the way in which the form of the anchor (threaded bolt-ribbed bar-plain bar) affects the mechanical behaviour had to be estimated. Firstly, the effect of the type of anchor on the ultimate load is drawn against the types of anchor examined (Fig.7.114). Whereas the plain bar resisted low $[P_{ult}/\sqrt{f_{cc}}]$ values, the ribbed bars were marked by pull-out ultimate normalized values (average values of 2 tests) 6% higher than those of the threaded anchors. Although at first sight this might seem strange, in fact it might be connected with either better primary adhesion or the micro-mechanical interlocking effect which occurs in the ribbed and plain bars as result of their inevitable mild oxidation or a combination of both effects. The primary adhesion might be higher in the ribbed and plain bars as a result of the better wetting conditions prevailing at the plain or ribbed bar-resin interface which are better than the ones at the threaded surface-resin interface,

because the relatively denser pitch of the threading (Plates 34, 37) enables air bubbles to disrupt the overall wetting of the threading by the resin.

This possibility is not unrelated to the lower displacement values $[(\delta_{10in1})\sqrt{f_{cc}}]$ and $[(\delta_{20in1})\sqrt{f_{cc}}]$ that the ribbed bars exhibited in relation to threaded anchors, as can be seen from Fig.7.114. The same effect of better wetting seems also to be the reason for the high stiffness of the plain bars at the early stage of loading.

$(\delta_{10in1})\ \sqrt{f_{cc}} = 1038$ for the plain bar

$(\delta_{10in1})\ \sqrt{f_{cc}} = 1180$ for the bolt

$(\delta_{20in1})\ \sqrt{f_{cc}} = 1994$ for the plain bar

$(\delta_{20in1})\ \sqrt{f_{cc}} = 2647$ for the bolt

The lower ultimate pull-out values of plain bar and the progressively reducing differences in the $[\delta_{in1}\sqrt{f_{cc}}]$ values between threaded and ribbed bar, prove that the mechanical threading becomes effective not in the lower levels of loading.

It must be pointed out here that the variation of $[(\delta_{10in1})\sqrt{f_{cc}}]$ and $[(\delta_{20in1})\sqrt{f_{cc}}]$, rates are calculated (Appendix H) on the assumption that the correction coefficient for normalizing the different values of the concrete strength which were calculated for the threaded anchors are also applicable to the ribbed and plain bars.

7.12.8. The type of adhesive

The different types of adhesives used were:

- Two types of low viscosity epoxy resin with almost similar wetting properties (γ, θ) as can

be seen from Table 7.10 - Section 7.7.3, but different mechanical ones.

- One type of thixotropic epoxy resin which was formulated by using the same type of one of the low viscosity resins (type LV) and adding different fillers and thixotropic agents.
- A whole series of grouts with low adhesive strength to concrete involving one specially formulated low strength PMMA grout and three types of cementitious grouts. All of these materials had led to very low ultimate pull-out values and extensive anchor displacements. These adhesive anchor properties preclude their use as anchoring devices under the conditions set within the present research project. (They might prove to be useful anchors if, for example, the embedment length were increased substantially).

The discussion about the types of adhesive is, therefore, limited to the three types of epoxy resins used. The ultimate values $[P_u/\sqrt{f_{cc}}]$ each of these types had reached is shown in Fig.7.115 where also the variation of the displacement values $[(\delta_{inl})\sqrt{f_{cc}}]$ is plotted at the levels of 10, 20 and 30 kN after recalculation in order to take into account the concrete strength - effect, Appendix H.

The two types of low viscosity epoxy resin behave in a slightly different way in terms of $[P_u/\sqrt{f_{cc}}]$ (variation of $[P_u/\sqrt{f_{cc}}]$ values of 3.5%) and differently in terms of displacements (differences in $[(\delta_{inl})\sqrt{f_{cc}}]$ values from - 31%

to +5.8%). This conclusion reflects the effect of wetting properties of adhesive on the ultimate pull-out values [$P_u/\sqrt{f_{cc}}$], which seem to be independent of the mechanical properties of the adhesive, provided they are over a certain minimum value. (It must be stressed that the second low viscosity resin used of type LV had a modulus of elasticity 7.8% higher and an ultimate tensile strength 3.7% lower than those of the standard resin of C1380 type).

By examining the differences in [$(\delta_{inl})\sqrt{f_{cc}}$] values the following are found:

- Differences at level of 10.00 KN: -31.3% (lower values for LV).
- Differences at level of 20.00 KN: -7% (lower values for LV).
- Differences at level of 30.00 KN: +5.9% (lower values for C 1380).

By taking into consideration the fact that the low load level displacements (up to 10 kN) are less reliable than those at higher load levels, due to the effect of a whole series of factors affecting the values of primary adhesion, (among which, the percentage of cement matrix mortar in the concrete-resin interface, the microroughness of boring, the microroughness of steel etc), and due to the less accurate measurements of the load, it can be concluded that the displacement values [$(\delta_{inl})\sqrt{f_{cc}}$], are also not highly dependent on the mechanical properties of the adhesive used, since their variation at high load levels is found to be between -7% to +5.9%.

7.12.9. The effect of specimen size

Provided that the same system of fixing the specimen in

the machine is used, the specimen size affects the field of stresses across the concrete-adhesive, and adhesive-steel interfaces.

As shown in Fig.7.116 there is a decrease in the ultimate pull-out [$P_u/\sqrt{f_{cc}}$] rate with decreasing specimen size in both cases i.e. in thin annulus (t=2mm, t/d=0.16) and the thicker one (t=4mm, t/d=0.33). The decrease was found to be 46% for thin and 20% for thick resin shells.

The whole phenomenon can be explained by the role of compressive stresses, which cause the rotation of the principal tensile stress of the concrete elements in the vicinity of interface from its initial position a-a (a line inclined 45°) to another, b-b, closer to the horizontal line, Fig.7.116. As a result, the failure line moves from its position cc to a steeper inclination, dd, (Fig.7.116) which results in smaller cone diameter. The presence of compressive stresses also causes a reduction of the interfacial area, which is critical in respect of the tensile principal stress, thus leading to a smaller cone height. Both hypotheses were confirmed by tests 3.26-3.27. (Section 7.11.2.9). With reduced cone height and diameter the normalized ultimate pull-out forces ($P_u/\sqrt{f_{cc}}$) are expected to decrease in value.

The normalized displacements [$(\delta_{inl}).\sqrt{f_{cc}}$] were found to increase generally, but with the anchors with thicker resin shell exhibiting a smaller increase in displacement with decreasing specimen size.

7.12.10. The effect of reinforcement

The reinforcement generally needs more than one parameter in order to be fully defined. Reinforcement

ratio, bar spacing, and bar anchor and cover, at least, must be defined to allow a clear picture of the reinforcement of the specimen. However, examination of all these factors within the present research project was unrealistic. Thus, it was decided to examine the effect of reinforcement by varying the amount of reinforcement and keeping the rest of the aformentioned variables constant at values which are most likely to be found commonly in concrete substrates of existing structures (shear walls, columns, beams and slabs in order of frequency of fixing additional adhesive anchors). Hence, the specimens were designed with reinforcement matching the expected reinforcement configuration of an existing vertical load bearing member. The main parameter, however, after the completion of test series No.3, seems to be associated with the spacing of the bars, since in the case of concrete cone failure, it is this spacing which controls the geometry of failure and, hence, the ultimate pull-out values [$P_u/\sqrt{f_{cc}}$].

Thus, it makes sense to comment only on the displacement rates [$(\delta_{inl})\sqrt{f_{cc}}$] as they are illustrated in Fig.7.117, for the reinforcement scheme designed. In this figure, the specimens which showed a concrete cone failure and those which showed splitting failure form two distinct groups of results and they are considered separately. The normalized displacements in both groups show a remarkable decrease in the reinforced specimens. The decrease was substantially higher in the case of split specimens, where this decrease was calculated at an average of 20%, compared with unreinforced specimens.

7.12.11. The influence of the method of drilling, the method of insertion of resin and the eccentri city of the anchor

In one test (3.25) of test series No 3. the hole was drilled by means of a diamond drilling machine, which produces a smoother hole surface compared with a percussive rotary hand-held machine. The hole was drilled with 20mm diameter because this was the minimum diameter of the commercially available bits. Therefore the thickness of the annulus was 4 mm. In Fig.7.118 the effect of diamond drilling on the normalized ultimate values $[P_u/\sqrt{f_{cc}}]$ and on the normalized displacements $(\delta_{inl}\sqrt{f_{cc}})$ as calculated in Appendix H is shown. According to the values plotted there is a strong increase in the displacement rates, in relation to those of test 3.08 (t=4mm - percussive drilling) which is regarded as the reference test in this instance, but there is no apparent change in the ultimate pull-out value. This means that diamond drilling allows much greater slip across the interface concrete resin, and does not seem to affect the final pull-out load.

In Test 3.15 the resin was injected by an epoxy injection machine with a pressure up to 0.30 MPa, instead of being poured into the gap. The effect of this method of insertion of resin is apparent in Fig.7.118, where an increase of about 32% in the normalized pull-out value $[P_u/\sqrt{f_{cc}}]$ and a decrease of an average 30% in normalized displacements $[\delta_{nl}\sqrt{f_{cc}}]$ were calculated. This overall enhancement of mechanical behaviour can be attributed to the penetration of concrete by the low viscosity resin injected at the interfacial area which, on the one hand, improves the mechanical interlocking and, on the other, increases the

concrete tensile strength.

Finally, due to a mistake in fixing, the 12mm diameter anchor of test 3.11. was placed with an eccentricity of 3,0mm in a hole of 20mm diameter, so the opportunity arose to check this factor also, which must occur frequently in practice. A considerable decrease of 35% in normalized ultimate pull-out value [$P_u/\sqrt{f_{cc}}$] in relation to that of symmetrically placed anchor (Test 3.08) and an increase of 93% in the normalized displacement at 20 kN and of 2% in the normalized displacements at 30 kN level were found.

7.13. The stress and strain distribution in the structural components of the system

The strains in the steel, resin, and concrete were measured in 13 tests in all as can be seen in Table 7.2, by means of strain gauges of a different type for each material (Section 7.8.6). In some tests, however, a malfunction of the measuring system occurred, mainly due to badly fixed leads or defective soldering of the leads on the strain gauges. In this way, the data of resin strains were lost in two positions in Tests 3.03 and 3.05. The same happened for steel strain in one position in Test 3.03 and for concrete strain in one rosette in Test 3.01 and 3.03 and in three rosettes in Test 3.13 The rosette gauges recorded the strains along one or two directions only, in these cases.

However, this loss of information did not affect the overall definition of the strain distribution in the materials involved in the system, mainly due to the adequate number of tests monitored.

The data were processed by the data acquisition and recording system Section 7.8.7 and reported in the form of tables and curves. From the whole series of data the strains related to pull-out loads of 10, 20, 30 kN and that of failure were then selected and presented in Tables 7.14 (steel), 7.15 (resin) and 7.16 (concrete). In addition, the principal strains of concrete were calculated and tabulated (Table 7.17).

7.13.1. The steel strains

The distribution of steel strain along the axis of the anchor is illustrated in Fig. 7.122 (Test 3.01 - reference test), Fig 7.127 (Test 3.02-l=7.0d), Fig 7.130 (Test 3.03 - l=5d), Fig 7.135 (Test 3.04-plain bar), Fig 7.140 (Test 3.05 - ribbed bar) and Fig 7.142 (Test 3.15 - injected resin).

The values of steel strain at the load levels of 10, 20, 30, 40 kN are presented in Table 7.14 below.

Table 7.14. Steel strains measured [με]

Test 3.01	S16	S15	S13
P=10	740	407	184
P=20	1490	1050	496
P=30	2310	1830	905
P=33.3	2410	2250	1030

Test 3.02	S16	S15	S13
P=10	575	57	89.4
P=20	1380	5.4	310
P=25	1760	7.8	410
P=28.9	1860	-418	478

Test 3.03	S16	S15	S13
P=5		339	331
P=10		754	731
P=15		1130	1130
P=20.1		1540	1540

Test 3.04	S16	S15	S13
P=5	251	87.6	51
P=10	512	200	122
P=15	885	394	234
P=20	1190	559	643
P=22.5	745	768	537

Test 3.05	S16	S15	S13
P=10	319	237	118
P=20	793	567	257
P=20	1400	1000	470
P=35	1820	1240	619
P=38.1	2110	1320	746

Test 3.15	S16	S15	S13
P=10	737	292	146
P=20	1530	779	399
P=30	2310	1420	793
P=40	2350	2260	1310
P=45	2350	2570	1610

S13, S15, S16: Strain gauges for strain measurement at the bottom, middle and top of the bolt. For directions and positions of gauges for S13, S15, S16, see Fig 7.7

Since the gradient in steel stress towards the bottom of the hole is linearly dependent on the bond shear stress applied at the steel-resin interface, Eq.5.16, the inclination of the steel strain curve at every point indicates the size of the relevant bond shear stress with resin. For Test 3.01, Fig.7.122 in the upper critical zone, it is shown that at 20 kN the bond stress became ineffectual and the lower level bond stress was mobilized to carry the tension of the anchor. Conversely, in Test 3.02, Fig.127 there was a steady inclination of the steel strain curve in relation to the depth of the anchor. In Test 3.03, Fig. 7.130, the steel strain was invariable up to the 2/3 of the anchor length. However, since the strain gauges were densely placed due to the short anchor length in this test, the only reliable value is that of the upper gauge S16, which can be related to the calculated strain at the free section of the anchor 20mm higher. The comparison shows that the steel strain was almost constant along the first 20mm of the anchor length. For the plain anchor (Test 3.04) the slope of the strain curve, Fig.7.135, shows a gradual decrease changing to an increase in the later stages of loading for the uppermost strain, whereas the strain at the middle exhibited a decrease throughout. The same performance is shown in the anchor with injected resin (Test 3.15.)-Fig.7.142. The ribbed bar anchor (Test 3.05) exhibited a steel strain curve with an inclination increasing with load, Fig.7.140.

These considerations lead to the conclusion that anchor 3.01 (threaded bar) exhibited a bond behaviour inferior to anchor 3.02. (of the same type) throughout the whole spectrum of loading and to anchor 3.04 (plain bar) up to

22.5 kN level, anchor 3.05 (ribbed bar) throughout the test loading and anchor 3.15 (injected bar) throughout the whole range of loading.

The inferior bond performance of anchor 3.01. in relation to anchor 3.02 can be attributed to the possible existence of defects across the steel-resin interface, although this could not be proved. Despite this inferior steel-resin bond characteristic, anchor 3.01 exhibited better overall behaviour in terms of P-δ relationship due to longer embedment length. Hence, it can be concluded that the better overall behaviour of anchor 3.01 (threaded bar - l=8.3d) compared with 3.02 (threaded bar l=5d) would have been even better if this anchor 3.01 had had similar steel-resin bond behaviour to that of anchor 3.02.

The similarity of the behaviour of anchor 3.04 with 3.15 throughout its range of loading demonstrates the possible beneficial effect of micro-interlocking. This is provided by the slight oxidation of the plain bar (3.04), which is not met in the zinc electroplated steel of threaded bars. The injection of resin (3.15), which reduces the possibility of flaws across the anchor-resin interface, has also a noticeably beneficial effect on the overall bond behaviour of the anchor expressed by strong inclination of the strain distribution curve in the upper part, even in the latest stage of loading. Finally, it seems that the slight oxidation of the ribbed bar, combined with the interlocking effect of the existing ribs, leads to its relatively better overall bond behaviour.

7.13.2. The resin strains

The resin strain gauges were placed in the middle of the resin thickness and measured the normal strain in the longitudinal direction of resin (which was activated by the shear stresses across the steel - resin interface and the concrete - resin and resin - steel contact at the bottom of the hole). The resin strains measured are shown in Table 7.15.

Table 7.15. Resin strains measured [με]

Test 3.01	S12	S11	S10
P=10	100	286	382
P=20	314	506	1070
P=30	917	880	1650
P=33.3	2360	830	1780

Test 3.02	S12	S11	S10
P=10	84.6	176	442
P=20	294	626	1120
P=25	413	947	1460
P=28.9	560	1250	1760

Test 3.03	S12	S11	S10
P=5			744
P=10			1390
P=15			1820
P=20.1			2120

Test 3.04	S12	S11	S10
P=5	51	-50	-213
P=10	126	-125	-198
P=12.3	161	-161	-185
P=15	236	-236	1190
P=20	47	-1460	2340
P=22.5	955	-337	2340

Test 3.05	S12	S11	S10
P=10	60		
P=20	168		
P=20	163		
P=35	325		
P=38.1	-880		

Test 3.15	S12	S11	S10
P=10	27	117	233
P=20	60	228	606
P=30	-24	464	1380
P=40	160	260	2380
P=45	310	967	2380
P=46.3	669	-751	2380

S10, S11, S12: Resin strain gauges at the bottom, middle and top of the resin shell. Positioning of these is illustrated in Fig 7.7

The graph of resin strain versus depth of anchor has for anchor 3.01, Fig 7.121, a form different from that for anchors (3.02), Fig 7.126 and (3.15), Fig 7.141, at the later stage of loading (Anchor 3.02 according to the previous discussion exhibited better steel-resin bond behaviour than 3.01).

Because the interdependencies are complicated in the case of the resin strain, it is impossible to comment upon the measured strains in the same way as for the steel strains.

Some qualitative consideration, however, can be applied. The tensile strain in the resin depends on the steel - resin and on the resin - concrete adhesive tensile (at the bottom) and shear (lateral) behaviour, which in turn depends on the cracking state of the concrete.

It is characteristic that Anchor 3.01, which exhibited inferior performance to anchor 3.02, tends to develop high resin strains at both ends at load levels higher than approximately 25.0 kN (75% of the ultimate load) up to 30 kN. At the level of about 25.0 kN a crack is expected at point C1, Fig 7.8, (60mm deep and 10mm from the hole surface towards the concrete bulk) as is shown in Fig 7.119 where the concrete strain exceeds the ultimate concrete tensile strain of 100 με. The same is true for anchor 3.02. also, and it seems that it is the relatively better bond response of anchor 3.02, as mentioned before, which differentiates the form of the resin strain envelope in this case. Similar considerations can be applied for loads up to 30 kN to anchor 3.15, which, without doubt, exhibited very much better behaviour owing to the limitation of flaws across the interface and the penetration of concrete by the resin.

In the latest stage of loading (near the failure) the behaviour of both 3.01 and 3.15 anchors were similar.

An important point is that the maximum measured resin strain in anchor 3.15 was 2380 με, which is very much lower than the ultimate value, being found in the region of 5,000-6,000με, Figures 7.150, 7.151. This means that the

resin tensile failure occurs after the concrete failure in the combined mode, Section 7.16.

7.13.3. The concrete strains

At three points in the concrete (C1, C2, C3), Fig.7.8 the strains were monitored by means of rosette type strain gauges glued on precast mortar cubes which were accurately placed in concrete as described in Section 7.8.6. These points were selected in order to be very close to the expected failure surface of the concrete. The data obtained for each point consisted of continuous measurement of the values of concrete strains along three axes (vertical, horizontal and a third in the plane of the first two and inclined at 45° to the horizontal). From these data the principal strains and their inclination to the horizontal axis were calculated (Table 7.17).

The strains measured and the calculated principal values together with their inclination are presented in Tables 7.16, 7.17 and illustrated in a series of figures for each anchor, Fig.7.120-7.145, where the uniaxial ultimate tensile concrete strain of 100 με taken from the available literature, Heilman et al /61/, is also indicated.

Table 7.16 Concrete strains measured (με)

	Point C1			Point C2			Point C3		
3.01	εz	εy	εs	εz	εy	εs	εz	εy	εs
P=10	15	-9.6	-9.6		-84		-14.40	6.6	-14.4
P=20	37.2	-13.8	-26.4		-19.2		-18.6	-8.4	-13.2
P=30	-13.8	-27	-154		224		37.2	-6.6	31.8
P=33.3	-18.0	-1.8	-185		637		93	-10.2	51.6

	Point C1			Point C2			Point C3		
3.02	εz	εy	εs	εz	εy	εs	εz	εy	εs
P=10	12.60	-8.4	16.2	0.00	7.2	9.6	0.6	4.2	-9.0
P=20	45	-31.2	52.2	-7.2	0.0	16.80	5.4	9.6	-28.0
P=25	138	-36	146	74.4	-41.4	39.0	9.6	9.0	-59.4
P=28.9	346	-40.2	317	112	-62.4	66.6	-18	4.8	-103

	Point C1			Point C2			Point C3		
3.03	εz	εy	εs	εz	εy	εs	εz	εy	εs
P=5	4.2		68.4	-1.8	814	84	-3.6	4.8	-4.8
P=10.0	-1.2		92.4	-14.4	581	77.4	-18	8.4	-9.6
P=15.0	63.0		317	-66.6	532	126	-67.8	-3.0	-55.2
P=20.1	1570		2540	-9	535	133	-32.4	7.8	-77.4

	Point C1			Point C2			Point C3		
3.04	εz	εy	εs	εz	εy	εs	εz	εy	εs
P=5	6.6	-12.6	-6.6	10.2	-2.4	4.8	0.0	1.80	-10.2
P=10	12.0	-28.8	-14.4	27.6	-13.2	10.2	0.0	5.4	-22.2
P=15	16.2	-52.2	-21.0	49.2	-25.2	12.6	-2.4	-1.2	-30.0
P=20	9.0	-87	-21.0	42.6	-52.2	-6.6	-11.4	-12.6	-58.2
P=22.5	-4.2	-122	1.2	40.2	-60.0	-16.8	-17.4	-30	-75.6

	Point C1			Point C2			Point C3		
3.13	εz	εy	εs	εz	εy	εs	εz	εy	εs
P=10			40.2					-135	-10.2
P=20			80.4					-169	-90.6
P=30			106					-247	-33.6
P=35.9			179					-79.2	-57.6

	Point C1			Point C2			Point C3		
3.14	εz	εy	εs	εz	εy	εs	εz	εy	εs
P=10	29.4	-0.6	-7.80	14.4	-7.2	0.6	2.4	36.6	-5.4
P=20	72.6	-1.8	-19.8	9.6	3.0	9.0	5.4	64.2	-5.4
P=30	111	-113	-16.8	-116	40.8	43.8	5.4	66.6	-4.8
P=40	118	-69.0	-28.2	3.01	142	78.0	4.2	67.8	-3.6
P=50	207	-160	127	96.6	692	915	-1.8	42.6	13.8

	Point C1			Point C2			Point C3		
3.17	εz	εy	εs	εz	εy	εs	εz	εy	εs
P=5	8.4	1.2	9.6	4.2	4.8	18	0.0	0	-4.2
P=10	5.4	-13.2	14.4	78	6.0	35.2	-5.4	-12	-25.2
P=15	113	-54	82.8	29.4	6.6	42.6	-18.6	-46.8	-46.2
P=17.8	412	-80.4	272	17.4	10.8	87.6	-36	-73.2	-60.6

The Points C1, C2, C3 are illustrated in Fig 7.8,
$C_1(y_o=18,\ z_o=60)$, $C_2(y_o=40,\ z_o=50)$, $C_3(y_o=70,\ z_o=35)$,
ε_z, ε_y, ε_s:Concrete strain measured along the z (vertical), y (horizontal and s (45^o inclined to y) axes.

Table 7.17 Principal strains of concrete (με)

$e_{11}=(e_z+e_y)/2+(1/\sqrt{2})(\sqrt{(\varepsilon_z-e_s)^2+(e_s-e_y)^2}$
$e_{22}=(e_z+e_y)/2-(1/\sqrt{2})(\sqrt{(\varepsilon_z-e_s)^2+(e_s-e_y)^2}$
$\tan 2\varphi=(2e_s-e_z-e_y)/(e_z-e_y)$

$\phi=0$; how about ??
In Table 7.18

TEST 3.01

	C1					
	ε_{zz}	ε_{yy}	ε_{ss}	ε_{11}	ε_{22}	tan2φ
P=10	15	-9.6	-9.6	20.10	-14.70	1
P=20	37.2	-13.8	-26.4	57.55	-34.15	1.49
P=30	-13.8	-27	-154	113.38	-154.18	20.24
P=33.3	-18	-1.8	-185	165.41	-185.21	-21.62

C3

	ε_{zz}	ε_{yy}	ε_{ss}	ε_{11}	ε_{22}	tan2φ
P=10	-14.4	6.6	-14.4	10.95	-18.75	-1
P=20	-18.6	-8.4	-13.2	-8.39	-18.61	.06
P=30	37.2	-6.6	31.8	42.72	-12.12	-.75
P=33.3	93	-10.2	51.6	94.01	-11.21	-.20

: TEST 3.02

C1

	ε_{zz}	ε_{yy}	ε_{ss}	ε_{11}	ε_{22}	tan2φ
P=10	12.6	-8.4	16.2	19.68	-15.48	-1.34
P=20	45.0	-31.2	52.2	66.10	-52.30	-1.19
P=25	138	-36	146	179.84	-77.84	-1.09
P=28.9	346	-40.2	317	406.35	-100.55	-.85

C2

	ε_{zz}	ε_{yy}	ε_{ss}	ε_{11}	ε_{22}	tan2φ
P=10	0	7.2	9.6	10.08	-17.28	-0.72
P=20	-7.2	0	16.8	17.12	-24.32	5.67
P=25	74.4	-41.4	39	78.63	-45.63	-.39
P=28.9	112	-62.4	66.6	121.52	-71.92	-.48

C3

	ε_{zz}	ε_{yy}	ε_{ss}	ε_{11}	ε_{22}	tan2φ
P=10	.6	4.2	-9	13.94	-9.14	-6.33
P=20	5.4	9.6	-28	43.07	-28.07	-16.90
P=25	9.6	9	-59.4	78.01	-59.41	229
P=28.9	-18	4.8	-103	90.49	-103.69	-8.46

TEST 3.03

C2

	ε_{zz}	ε_{yy}	ε_{ss}	ε_{11}	ε_{22}	tan2φ
P=5	-1.8	814	84	925.92	-113.72	-.79
P=10	-14.4	581	77.4	645.32	-78.72	-.69
P=15	-66.6	532	126	550.50	-85.10	-.36
P=20.1	-9.0	535	133	564.52	-38.52	-.48

C3

	ε_{zz}	ε_{yy}	ε_{ss}	ε_{11}	ε_{22}	tan2φ
P=5	-3.6	4.8	-4.8	7.44	-6.24	-1.29
P=10	-18	8.4	-9.6	9.25	-18.85	-.36
P=15	-67.8	-3	-55.2	2.58	-73.38	-.61
P=20.1	-32.4	7.8	-77.4	55.84	-80.44	-3.24

TEST 3.04

C1

	ε_{zz}	ε_{yy}	ε_{ss}	ε_{11}	ε_{22}	tan2φ
P=5	6.6	-12.6	-6.6	7.25	-13.25	.38
P=10	12	-28.8	-14.4	12.87	-29.67	.29
P=15	16.2	-52.2	-21	16.34	-52.34	.09
P=20	9	-87	-21	12.27	-90.27	-.38
P=22.5	-4.2	-122	1.2	24.11	-150.31	-1.09

C2

	ε_{zz}	ε_{yy}	ε_{ss}	ε_{11}	ε_{22}	tan2ϕ
P=5	10.2	-2.4	4.8	10.26	-2.46	-.14
P=10	27.6	-13.2	10.2	27.82	-13.42	-.15
P=15	49.2	-25.2	12.6	49.21	-25.21	-.02
P=20	42.6	-52.2	-6.6	42.64	-52.24	.04
P=22.5	40.2	-60	-16.8	40.68	-60.48	.14

C3

	ε_{zz}	ε_{yy}	ε_{ss}	ε_{11}	ε_{22}	tan2ϕ
P=5	0	1.8	-10.2	12.04	-10.24	-12.33
P=10	0	5.4	-22.2	27.75	-22.35	-9.22
P=15	-2.4	-1.2	-39	35.41	-39.01	-62
P=20	-11.4	-12.6	-58.2	34.21	-58.21	77
P=22.5	-17.4	-30	-75.6	28.59	-75.99	8.24

TEST 3.14

C1

	ε_{zz}	ε_{yy}	ε_{ss}	ε_{11}	ε_{22}	tan2ϕ
P=10	29.4	-.6	-7.8	41.20	-12.40	1.48
P=20	72.6	-1.8	-19.8	101.97	-31.17	1.48
P=30	111	-113	-16.8	112.13	-114.13	.14
P=40	118	-69	-28.2	131.85	-82.85	.56
P=50	207	-160	127	234.21	-187.21	-.56

C2

	ε_{zz}	ε_{yy}	ε_{ss}	ε_{11}	ε_{22}	tan2ϕ
P=10	14.4	-7.2	.6	14.81	-7.61	.28
P=20	9.6	3	9	10.56	2.04	-.82
P=30	-116	40.8	43.8	75.43	-150.63	1.04
P=40	-301	142	78	192.33	-351.33	.71
P=50	96.6	692	915	994.19	-205.59	1.75

C3

	ε_{zz}	ε_{yy}	ε_{ss}	ε_{11}	ε_{22}	tan2ϕ
P=10	2.4	36.6	-5.4	49.71	-10.71	-1.46
P=20	5.4	64.7	-5.4	85.21	-15.11	-1.36
P=30	5.4	66.6	-4.8	87.01	-15.01	-1.33
P=40	4.2	67.8	-3.6	86.80	-14.80	-1.25
P=50	-1.8	42.6	13.8	43.56	-2.76	-.30

TEST 3.17

C1

	ε_{zz}	ε_{yy}	ε_{ss}	ε_{11}	ε_{22}	tan2ϕ
P=5	8.4	1.2	9.6	10.80	-1.20	-1.33
P=10	5.4	-13.2	14.4	16.63	-24.43	-1.97
P=15	113	-54	82.8	128.58	-69.58	-.64
P=17.8	412	-80	272	433.91	-101.91	-.43

C2

	ε_{zz}	ε_{yy}	ε_{ss}	ε_{11}	ε_{22}	tan2φ
P=5	4.2	4.8	18	18.01	-9.01	45
P=10	7.8	6	35.2	35.22	-21.42	-31.44
P=15	29.4	6.6	42.6	45.12	-9.12	-2.16
P=17.8	17.4	10.8	87.6	87.69	-59.49	-22.27

C3

	ε_{zz}	ε_{yy}	ε_{ss}	ε_{11}	ε_{22}	tan2φ
P=5	0	0	-4.2	4.20	-4.20	---
P=10	-5.4	-12	-25.2	8.13	-25.53	5
P=15	-18.6	-46.8	-46.2	-12.68	-51.72	1.03
P=17.8	-36	-73.2	-60.6	-35.05	-74.15	.32

In Fig.7.119 it is demonstrated that the concrete at point C1 enters the region of concrete cracking strain at a load of approximately 27.0 kN, which is equal to 75% of the ultimate anchor pull out load. At this level, point C3 (52mm further out in the radial direction and 15mm higher) shows a principal tensile strain of only 35με, far below the ultimate tensile strength of concrete. The inclination of principal strains at point C1 shows that the corresponding failure surface can not have been involved in the concrete cone at its initiation which is true but it could have been at the post-cracking stage (see Table 7.12 according to which C1 was positioned outside the cone failure, in fact about 10 mm deeper). Point C3 became critical just at pull-out.

The comparison of the inclination of principal strains at all load levels in points C1, C2, C3, between specimens 3.01 and 3.02 shows that generally there was a flatter failure surface in 3.02 that in 3.01.

Table 7.18. Inclination of the principal concrete strains to the horizontal

	Point C1		Point C2		Point C3	
P	Anc.3.01	Anc.3.02	Anc.3.01	Anc.3.02	Anc.3.04	Anc.3.02
P=20	+28	-25	-	+40	+14.6	-43.3
P=25	-	-	-	-10.7	-	+44.9
P=28.9	-	-23.7	-	-12.8	-	-41.6
P=30	+43.5	-	-	-	-	-
P=33.3	+43.6	-	-	-	-	-

* φ inclination to the vertical (positive anticlockwise).

It is indicative that for anchors 3.01 and 3.02, Table 7.16, the shear (the effect of which is described by ε_{ss}) becomes decisive at load levels above 75% of the ultimate load. This seems to have something in common with the redistribution of shear stress after the progressive shear failure at the top of the anchor.

In anchor 3.04 the concrete principal strains at all points were very much lower than the ultimate concrete tensile strain, which confirms the pull-out failure of the anchor across the steel resin interface.

In anchor 3.14 (high strength concrete), although point C1 reached the ultimate strength at about 20.0kN, point C2 entered the area of ultimate tensile strain at 31.0kN whereas the principal tensile strain at C3 was kept below 100με throughout the test loading.

In this anchor the ratio of vertical to 45^0 inclined strain for the point C1 was much higher than in Tests 3.01 and 3.02. This means that the vertical and not the shear stress mainly contributed to high values of principal stresses. This fact can be attributed to enhanced bond behaviour and to fewer microcracks in the upper part (due to

the increased concrete strength) which resulted in lower shear stresses along the anchor (see Fig 6.6, comparison between the values of shear stresses in uncracked concrete and in that with a stabilized crack).

The inclination of principal strains at failure were for Anchor 3.02 flatter than that of 3.14. in all points.

	Point C1		Point C2		Point C3	
	An3.02	An314	An3.02	An3.14	An3.02	An3.14
Spec.3.02:P=28.9kN	-23.7°		-12.8°		-41.6°	
Spec:3.14:P=50.0kN		29.2°		-30°		8.3°

Finally, in Anchor 3.17 (non-shrink grout as adhesive) Point C1 only entered the area of critical tensile strain (Fig.7.143) whereas points C2, C3 were kept below it. The anchor failed by pull-out along a cohesive grout failure and by grout failure (Fig.7.74), which in this case had an ultimate value of 100με for the particular material used.

It appears, therefore, that the concrete failed at a load of about 13.0 kN, which is equal to 73% of the ultimate pull-out value of the anchor.

7.14. The results of the direct shear tests

The tests of the direct shear were carried out on:

- Partially bonded anchors along an anchor length of usually 10mm (Fig.7.92.-7.94).
- On specimens consisting of 40 mm concrete cubes and steel parts (Fig.7.15.) as described in section 7.9.2.2.

In all tests the applied shear stress and the displacement of the anchor or the relative slip between the

components of the specimen were measured via the data acquisition and recording system already described, Section 7.8.7, by taking into account the calibration of the different components involved, Appendix E. Only one test per parameter (varying value of each parameter) was carried out.

7.14.1. Partially bonded anchors

The data obtained from these tests, Plates 38-41,were:

- The type of failure.
- The $P=P(\delta)$ and therefore the $\tau_{ac}=\tau_{ac}(\delta)$ relationship, (Table 7.19 and Fig 7.92-7.94).

Table 7.19. Summary of pull-out data of partially bonded anchors/ local bond - local slip data.

Test	Relevant specimen of series No.3	fcc [MPa]	fct [MPa]	Mode of failure	Py failure load	$\delta_{1.5}$ (μm)	$\delta_{3.0}$ (μm)	$\delta_{4.5}$ (μm)	$\delta_{6.0}$ (μm)	$\delta_{7.5}$ (μm)	$\delta_{9.0}$ (μm)	$\delta_{10.5}$ (μm)	δ_y (μm)
4.01	3.01	19.56	2.63	C	10.20	22	86	219	330	436	528		844
4.02	3.14	51.78	3.69	R+C+Spl.	10.50	174	393	609	757	923	1060	1330	1330
4.03	3.03	21.29	2.64	C	8.18	118	245	363	519	642			778
4.04	3.22	20.66	2.25	I	7.74	67	161	264	425	593			599
4.05	3.25	22.25	2.25	C	8.03	104	221	383	658	1040			1480
4.07	3.06	23.11	2.71	R	8.60	84	324	621	816	1130			1300

Modes of failure
C: concrete failure
I: interface failure
R: resin failure
Spl: Concrete splitting

Displacements
$\delta_{1,5}$-$\delta_{10,5}$: displacement at load levels 1.5kN-10.5kN.
δy: displacement at failure

These data are illustrated in the aformentioned Fig.7.92-7.94. Three anchors, anchor 4.01 (reference anchor), anchor 4.03 (adhesive of LV type) and anchor 4.05 (adhesive of GEL type) were failed with concrete cone. Anchor 4.02. failed in the splitting mode, whereas anchor 4.04 (plain bar) failed by pull-out of the anchor along the steel-resin interface. Finally anchor 4.07 (thick adhesive

layer, t=8mm) exhibited an almost pure shear failure of adhesive.

In the splitting mode of failure horizontal cracks starting from the top fibre of resin and causing a separation of the concrete cone were identified. The crack line involved aggregate-mortar interfaces for the greater part.

Anchor 4.04 (plain bar) failed at a steel-resin shear (local) stress of 20.54 MPa, which compared with the average failure shear stress of anchor 3.04 (fully bonded anchor made of plain bar) of 5.97 MPa (Section 7.11.1.), is 244% greater. Bearing in mind that the average value of the shear stress along the fully bonded anchor does not deviate too much from the maximum value of local shear stress, Fig 5.5, 6.4, this increase of 244% in shear stress strength of partially bonded anchor can only be attributed to the much more reliable insertion of resin in this case than in the relevant fully bonded anchor. As a result, the flaws across the steel-resin interface must have been strongly reduced in number and size and the interfacial shear strength increased to a large extent.

Anchor 4.07, Fig 7.94, failed at a load of 8.6 kN, which corresponds to a shear stress of 22.82 MPa at the resin - steel interface or a principal stress of 32.18 MPa in the resin.

All the anchors except Anchor 4.01. were designed to be bonded along a 10mm length. This length was actually 13mm for Anchor 4.01. Thus, there was a need to convert the values of δ found for anchor 4.01 to the equivalent for an idealized Anchor 4.01 with 10mm length. The correction, Appendix I, was based on the relationships reported in

section 7.12.4. In Fig.7.146.a the corrected relationship $\tau=\tau(\delta)$ is illustrated by the dashed line. In anchor 4.03., the bolt was found to be eccentrically placed with a deviation of 1.00mm from symmetrical position. The correction made, Appendix I, was based on section 7.12.11. and the corresponding curve is illustrated in Fig.7.146.a.

As can be seen in Fig.7.92-7.94 where a regression analysis is made for the curve fitting to each test, anchor 4.01 (reference anchor) exhibited an almost linear behaviour in terms of $\tau=\tau(\delta)$ law.

The behaviour of anchor 4.02 with split concrete cone and that of anchor 4.03 (LV adhesive), were the same, whereas the law for the anchor 4.04 (plain bar) was deviating from linearity with continuously decreasing stiffness. The use of a gel type of adhesive, Test 4.05, led to a significantly flatter curve which is better defined by a logarithmic function. The increased thickness (Test 4.07) resulted in a more ductile behaviour expressed by a power function with an exponent significantly higher than 1.0.

The effects of the different variables are shown in Fig.7.146. The use of LV type of adhesive caused a stiffer local bond - local slip relationship in general, whereas, the use of GEL type a less stiff one, Fig.146a. Both effects were the same as the effect of these variables on the overall slip of the fully bonded anchor, Fig.7.95. The plain bar, although showing a somewhat stiffer characteristic, Fig.7.146.b, failed at a lower level of shear. This behaviour is similar to that of the fully bonded anchor, Fig. 7.97. The 8mm thickness of resin caused less stiff behaviour in terms of local bond-local slip law

(Fig.7.146.c) as was the case for the overall load-overall slip relationship, Fig.7.101 for the same thickness. Finally, the specimen which failed by splitting mode exhibited less stiff behaviour than that of concrete cone failure in terms of $\tau=\tau(\delta)$ law, Fig.7.146.d, in almost the same way as the corresponding fully bonded anchors, Fig.7.106.

The comparison between the data obtained and those reported by Eibl et al, /5/, is illustrated below:

Table 7.20. Comparison between the results of partially bonded anchors reported by Eibl et al /5/, and those of the present work

	δ[μm]	δ[μm]	δ[μm]	δ[μm]	δ[μm]
τ[MPa]	According to Eibl et al /5/	According to pres. work	According to pres.work after the correction due to l= (3.6)d	According to pres.work after the correction due to strength f=800	According to pres.work after the correction due to presence of compressive stress
(a)	(b)	(c)	(d)	(e)	(f)
5.0	6	60	15	6	6
10.0	8	200	50	19	19
15.0	12	650	130	50	50
20.0	40	1200	300	114	114

Remarks
The values of δ[μm] according to present work are progressively and accumulatively corrected, columns d-f.

The final differences between the values reported and those of present work, columns b and f, are caused by the effects of:

a) the different bonding length (which in the work of Eibl et al /5/, was 36mm instead of 10mm in present work),

b) the different geometry of specimens (200mm cubes with a 75mm hole filled with polymer concrete of 70 and 100 MPa compressive strength in the work of Eibl et al)

c) the difference in compressive strength of the

material surrounding the anchor

d) the kind of adhesive which was epoxy resin in the present work and polyester mortar in reference /5/

e) the size of specimen which, in the case of reference /5/, allowed the presence of a field of compressive stresses around the bonded part of the anchor.

7.14.2. The direct shear tests

Three different types of double direct shear tests were carried out, i.e. tests in which:

- the concrete - resin - concrete interface,
- the concrete - resin - steel interface, and,
- the interface involving steel - resin - steel,

were sheared.

For all the tests the data obtained were:

- The type of failure.
- The $\tau = \tau(\delta)$ relationship.

In the tests of the first series (concrete to concrete adhesive joint) a concrete failure was commonly involved. The detailed mode of failure for each test is shown in Table 7.21. In the second series (concrete to steel joint) the type of failure was usually adhesive failure which, in Test 4.19, also involved resin failure.

In the third series (steel to steel joint) the failure was a typical adhesive failure.

The $\tau=\tau(\delta)$ relationship for every system was obtained in the form of continuous recording of pairs of P and δ values, Table 7.21, and in the form of P-δ curves, which then were converted into $\tau=\tau(\delta)$ curves, illustrated in Fig.7.147, 7.148, 7.149.

In the concrete-resin-concrete adhesive joint, the increasing thickness of resin caused larger displacements and higher ultimate local bond stress in general.

The GEL type of adhesive caused a lowering of the ultimate local shear stress and a significant increase in displacements, whereas the LV type caused slightly stiffer behaviour with slightly higher ultimate shear stresses.

In the concrete-resin-steel adhesive joint the effect of GEL type of resin was the same whereas the increase of the minimum resin nett thickness led to increased displacements initially, which then (at a stress level of approximately 8.0 MPa) became smaller in relation to those corresponding to t=2mm minimum resin thickness.

It must be pointed out, however, that in this case the effect of the resin between the threading is unknown and might have influenced the overall response of the adhesive joint.

Finally, the local displacements of steel-resin-steel interfaces were found of the same size of order in relation to the ones of the concrete - resin - steel and concrete - resin - concrete interfaces.

Table 7.21. Direct shear tests

TESTS 4.09.-4.13./Concrete-Resin - Concrete direct shear

	TEST 4.09*		TEST 4.10		TEST 4.11		TEST 4.12		TEST 4.13	
	C1380/t=2mm		C1380/t=8mm		C1380/t=2mm		LV/t=2mm		GEL/t=2mm	
P [kN]	τ[MPa]	δ[μm]	τ[MPa]	δ[μm]	τ[MPa]	δ[μm]	τ[MPa]	δ[μm]	τ[MPa]	δ[μm]
1.0	2.39	614	1.23	800	1.04	108	1.04	168	0.975	847
2.0	4.78	1020	2.46	1220	2.08	340	2.08	340	1.95	1240
3.6	7.17	1237	3.69	1480	3.12	619	3.12	550	2.93	-
4.0	9.56	-	4.91	1780	4.16	760	4.16	570	3.9	-
5.0	11.95	-	6.15	1980	5.2	842	5.2	630	4.88	-
6.6	14.34	-	7.37	2120	6.24	933	6.24	670	5.85	-
7.0	16.73	-	8.60	2190	7.28	988	7.28	720	6.83	-
8.0	19.12	-	9.83	2290	8.32	1060	8.32	780	7.8	-
9.0	21.51	-	11.06	2110	9.36	-	9.36	840	8.77	-
10.0	23.9	-	12.29	2600	10.4	-	10.43		9.75	-
Py	3.21	1270	10.2	2700	8.61	1120	96.4	870	2.63	1420
(τ_y)	(7.67)		(12.04)		8.95		(10.02)		(2.56)	
Interface: [mm]x[mm]	38X11mm		37X11		37X13		37X13		38X13.5	
Mode of failure	1st Inteface		1st Interface		1st Interface		1st Interface		1st Interface	
	100% Adhes.		100% Adhes.		50% Adhes. 50% Concrete		100% Adhes.		30% Adhes. 30% Resin 40% Concrete	
*One interface only	2nd Interface		2nd Interface		2nd Interface		2nd Interface		2nd Interface	
	95% Adhes. 5% Concrete		90% Adhesive 10% Concrete		50% Adhes. 50% Concrete		50% Adhes. 50% Concrete		30% Adhes. 30% Resin 40% Concrete	

TESTS 4.14, 15, 19 Concrete-Resin - Steel direct shear

	TEST 4.14 (Ref.test)		TEST 4.15 (t=3.5)		TEST 4.19 (GEL)	
P [kN]	τ[MPa]	δ[μm]	τ[MPa]	δ[μm]	τ[MPa]	δ[μm]
1.0	1.25	287	1.25	410	1.25	573
2.0	2.50	570	2.50	700	2.50	1040
3.0	3.75	870	3.75	810	3.75	1537
4.0	5.00	1200	5.00	930	5.00	1960
5.0	6.25	1270	6.25	1000	6.25	2390
6.0	7.50	1370	7.50	1075	Py=5.11	2420
7.0	8.75	1480	8.75	1150		
8.0	10.00	1540	10.00	1330		
9.0	11.25	1570	11.25	1440		
10.0	12.50	1650	12.50	1520		
11.0	13.75	1700	Py=13.80	1570		
12.0	15,00	1750				
13.0	16.25	1830				
14.0	17.50	1920				
14.3	17.88					
Mode of failure	100% Adhesive		100% Adhesive		50% Adhesive 50% Resin	

TEST 4.20 Steel-Resin-Steel direct shear

[kN] P =	1.0	2.0	3.2	4.0	5.0	6.0
[kN] δ =	227	441	615	697	1097	1125
[MPa] τ =	1.25	2.50	3.75	5.00	6.25	7.50

7.15. The results of resin tensile tests

The P=P(ε) curves for the epoxy resins of types C1380 and LV are shown in Figures 7.150 and 7.151. As can be seen, both types of resin exhibited an almost linear behaviour up to yield, which for type C1380 took place at 12.94 MPa whereas for resin of type LV it occurred at 12.48 MPa. The latter, however, showed a modulus of elasticity of 2340 MPa while for the former this value was 2157 MPa.

7.16 Sequence of the failure in the combined mode of failure

The analysis of the distribution of concrete principal strains obtained, Table 7.17, showed that, apart from Anchor 3.03 (l=5 d), in the anchors which failed by concrete cone failure (Anchor 3.01-Fig 7.119, Anchor 3.02-Fig 7.123, Anchor 3.17-Fig 7.143) at the most critical point monitored (for Anchor 3.01 and 3.17 60% of the embedment length deep and for Anchor 3.02 70%), the concrete principal tensile strain first exceeded the ultimate tensile strain of 100 με at about 75% of the ultimate pull-out load. In Anchor 3.14 (C50), although the first crack must have occurred at a load level of about 40% of the ultimate pull-out load, the strain corresponding to 75% of the load was 125 με, very close to the crack strain of 100 με.

For the epoxy bonded anchors this means that:

The anchor 3.01 cracked at a point (0.6)l deep at

$P \approx 25$ kN/$P_{ult} = (33.3)0.75$

The anchor 3.02 cracked at a point (0.7)l deep at

$P \approx 22$ kN/$P_{ult} = (28.9)0.75$

At this load level the corresponding values of slip were:

Anchor 3.01: 745 μm

Anchor 3.02: 764 μm,

as can be seen from the corresponding P=P(δ) relationships, Fig 7.58 and 7.59 respectively, or calculated upon the fit curves given in Table 7.13.

This, according to Eq.(5.2), (5.3), by taking $w_s = 745$ or 764 μm, implies that in both cases the local steel-resin slip $\delta_{s,r}$ is lower than 1125 μm, which is the ultimate slip for the steel-resin interface, Fig 7.149. The same is true for the concrete-resin interface with critical value 1237 μm as can be taken from Test 4.11, Fig 7.147.

In addition, if the theoretical and finite element analyses were considered, at the moment of the first crack (P=25 kN, for the standard anchor with l=(8.3)d) the interfacial concrete-resin and steel-resin shear stresses would be:

- according to theoretical analysis:

$\tau_{c,r} = (1.91)(25/10) = 4.85$ N/mm^2,

$\tau_{s,r} = (4.85)(16/12) = 6.47$ N/mm^2

- according to finite element analysis:

$\tau_{c,r} = (1.78)(25/10) = 4.45$ N/mm^2,

$\tau_{s,r} = (4.45)(16/12) = 5.93$ N/mm^2

Both values are below the ultimate values of $\tau_{c,r}$=8.95 N/mm^2 and $\tau_{s,r}$=7.50 N/mm^2 obtained from the tests, Table 7.21.

The last two criteria (anchor slip at cracking below the ultimate slip and calculated interfacial shear stress below the corresponding ultimate value) imply that concrete fails before the bond between concrete and resin enters the critical state.

The resin-steel bond enters criticality at slip values of $\delta_{s\,r}$=1125 μm, corresponding to τ=7.50 N/mm^2, Table 7.21, Test 4.20. At this moment the slip between concrete and resin is δ=1069 μm (as can be taken from Fig.7.147, for $\tau_{s\,r}$=5.62 N/mm^2, because $\tau_{c\,r}=\tau_{s\,r}(d/d_o)=(7.5).(12/16)$=5.62 N/mm^2, Section 5.2).

The pull-out load which had caused this value of the interfacial shear stress, would have been:

- according to finite element analysis:

  P = (5.62/1.78)10 = 31.5 kN

- according to theoretical analysis:

  P = (5.62/1.91)10 = 29.2 kN

and the corresponding resin strain:

$\varepsilon_{r\,o}$=1730 με, according to the P=P(ε_r) relationship experimentally obtained, Fig 7.121, for P=31.5 kN.

Yet this value of 1730 με of resin strain calculated at the moment of the interfacial bond failure is less than the ultimate strain of the particular resin obtained by tests, which was equal to 6000 με for C1380, Fig 7.150. This means that the bond failure takes place before the resin enters criticality.

Thus, the overall conclusion is that the sequence of the failure of the particular components in the combined mode of

failure, is:

- concrete failure
- bond failure in the remaining embedment
- resin tensile fracture

7.17 Concluding remarks

Five series of tests were carried out in all.

- The aim of series No 1 was to decide upon the size of specimen in accordance with BS 5080 Part 1-1974, and the way of fixing the strain gauges for concrete and steel.
- Series 2 involved 7 tests. The aim of this series was to check the final size of specimen in relation to the anchor diameter and to identify the effect of the main parameters, which were then considered in the design of the main test series (No 3).
- Test series No 3 consisted of 34 tests of fully bonded adhesive anchors the main purpose of which was to examine the influence of the following parameters:
  1) The concrete strength
  2) The embedment length of the anchor
  3) The thickness of resin
  4) The diameter of the anchor
  5) The type of anchor
  6) The type of resin
  7) The method of drilling the hole
  8) The amount of reinforcement in concrete
  9) The size of the specimen

10) The method of inserting the resin into the gap

- Test series No 4 comprised 7 tests of partially bonded anchors, along a bonding length of 10 mm, and 9 tests of direct double shear tests. The aim of the partially bonded anchor test was to formulate the local bond - local slip relationship for the fully bonded types of anchors. The aim of the direct double shear tests for the concrete - resin - concrete, concrete - resin - steel and steel-resin-steel interfaces was to find the local bond - local slip relationships for these interfaces. The results of this test series fed back the theoretical analysis (Chapter 5) and the finite element elastic analysis of the specimen used (Chapter 6).
- The aim of test series 5 was to provide data on the tensile stress- strain properties of resins used.

The presentation and discussion of the results obtained in the main series No 3, were conducted according to the following major characteristics of the mechanical behaviour of the anchor:

a) Mode of failure (combined, involving concrete double cone failure, concrete splitting, adhesive failure, steel failure)
b) Fundamental relationship of load to displacement of the anchor, $P=P(\delta)$

c) Stress and strains of all the anchor components (steel-resin-concrete)

A detailed discussion of the influence of the parameters on the failure characteristics was presented, the main points of which are:

a) A substantial decrease in embedment length results in increase in the value C_r, the average value of cone height normalized with respect to embedment length, that is:

$$C_r = C_1 + C_2 / 21$$

where:

C_1 :maximum value of cone height measured

C_2 :minimum value of cone height measured

l :embedment length

b) C_r values increase with decreasing anchor diameter.

c) Increased in resin thickness leads to an increase in the values C_r and in the cone base.

d) An increase in concrete strength causes shallower and steeper concrete cones which have single rather than double conical lateral surface.

e) The same effect as above is found with the insertion of resin by means of injection.

f) Ribbed bars lead to shallower concrete cones in relation to those of threaded anchors.

g) Reinforcement of the concrete results in shallower concrete cones.

h) The same effect is found with the reduction of the size of the specimen.

In all the split concrete specimen cracks starting at a point (0.20-0.25)l deep and going upwards at 30° - 45° were found. These cracks cause an increase in the radial pressure across the concrete-resin interface. Thus, concrete splitting becomes more likely.

The effect of the parameters on the constitutive law P=P(δ) was discussed by means of the fit curve for each relationship obtained experimentally. However, since the concrete strength had different values in almost all the tests, a parameter was sought which could incorporate this variation, and which then would be the basis for the examination of the effect of the rest of the parameters.

Thus, it was found that the values of $Pu/\sqrt{(f_{cc})}$ of ultimate pull-out load normalized with respect to concrete strength are almost independent of the concrete strength. The values $[(\delta_{10in1})\sqrt{(f_{cc})}]$, $[(\delta_{20in1})\sqrt{(f_{cc})}]$ and $[(\delta_{30in1})\sqrt{(f_{cc})}]$ of the anchor displacement normalized with respect to the concrete strength were found to be linearly dependent on the concrete strength.

The influence of the rest of parameters was examined against these normalized values of P_u and δ. Thus, it was found that:

- The ratio of embedment length to anchor diameter is dependent on the normalized value $P_u/\sqrt{(f_{cc})}$ with a second order function up to a value of about 8. Above this limit it seems that the l/d ratio has no effect at all (Fig.7.110). This ratio has an almost linear relationship with the normalized values

$[(\delta_{10in1})\sqrt{(f_{cc})}]$ and $[(\delta_{20in1})\sqrt{(f_{cc})}]$, Fig. 7.111, causing by its decrease an increase in normalized displacements.

- By decreasing the anchor diameter there is an almost linear decrease in $P_u/\sqrt{(f_{cc})}$ down to a certain limit, Fig. 7.112. Below this limit the relationship $[P_u/\sqrt{(f_{cc})}]$-d, changes to a curve of higher order. Decreasing diameters cause a higher order increase in the normalized values of displacements at 10 KN and 20 kN loading $[(\delta_{10in1})\sqrt{(f_{cc})}]$, $[(\delta_{20in1})\sqrt{(f_{cc})}]$, Fig. 7.112.
- Increased thickness of resin causes an increase in $P_u/\sqrt{(f_{cc})}$ up to a value of ratio of resin thickness to anchor diameter of about 0.4. Above this value there seems to be no influence at all, Fig. 7.113. Increased thickness results also in a decrease in the values $[(\delta_{10in1})\sqrt{(f_{cc})}]$, $[(\delta_{20in1})\sqrt{(f_{cc})}]$ $[(\delta_{30in1})\sqrt{(f_{cc})}]$ up to a t/d ratio of approximately 0.60 and in an increase of these values for t/d > 0.60.
- From the different types of anchors used, the ribbed bar anchors exhibited the higher $P_u/\sqrt{(f_{cc})}$ and the lower $[(\delta_{10in1})\sqrt{(f_{cc})}]$, $[(\delta_{20in1})\sqrt{(f_{cc})}]$ values.
- The highest $P_u/\sqrt{f_{cc}}$ values and the lowest $[(\delta_{10in1})\sqrt{(f_{cc})}]$, $[(\delta_{20in1})\sqrt{(f_{cc})}]$ and $[(\delta_{30in1})\sqrt{(f_{cc})}]$ values were shown by the LV type of a low viscosity resin, whereas the lowest normalized load values and the highest

normalized displacements by the GEL type of resin, Fig. 7.115.

- The size of specimen affects to a high degree the normalized pull-out values $P_u/\sqrt{f_{cc}}$. There has been shown to be a considerable decrease in above value with decrease in the size of the specimen, Fig. 7.116. There is also a decrease in the values of displacements $\delta_{j1n1}\sqrt{f_{cc}}$, normalized with respect to concrete.

- Since the reinforcement ratio was varied in only two tests and because the concrete cone seemed to be controlled by the spacing of bars, there is some reservation in commenting on the effect of reinforcement on $P_u/\sqrt{f_{cc}}$ values, although it is doubtless positive. The influence of the increasing reinforcement ratio on the decrease in normalized values of the displacements $\delta_{10in1}\sqrt{f_{cc}}$ and $\delta_{20in1}\sqrt{f_{cc}}$ was more apparent in the split specimens, Fig. 7.117.

- There was found to be a decrease in the $P_u/\sqrt{f_{cc}}$ and an increase in $\delta_{10in1}\sqrt{f_{cc}}$, $\delta_{20in1}\sqrt{f_{cc}}$ and $\delta_{30in1}\sqrt{f_{cc}}$ values due to possible eccentricity of the anchor in relation to the hole axis and due to the diamond boring instead of percussive boring. Conversely, the injection of resin caused a substantial increase in the normalized pull-out values and an equally considerable decrease in the normalized displacement value, as expected.

Finally, the profiles of strain distribution of resin

and steel were drawn. The main characteristic of these profiles is that there is generally a decrease in steel strain towards the bottom of the anchor, as expected, whereas the opposite is true for the resin tensile strain. The maximum resin tensile strain in the most critical area just before failure of the anchor, however, was found to be far lower than the ultimate value.

The concrete principal strains were calculated at particular points which were designed to be near the failure surface. The analysis of the distribution of concrete strains, showed that in the anchors which failed in the combined mode at the most critical point monitored (at a depth of (0.6)l) the concrete principal strain first exceeded the ultimate tensile strain at a load level of about 75% of the pull-out load at failure.

This load can be regarded as the generalized cracking load.

The sequence of failure of the different links in the combined mode is:

- concrete failure
- bond failure
- resin fracture

The constitutive laws $\tau=\tau(\delta)$ for the partially bonded anchors show a remarkable similarity to those for the fully bonded anchors for each particular parameter examined.

The constitutive relationship $\tau = \tau(\delta)$ for the direct double shear tests were, for thin resin with low viscosity, almost linear for both the concrete - resin and resin - steel interfaces.

The tensile stress - strain relationship of the low viscosity resins used was found to be linear, as expected.

8. PRESENTATION AND DISCUSSION OF THE STRESSES AND STRAINS DERIVED FROM THEORETICAL AND FINITE ELEMENT ANALYSIS, AND EXPERIMENTAL VALUES

In this section the results (stresses, strains and displacements of steel, resin and concrete) obtained from:

- theoretical analysis,
- finite element analysis,
- experimental programme

are compared so that similarities and differences may be identified and discussed.

In order to discuss comparable physical quantities and properties, the model analysed was exactly the same as the standard experimental specimen (specimen 3.01).

The comparison of the stresses and strains was made for the pull-out load levels of 10kN, 20kN and 30kN. Since both the theoretical and the finite element analysis were elastic, the stress and strain distributions for P=20kN and 30kN were calculated proportionally from those derived from the analyses for P=10kN. The stress and strain distributions and the anchor displacement of the theoretical analysis are shown in Sections 5.2, 5.3, Figures 5.4, 5.5, and Appendix A.4. Those of finite element analysis are shown in Figures 6.3, 6.4, 6.5 and 6.6.

The relevant experimental results were stated in Sections 7.13.1 (steel strains), 7.13.2 (resin strains), 7.13.3 (concrete strains) and in Tables 7.14 (steel strains), 7.15 (resin strains), 7.16 (concrete strains), 7.17 (concrete principal strains) and 7.18 (inclination of principal strains).

In order to facilitate the comparison, Figures 8.1 and 8.2 are drawn, in the first of which the strains of steel and resin and the anchor displacements are shown, whereas in the second the shear stresses in the resin-concrete interface and the strains in the surrounding concrete are illustrated.

8.1. Discussion of steel and resin strains, anchor displacements and interfacial shear stress distribution.

As can be seen from Fig 8.1. the values of strains and stresses calculated by the finite element analysis are in good agreement with those calculated by the theoretical analysis and the experimental results. A comparison shows that:

The steel strains derived from the finite element analysis are closer to the experimental values than those derived from theoretical analysis for P=10kN and P=20kN. At P=30kN the strains derived from both analyses deviate more from the strains measured experimentally. When viewed against the values calculated by theoretical analysis, the values computed show a maximum divergence of 3% at the upper part of the anchor. When compared with the values obtained experimentally they show a difference of 17% at the uppermost strain gauge position for P=10kN, 17% for P=20kN and 20% for P=30kN, Fig. 8.1 (a). The difference is greater at higher external loads because of the progressive cracking of concrete, which was not taken into account in the finite element analysis. The same is true for the results of theoretical analysis also.

The resin strains derived from theoretical analysis,

show a deviation of 48% from the values obtained by tests in the middle, but tend to be closer in the lower half of the anchor at low load levels, (P=10kN), Fig 8.1.b. They diverge considerably from them in the upper part of the anchor (maximum difference 56% for P=10kN). It must be mentioned that, for sake of simplicity , in the theoretical analysis the resin tension was regarded as very low in relation to that of steel or concrete and omitted because the ratio $(E_r A_r)/(E_s A_s)$ was negligible in relation to $(E_c A_c)/(E_s A_s)$. Section 5, Eq.(5.11), Eq.(5.12). At higher loads, however, the quantity $(E_r A_r)/(E_s A_s)$ becomes greater in relation to $(E_c A_c)/(E_s A_s)$ because the modulus of elasticity of concrete decreases due to progressive cracking, and thus the assumption made diverges from reality.

The resin strains derived from the finite element analysis were higher than those obtained experimentally in the upper half of the anchor (maximum divergence of 62%), whereas, they were lower than these in the middle and lower part (difference -65%) for low load (P=10kN), Fig 8.1.b. This divergence increases with a progressive increase in loading, becoming maximum for loads near the ultimate load, and might be attributed to two factors. The first is related to the elastic properties of tensile links between steel and resin at the bottom, which were taken into account in the finite element analysis, Section 6.2. They had a coefficient (spring constant) equal to 2a, where a is the coefficient of the $\delta=a\tau^m$ relationship of the shear slip elements across the steel-resin and resin-concrete lateral interfaces. The lower the values of a, the greater the resin strain becomes Fig 6.3, model

I.1. Thus, this coefficient should be corrected towards values around a. The second factor causing low values of resin strain computed by finite element analysis could be that the resin thickness in the finite element analysis was taken as 2 mm, whereas, the real average thickness is about 2.6 mm due to identation of resin in the thread of the anchor. Yet, the thicker the resin layer, the higher its strain (finite element analysis - model II). Thus, if the thickness of resin had been taken as 2.6 mm, substantially higher values of resin strain would have been found.

The values of interfacial shear stresses along the concrete-resin interface were only calculated by theoretical and finite element analyses. The comparison shows a difference with changing sign from the top to the bottom of the anchor. The absolute value of this difference in the uppermost point is 32%, dropping to 22% at a depth of 10mm and to less than 10% along the remaining 90% of the anchor length.

The displacement of steel derived from theoretical analysis at P=10kN was 0.257 mm, that from finite element analysis 0.337 mm and the experimental value 0.267 mm, which is between the above values but closer to that calculated theoretically, Fig 8.1. More specifically the displacements of the steel anchor at P=10kN were calculated as 0.337 mm for the standard model, 0.305 mm for that with resin thickness of 4 mm, 0.439 mm for that with anchor diameter of 8 mm, 0.367 mm for the model with a full depth crack starting at 0.2 l and 0.337 mm for a stabilized crack starting at the same point, Fig 6.3. The values of the anchor slip measured experimentally at P=10kN were 0.267 mm

for the standard model, 0.822 mm for the anchor with 8 mm diameter, 0.140 mm for the anchor with 4 mm thickness of resin and 0.523 mm, average for all split specimens, Fig 6.3. There is a good agreement for the standard model and for that with a fully developed crack starting at a depth of (0.2)1. Whereas, there is a considerable difference in the case of anchor diameter of 8 mm and resin thickness of 4 mm.

The comparison of the anchor displacement derived from finite element and theoretical analyses at the standard model at P=20 and 30kN with those obtained experimentally is shown in Fig 8.1.c. There is still good agreement between the calculated and measured displacements.

The analysis confirms that small diameters and cracks lead to great displacements of anchors. The accuracy of the steel displacements of the standard model computed can be slightly improved by increasing the stiffness of the tensile slip elements bridging the steel-resin and resin-concrete elements at the bottom of the anchor, Fig 6.3.d. Their stiffness was calculated upon the assumption that in the law $\delta=a_t\sigma$ the coefficient a_t has a value double the corresponding a of the $\delta=a\tau$ law, for the lateral slip elements.

8.2. Discussion of concrete strains.

The concrete radial strains, ε_{yy}, calculated by the finite element analysis in a radial section at a distance of 18mm from the anchor axis and at a depth of 60mm, representing the centre of concrete strain gauge, show a difference of 25% at P=10kN, 71% at P=20kN, and 33% at P=30kN over them measured. For the vertical concrete strains ε_{zz} these differences were 37% at 10kN, 49% at 20kN

and there was a change of sign at 30kN at this particular point. The concrete tangential strains, ε_{xx}, were not measured. The comparison between the values of concrete radial strains calculated theoretically with those measured at the particular point, shows a difference of 27% at P=10kN, 0% at P=20kN and 22% at P=30kN in radial strain. The vertical strains calculated deviated by 7% at P=10kN and 22% at P=20kN from those measured, whereas they changed from negative to positive at P=30kN.

The differences in the latter can be attributed to the assumption made that the shear stress distribution across the concrete boreface can be simulated for the Mindlin solution by three concentrated vertical forces acting at depths of 16.5mm, 49.5mm and 84mm in the z axis. It is reasonable to expect a better approximation with the use of a greater number of concentrated vertical forces simulating the interfacial shear stress action on the concrete boreface.

8.3. Summary of main comparison

There are differences in the strains of the anchor components calculated by theoretical and finite element analysis and those measured.

More specifically, for the results of finite element analysis:

- The differences between steel strains derived from the analysis and those measured were dependent on the external load level ranging for the middle of the anchor from 5% at P=10kN to 37% at P=30kN (with the values measured being higher).

- The relevant resin strains were from (62%) higher (in the upper part of the anchor at 10kN) to 48% lower (in a point 50 mm deep under pull-out load of P=30kN) than the measured ones.
- The corresponding radial concrete strains computed at a section extending 18 mm from the axis were found to be between 25% and 71% higher than those measured, depending on the external load.
- The vertical concrete strains computed in the same section were found to be 37%-49% lower than those measured up to P=20kN, and changed sign at P=30kN.
- The anchor displacement calculated was 26% higher than the one measured in the standard model, 118% higher than the corresponding one in the case of resin thickness of 4 mm, 35% lower in the case of split specimens (initiation of split by an upwards directed crack reaching the surface and starting at 0.21) and 46% lower than the value measured in the case of 8 mm anchor diameter, Fig 6.3.

For the strains derived theoretically, the differences over those measured were also dependent on the pull-out load level as expected.

- The steel strains calculated were lower than those measured by between 10% at P=10kN and 40% at P=30kN, in the middle of the anchor.
- The relevant range for the resin strains was between 48% maximum at P=10kN and 50% at P=30kN

in the middle of anchor, the measured values always being higher.

- The respective concrete radial strains, ε_{yy}, calculated were lower than those measured by between 27% at P=10kN and 22% at P=30kN.
- The vertical concrete strains, ε_{zz}, calculated theoretically were found to be lower than those measured, about 7% at P=10kN and 22% at P=20kN, whereas they changed sign at P=30kN.

The comparison between the tangential concrete strains, ε_{xx}, derived from the two analyses shows that the values calculated theoretically were 114% higher than those obtained from finite element analysis at the upper most point examined (5 mm deep), and they tend to be lower towards the bottom of the anchor, Fig 8.2.

The comparison of the distribution of the interfacial shear stress calculated theoretically with that obtained from the elastic finite element analysis shows differences of 32% maximum. The theoretically derived values were higher in the upper part and, in the lower part of the anchor, lower than those computed by the finite element analysis.

8.4 Prediction of the failure mechanism

Assuming that the behaviour of an anchor system remains linearly elastic up to failure, it is possible to predict the pull-out load, which causes the first crack in concrete using as failure criterion the ultimate tensile principal strain on a plane involving the anchor axis.

From both analyses the concrete radial and vertical

stresses and strains at different sections and the vertical shear stresses on planes involving the axis were derived. Thus, the principal tensile stresses and strains can be calculated for the examined load level of P=10kN at these sections.

The pull-out load which causes the first crack in each section is proportional to P=10kN with the ratio of the ultimate tensile concrete strain to the principal tensile strain at P=10kN. The ultimate concrete tensile strain according to Heilman et al /61/, can be taken as 100 με. The minimum value of the loads calculated in this way in the different sections examined will be the critical cracking load of the system.

In a similar way, the load causing bond failure can be calculated from the ultimate value of shear stress derived from test series No 4, Fig 7.147, 7.149 and the load causing the resin tensile failure from the critical resin strain obtained from test series No 5, Fig 7.150, 7.151.

The sequence of failure in the combined mode is governed by the weakest link (concrete tension-interfacial bond-resin tension).

Thus, according to finite element analysis, this first crack load was calculated as P_{cr}=10(100/64.6)=15.5 kN, Appendix C.3. whereas, according to theoretical analysis as P_{cr} = 10(100/26.8) = 37.3 kN, Appendix A.4.6.7.

For the same model the corresponding bond failure was calculated, on the assumption that all mechanisms were operative, as:

P_b = (8.95/1.79)10 = 50.0 kN, according to finite element analysis and Table 7.21

and

P_b = (8.95/1.91)10 = 46.85 kN, according to theoretical analysis

where:

8.95[N/mm²]: the critical concrete-resin interfacial shear stress

1.79[N/mm²]: the value of concrete resin shear stress, at z=60 mm deep, theoretically calculated

1.91[N/mm²]: the value of concrete resin shear stress, at z=60 mm deep, computed by finite element analysis

12/16[mm] : the steel and hole diameter, Section 5.2

The relevant pull-out loads leading to the critical values of tensile strain of resin (on the assumption that all mechanisms i.e. concrete tension, interfacial bond, resin tension were operative) were:

P_r = (1780/134)10 = 132.8 kN, after the finite element analysis

and

P_b = (1780/300)10 = 59.3 kN, after the theoretical analysis which is closer to the experimental results in the lower part of the anchor

The value of 1780 με of resin strain at failure was taken from Fig 7.121.

The critical tensile load the resin alone can carry is calculated as:

P_{tr} = ($\pi(16^2-12^2)/4$)(6000.10^{-6} 2157) = 1.14 kN

The prediction of the split load can be calculated in

the same way from the tangential tensile strain of concrete, which were calculated by both the theoretical and finite element analysis. Thus,

$$P_{split} = (100/\varepsilon_{xx})10 \text{ [kN]}$$

And for the particular example analysed

$$P_{split} = (100/22)10 = 45.45 \text{ kN},$$

according to finite element analysis and

$$P_{split} = (100/16)10 = 62.5 \text{ kN},$$

according to theoretical analysis.

The above considerations lead to the following sequence of failure according to finite element analysis:

- cracking of concrete (at P_{cr}=15.5kN)
- bond failure (up to 50kN according to theoretical analysis)
- resin tensile failure (up to the failure of the system)

For the particular model analysed the combined mode took place because the corresponding cracking load of concrete is lower than the split load.

8.5 Concluding remarks

The profiles of steel strain distributions along the anchor obtained experimentally are in good agreement with those predicted by the theoretical and finite element analysis (differences in the region of 5%-40%) for the middle of the anchor. The same is almost valid for the anchor displacement of the standard model.

The corresponding resin strain values varied to a higher degree (differences about 45%-50% at P=10kN between the values measured and those calculated by finite element or

theoretical analysis).

The theoretically, or by finite element analysis, calculated radial and vertical concrete strains are in good agreement with those computed by finite element analysis and exhibit a difference 0%-49% in relation to those measured, with only one exception (radial strain at P=20kN which was 71% higher than the value measured).

Finally, the comparison between the tangential concrete strains ε_{xx} derived from both analyses, shows a difference of 114% at the top of the anchor.

There is a deviation of 10% - 32% between the values of interfacial shear stress calculated by the theoretical analysis and those by finite element analysis.

The approximation of concrete strains according to theoretical analysis could be improved by introducing a greater number of concentrated vertical loads simulating the interfacial shear action along the concrete boreface in the Mindlin solution. The approximation of resin strains derived from the finite element solution could be improved by correcting the stiffness of the tensile slip elements at the bottom of the anchor, which in this study was calculated upon the assumption that the coefficient of local stress-local slip relationship was double the corresponding value of the lateral shear slip elements.

9. CONCLUSIONS

The results obtained in the investigation have been discussed in detail in the previous sections of the thesis and allow the following main conclusions:

1. An adhesive anchor is, in effect an adhesive joint and as such, this aspect of its mechanical behaviour is governed by adhesion across the concrete-resin and resin-steel interfaces. The main components of adhesion are the mechanical interlocking and the specific adhesion which consists of the primary (chemical) and the secondary (physical) adhesion. The mechanical interlocking in the adhesive anchors is initiated, on the one hand, across the resin-concrete interface by boring and by the pores of the concrete mass, and on the other, is formed along the resin-steel interface by the shape of the outer surface of the anchor and possibly due to existing microcracks.

   The specific adhesion across the concrete-resin interface, especially in the case of epoxy resins, is established by means of the dipole interaction between the two phases, concrete and epoxy resin, both of which are polar, and by hydrogen bonds. Regarding the wetting equilibria, because the surface energies of epoxy resins used in such applications are very much lower than that of the concrete surface, the criteria for maximisation of the specific adhesion are almost completely fulfilled. Besides, chemical bonds along quartz aggregates and epoxy resins are reported. However, it is uncertain

whether chemical bonds exist on any concrete-epoxy resin interface. The specific adhesion of the resin-steel interface is ensured mainly by the hydrogen bonds between the hydroxyls contained in the epoxy resin and the electronegative iron atoms of steel.

2. Due to the shrinkage of the resins and the incomplete contact between the liquid resin and the concrete or steel substrate, the theoretical adhesive bond strength is reduced. The size of the unwetted area (the flaw) controls the value of the ultimate interfacial strength. This is indicated by the fracture mechanics approach. Since the size of the flaw decreases due to an increase in the spreading coefficient of the interface, the best results in terms of interfacial strength can be achieved by using low surface energy resin.

3. The criteria for achieving high adhesion are fulfilled by polymers, among which the most important for use in structural applications are the thermosetting materials, or resins. Amongst these, epoxy resins are the most commonly used owing mainly to their polar nature, which results in high adhesive strength. The properties of epoxy resins can be modified by a whole series of additives to adapt to the particular requirements.

4. A theoretical analysis can be made based upon the assumption that all the materials involved behave

in a linear elastic manner and are homogeneous and that the value of resin axial force is negligible in relation to those of concrete and steel. Such an analysis results in closed expressions of the concrete-resin interfacial shear stress, Eq.(5.29), the concrete (P_c) and steel (P_s) forces, Eq.(5.36), the resin strain, Eq.(5.48) and the anchor displacement, Eq.(5.37), (5.38).

Any analysis of the strains and the stresses of the structural component of an adhesive anchor must take into account also the radial interfacial compressive forces which constitute the wedging action on the bore face. They consist of two components. The lateral pressure owing to micro and possibly to macro-interlocking across the steel-resin interface and to both micro - and macro-keying across the resin-concrete interface, is the first component. The second component is due to the combined shrinkage effect of resin and concrete. Both can be evaluated in a relatively simple way, Eq.(5.55) - Eq.(5.57).

The stresses of concrete at any particular point can be calculated using the Mindlin solution Eq.(5.51)-(5.54) and (5.58)-(5.61). In order to apply it the shear and radial actions across the resin-concrete interface must be simulated with a number of vertical and lateral concentrated forces.

5. A finite element analysis should take into consideration the constitutive law of the slip across the lateral steel-resin and resin - concrete interfaces,

as a function of the relevant interfacial shear stress. The adoption of linear elastic slip elements bridging the nodes of the elements across the interfaces is a way of taking into account the slip effect. The stiffness of these slip elements can be calculated from the $\delta=a\tau^m$ relationships obtained experimentally. Similarly, the stiffness of the tensile slip elements simulating the tensile interfaces at the bottom of the anchor can be defined. Since there is no information about the relevant tensile constitutive relationship $\delta=(a_t)\sigma^m$, the coefficient a_t was taken as double the corresponding value for the shear interfaces. A comparison of the results derived in this way shows that this coefficient should be corrected towards values close to that of shear stress relationship, a.

6. The mechanical behaviour of an adhesive anchor is dependent on the concrete strength, the embedment length, the diameter of the anchor and resin, the types of anchor and resin, the method of drilling, the amount of reinforcement, the size of the specimen and the method of insertion of resin. Their effect is quantified within certain range of values of each of the above variables examined in this thesis.

7. The mode of failure (concrete combined double cone failure, splitting, adhesive failure, steel failure) is dependent on these parameters. Adhesive failure takes place in the case of low adhesive strength

resins, and steel failure in anchors with small diameter and long embedment length.

A splitting mode of failure was observed in anchors with relatively large diameters, in those installed in small specimens, or adjacent or near to the edge of the specimen. Although the ratio of diameter of anchor to the size of specimen seems to control the mode of failure, resulting in splitting for high, and in concrete cone failure for low values, the limit of this ratio governing the mode of failure was not determined in this investigation. A common characteristic of all split specimens, however, is the presence of cracks starting at a point (0.20 - 0.25)1 deep and going upwards at 30°-45°. Apart from confirming the above concept, this might be of importance for defining the conditions under which splitting failure occurs.

8. The combined concrete failure involves concrete cone failure, interfacial adhesive failure and resin failure at the bottom of anchor. An increase in the value of cone height normalized with respect to the embedment length was caused by:

- decrease in embedment length
- decrease in anchor diameter
- increase in resin thickness
- decrease in concrete strength
- pouring the resin, instead of injecting it
- the use of threaded bars instead of ribbed bars
- absence of reinforcement

- large concrete specimen

9. The values of the ultimate pull-out load normalized with respect to concrete strength, $P_u/\sqrt{f_{cc}}$, were found to be almost independent of the concrete strength in all tests, Fig 7.108. This fact is important because it allowed the examination of the rest of the parameters against this value. The values of the anchor displacements at 10kN, 20kN, 30kN loading normalized with respect to concrete strength, $[(\delta_{10in1})\sqrt{f_{cc}}]$, $[(\delta_{20in1})\sqrt{f_{cc}}]$, $[(\delta_{30in1})\sqrt{f_{cc}}]$, were found to be linearly dependent on concrete strength, Fig 7.109. By the introduction of the coefficients λ_{10}, λ_{20}, λ_{30}, by which the displacements of any adhesive anchor must be divided in order to be normalized with respect to a particular concrete strength, it was possible to examine the effect of the different parameters on the anchor displacement. Further, both the relationships obtained (i.e. the constant value of $P_u/\sqrt{f_{cc}}$ and the relationship of the λ_{10}, λ_{20}, λ_{30} coefficients to the concrete strength) can be used in designing anchors. They allow the calculation of the anchor ultimate pull-out load and displacement in order to examine the fulfilment of the criteria of load carrying capacity and of serviceability on any concrete. Furthermore, they can be supplemented by the curves derived for the effect of all parameters examined on these two quantities, Figures 7.110-7.118. This means that any adhesive anchor can be designed in terms of calculation of its ultimate pull-out load and its

displacement based upon the relationships obtained for the parameters examined (an example is calculated in Appendix J).

10. The normalized values of pull-out load, $P_u/\sqrt{f_{cc}}$, are dependent:

- On the ratio of embedment length to anchor diameter by a second order function. The respective curve tends to become parallel to the f_{cc} axis at values of l/d of about 8.
- Almost linearly dependent on anchor diameter. Below a certain limit and towards zero, however, this line turns to a function of higher order.
- On the thickness of resin, with an approximately second order function which becomes constant at t/d values of approximately 0.40 in these tests.
- On the type of anchor. They are greatest for ribbed bars and least for plain anchors.
- On the type of resin, attaining a maximum value for low viscosity, low surface energy types of resin and a minimum for high viscosity resins.
- On the size of specimen being greater for the larger size of specimens (the size of specimen being sufficient to avoid local effects).
- On the presence of reinforcement, especially in the case of splitting mode. Greater values are reached in reinforced concrete specimens.
- On the method of insertion of resin, the injection resulting in remarkably higher $P_u/\sqrt{f_{cc}}$ values.

- On symmetrical fixing in relation to bore axis, lower values being reached if there is eccentricity.

11. The normalized values of displacements at 10, 20 and 30kN loading, $\delta_{inl}\sqrt{f_{cc}}$, were found to be dependent on:
    - The embedment length. They increase linearly with decrease in the ratio of embedment length to anchor diameter, Fig 7.111.
    - The anchor diameter; increasing sharply with decrease in the diameter, especially for diameters less than 10 mm, Fig 7.112.
    - The thickness of resin. They decrease almost linearly with increasing thickness up to a value of the ratio of thickness to diameter of 0.60, and then increase with higher values of this ratio, Fig 7.113.
    - The type of anchor and type of resin, being least for ribbed bars and low viscosity low surface energy resin and greatest for plain bars and gel type of resin, Fig 7.114 and Fig 7.115.
    - The size of the specimens, giving lower $\sqrt{f_{cc}}$ values (and more realistic) in the case of the larger specimen, Fig 7.116.
    - The reinforcement, decreasing almost linearly with increasing ratio of reinforcement, Fig 7.117.
    - The method of drilling, increasing if diamond drilling is used, Fig 7.118.
    - The method of insertion of resin, decreasing significantly if the resin is injected.

Finally, there is an increase in the normalized

values of displacements in the case of eccentricity of the anchor in relation to the hole axis.

12. The steel strain distributions obtained from both the theoretical and the finite element analyses are in good agreement with those obtained experimentally. The differences, which are dependent on the load level, were found to be in the middle of the anchor between 10% and 40% for the theoretical analysis and 5% and 37% for the finite element analysis for the whole range of loading up to failure, with the measured values always being higher than those calculated. The differences in resin strain between the values calculated by both analytical methods and those measured were found to be wider (the computed values were 62% higher in the upper part and 48% lower in the middle of anchor than the values measured over almost the whole range of loading up to failure. The theoretically derived values in the middle of the anchor were lower 48% to 50% than those measured).

The distribution of shear stress acting across the concrete-resin interface derived from the theoretical analysis does not deviate much from that computed by finite element analysis (32% maximum).

The anchor displacements derived from analytical

methods were found to be in good agreement with those measured (the theoretically derived values were 4% lower and the values computed by finite element analysis 26% higher than the values measured).

The differences between the concrete strains calculated analytically by both methods and those obtained experimentally were found to be:

- In the radial strains at a section extending 18 mm from the axis, between 0% and 27% for the theoretical and from 25% to 71% for the finite element analysis. The theoretically derived values were lower than the measured values and those computed by finite element analysis were higher than the measured values.
- In the vertical strains, between 7% and 22% for the theoretically calculated values and 37-49% for those computed by finite element analysis. All the theoretically derived values were lower than those measured, for loads up to P=20 kN.

The calculated concrete principal tensile strains show that, in the specimens with combined mode of failure, the first crack close to interface at a depth of 60% of the embedment length is expected at a

load almost equal to 75% of the ultimate pull-out load.

13. The sequence of the failure of the anchor components in the combined mode of failure is: concrete failure in the upper part - interfacial shear failure-resin failure at the bottom.

10. RECOMMENDATIONS FOR FURTHER WORK

In discussing the results obtained by the theoretical and the finite element analysis or the experimental work, various subjects needing further examination came to light. The most important of them are presented below.

1. The mechanism of the splitting mode of failure, needs further investigation in terms of a formulation of a relationship between the parameters influencing it (diameter of anchor, size of specimen and possibly others). In addition, the mechanism of initiation of a crack travelling upwards at 30°-45° to the vertical axis and starting from a point at (0.20-0.25)l below the upper specimen surface might be of importance.

2. More tests per variable would enable a more accurate mathematical formulation of the effect of each parameter on the normalized values of the pull-out load or on the anchor displacements. As a result, design charts based on the two criteria of normalized values $P_u/\sqrt{f_{cc}}$ and $\delta_{jinl}\sqrt{f_{cc}}$ obtained, could then be drawn.

3. Because the effect of dynamic loading is important for the design of anchors in structures under dynamic forces, it must be examined in detail.

4. The effect of time dependence of the resin properties will certainly affect the normalized values of displacements under long duration loads and needs

further research.

5. The effect of elevated ambient temperature on the normalized values of both the pull-out load and the anchor displacement is important. Although the heat deflection temperature of modern resinous materials has dramatically improved, the data on the mechanical behaviour of adhesive anchors under increased concrete temperature would be very important.

11. DESIGN RECOMMENDATIONS

In the following the existing specifications relating to the design of adhesive anchor systems and the contribution of this thesis are briefly presented and discussed.

A typical anchor system consists of:

- the anchor, (or group of anchors)
- the base plate, if any, which is anchored to concrete by means of the anchor (or anchors)
- the load carrying structural member, which is usually a single reinforcing bar welded or spliced to the anchor by special devices.
- the concrete substrate

The performance of an anchor system, therefore, depends on the interaction of these components and on their strength.

The tendency of all existing specifications is to ensure modes of failure which are accompanied by relatively large inelastic deflections, which are referred to as "ductile".

Excluding the existing concrete substrate the rest of the components can be designed to behave in a ductile manner.

The existing specifications refer only to the prediction of ultimate pull-out load in a general way (without taking into consideration all the parameters involved, Sections 7.11.2, 7.12, 7.13). They further state the requirements for safety factor and give closed expressions for the calculation of edge and group effects.

11.1. ACI Committee 355 - Anchorage to Concrete, /62/

According to a recent draft report of the committee,

while anchors may differ in their manner of load transfer, there are distinct similarities in how they function with respect to the concrete, once the load is transferred. Regardless of selected type of anchor and desired mode of failure, all anchor designs must consider the capacity of the concrete needed to sustain the design loading.

11.1.1. Basic equations for pull - out capacity of anchors

The pull-out strength of concrete for any individual anchor, unaffected by edge conditions, may be determined by:

$$F_u = \pi \; E^2 \; (2f'_t/3) \quad \ldots\ldots\ldots\ldots\ldots\ldots\ldots\ldots (11.1)$$

where:

E : the radius of the stress cone in inches

f'_t : the average splitting tensile strength of the concrete in psi

The stress cone radius (E) will vary with anchor size, type and the embedment, and will be discussed under specific types of anchors.

In addition, the draft of the committee ACI-355 refers to other proposed formulae, reported below.

For headed anchors, Eligehausen and Sawade /62/ derived from 170 test series with single anchors with failure of the concrete, the equation:

$$F_u = (16.5) \; (l_d^{3/2}) \sqrt{\beta_w} \; (N) \quad \ldots\ldots\ldots\ldots\ldots\ldots\ldots (11.2)$$

where:

l_d : embedment depth [mm]

β_w : cube compressive strength [N/mm²]

These tests included anchorage depths of 40 mm to 525 mm, with concrete strengths between 20 N/mm² and 50 N/mm².

Braestrup, et al, /62/ gives the predicted failure load as:

$$F_u = (0.21)(l_d)^2(1+(d_h/l_d))(\sqrt{\beta_w})\ [N] \quad .....(11.3)$$

where:

d_h : the diameter of the head of the anchor

Eq.(11.3) was deduced by applying the theory of plasticity to headed studs embedded in concrete. The failure load is assumed to be proportional to the concrete compressive strength.

Bode and Roik /62/ fitted data of a large number of tests to arrive at equation (11.4).

$$F_u = (12.2)(l_d^{3/2})(1+(d_h/l_d)(\sqrt{\beta_w})\ [N] \quad .....(11.4)$$

Cannon /62/ has developed an improvement to the ACI 349, Appendix B equation by assuming a decreasing angle of the failure cone for embedments less than six inches.

$$\text{for } l_d<3 \text{ inches, } a=28^\circ+1.1(l_d)^2 \quad .....(11.5)$$

$$\text{for } l_d>3 \text{ inches but } <6 \text{ inches, } a=45^\circ-0.79(6-l_d)^2 \quad .....(11.6)$$

The limiting tensile capacity of all anchorages is the tensile strength of the anchor steel: $A_s f_{ut}$

where:

A_s : the tensile stress area of the anchor steel

f_{ut} : the tensile strength of the anchor steel

Design of an anchorage may be based on the strength of anchor steel when the pull-out strength of the concrete, as determined above, exceeds ($A_s f_{ut}$).

11.1.2. Bonded (adhesive) anchors

These are anchors which depend on the strength of bond to transfer load to the concrete. They generally require deeper embedments to develop the strength of anchor steel

than headed anchors. Adhesive anchors exhibit elastic behaviour up to nearly maximum load. While they show relatively low coefficient of variation in comparison to torque controlled and drop-in anchors, the bond strengths vary considerably depending on the adhesive used and installation procedure. Anchor steel is generally composed of threaded rod, deformed rebar, or plain bars without deformations. Minimum embedment to develop strength will depend on the strength of concrete and anchor type.

Assuming a uniform stress distribution along the embedment length, the bond strength is in the order of 1300 psi (9 N/mm^2) with a coefficient of variation of 10%-15% for polyester and vinylester resin anchors installed in a concrete with compressive strength of 3,000 psi (20 N/mm^2).

The bond strength increases approximately with the square root of the concrete strength.

The pull-out capacity of resin anchors increases with increasing embedment length. However, after about nine anchor diameters the increase is not proportional to embedment, due to the high bonding effect resulting in high load transfer to the concrete at the top of the anchor. The bond failure is no longer uniform, and if the tensile load is sufficiently high, the failure initiates a concrete failure in the upper part of the anchor and then the bond fails in the remaining embedment length.

11.1.3. Group effect

The pull-out strength of concrete for multiple anchors is affected by the overlapping of stress cones. When the spacing is equal to or greater than 2E, the full value of individual capacities can be applied to all anchors.

However, there are difficulties in distributing a load evenly to widely spaced anchors.

When the spacing of anchors (S) is equal to or less than E, the multiple anchors act as a unit and capacity is controlled by the projected area (Ap) of the group and the group pull-out capacity (F_{ug}) can be determined by:

$$F_{ug} = (A_p).(f'_t)(2/3) \quad \text{.....(11.7)}$$

When S/E<1.0, the following formula can be used to calculate the projected area (A_p):

$$A_p = ((N_x-1)S_x+2E)((N_y-1)S_y+2E) - (0.86)E^2 \quad \text{...(11.8)}$$

where:

N_x, N_y: the number of anchors in the x and y directions

S_x, S_y: the average spacing of anchors in the x and y directions

When S_x and S_y = E, the above formula for projected area becomes:

$$A_p = ((N_x+1)(N_y+1) - 0.86)E^2 \quad \text{.....(11.9)}$$

When the average spacing (S) is greater than E but less than 1.5E, the failure pattern is composed of the formation of individual stress cones and failure is controlled by the lowest strength anchor in the group so that there is little if any increase in group pull out capacity above the capacities for S=E. Therefore: $A_p = A_{pE}$

When S is equal to or greater than E but less than 2E, the interference between individual stress cone development is less and capacity increases from that at S=E to that at S=2E so that:

$$A_p = A_{pE}+(\pi nE^2-A_{pE})(S-1.5E)(2/E) \quad \text{.....(11.10)}$$

where:

n:the number of tensile anchors in the group

Formula (11.7) can be used with the appropriate A_p to determine pull-out capacity of the multiple anchor group.

11.1.4. Edge effect

When anchors are located closer to an edge than the radius of the stress cone E, the capacity of the anchors nearest the edge are reduced by the loss of projected stress cone area and the reduced confinement of the lateral pressure. The capacity of anchors near an edge should be modified by the following edge factor (E_F):

$$E_F = 0.3 + 0.7\ a/E \quad \text{.....(11.11)}$$

where:

a: the distance from the anchor center to the near edge

For an anchor located in a corner, E_F equals the product of the two edge factors.

For one row of anchors near an edge out of a multiple row group, the modification of the group effect of the row nearest the edge by the edge factor is necessary and then the restriction of the capacity of anchor load of all anchors to that of the edge anchors follows.

11.1.5. Design criteria

These depend on:

- The types of loads.
  - Externally applied loads (dead, live, gravity loads, wind, earthquake, impact, dynamic).
  - Incremental displacements (temperature variations, creep, shrinkage).
  - Deflections, movements (settlements, inelastic structural displacements).

- The mode of failure.
    - Ultimate loads
    - Load deflections
    - Ductility
- Durability.
    - Fire resistance
    - Corrosion resistance
- The sensitivity of the system.
    - Degree of redundancy
    - Criticality in the event of failure
- The selection of anchorage and method of installation.

11.1.6. Safety factors

The proposed safety factors, according to the aformentioned criteria are shown in Table 11.1.

Table 11.1 Safety factors proposed by ACI 355

Type of Load		Mode of failure and durability		Sensitivity	Method of installation
• dead	2.0	• ductile	1.0	• redundancy not critical	• cast in place:1.0
• live		• ultimate			• post drilled:1.25
• gravity		• yield		• temporary	
• wind		• displacement		• permanent	
• wind pressure		• slip		• re-use	
• earthquake				• no redundancy	1.25
• cyclic		• fire			
• dynamic		• corrosion			
• impact	4.0	• flexure	1.5		

11.2. ACI 349 - Code requirements for nuclear safety related concrete structures, /63/

ACI 349, Appendix B (6), gives the concrete tensile capacity as the cone of uniform stress of $4\Phi(\sqrt{f'_c})$ acting on

the projected area of the stress cone.

$$U_p = (4\Phi)(\sqrt{(f'_c)}).(A_p) \quad \text{.....(11.12)}$$

where:

Φ : capacity reduction factor

A_p : effective projected area of stress cone

This stress cone angle is assumed to be 45^0. For non-ductile failures (concrete) a Φ factor of 0.65 is used.

Then the edge effect is mentioned, which, for an anchor installed too near an edge, results in failure of the anchor at the edge before developing the full concrete cone strength.

For concrete edge failures in tension, the minimum distance, m, for tensile failure is given as:

$$m = D\ [\sqrt{(F_u/56(\sqrt{f'_c}))}] \quad \text{.....(11.13)}$$

where:

D :anchor diameter [in]

F_u :ultimate tensile strength of anchor [psi]

f'_c :compressive strength with concrete [psi]

11.3. Prestressed Concrete Institute (PCI), /64/

Reinforcing bars, may be embedded into non-rusted metallic flexible interlocking conduit and grouted to provide a connection for a column base, column splice or other tension or compression connection. The required embedment length may be determined by:

$$l_e = (A_{s\,o})(f_y)/(\Phi)(\Sigma_o)(1200) \quad \text{.....(11.14)}$$

where:

$A_{s\,o}$:area of bar

f_y :yield strength of the bar

Σ_o :perimeter of the bar

Φ :0.85

The following limitations are recommended:

- The minimum concrete cover over the grouted reinforcing bar should be 3 inches.
- The conduit should have a minimum thickness of 0.023 in., and a minimum internal diameter of 3/4 in.
- The grout material should have a minimum compressive strength of 6000 psi.
- Confinement reinforcement consisting of spiral or ties having $A_{sh}=A_{so}f_y/\mu f_{ys}$ may be required to prevent splitting or bond failure between the conduit and the surrounding concrete, where μ the shear friction coefficient (usually μ=1.6).
- l_e should not be less than 6 in.

11.4. European Union of Agreement (UEAtc), /65/

This directive provides procedures to follow in order to obtain the basic characteristics of anchors installed in concrete. The philosophy is based on the limit state design, therefore, the following properties of the anchor are important:

- Ultimate carrying capacity.
- Serviceability characteristics.
- Durability characteristics.

It describes the procedures and requirements on tests to obtain reliable data but does not give any formula for the calculation of above properties. However, it gives the reduction of the pull-out load due to the group and edge effect as:

$$r_{ed}\ P = P\ (x_{ai})\ (x_{ari}) \quad \text{.....(11.15)}$$

where:

r_{ed} P: the pull-out load, reduced due to the group and edge effect

P : the maximum (original) pull-out load, equal to the sum of pull-out loads of the anchors

x_{ai} : reduction factor for the group effect.

$x_{ai} = (x_{ai1})(x_{ai2})(x_{ai3})$

x_{ai1}, x_{ai2}, x_{ai3}: the elementary reduction factors corresponding to the closeness of the anchor considered to anchors 1, 2, 3 etc respectively

x_{ari} : reduction factor for the edge effect

The values of x_{ai} and x_{ari} reduction factors are to be found by tests.

11.5. The contribution of the thesis to the design of adhesive tensile anchors

The results of this thesis allow:

- A more accurate calculation of the ultimate pull-out load in which the effect of the variables examined in this work can be taken into account. These variables were:

1. The concrete strength.
2. The embedment length.
3. The anchor diameter.
4. The resin thickness.
5. The type of anchor.
6. The type of resin.

7. The amount of reinforcement.
8. The method of insertion of resin.
9. The method of drilling the hole.
10. The eccentricity of the anchor in the hole.

- The calculation of the anchor displacement at different load levels taking into consideration the effect of the aformentioned parameters.

Thus, it is possible to design an individual adhesive anchor in order to fulfil the criteria of:

- Limit state of load carrying capacity.

$$\gamma\ (P_{des}) <= P_{ult} \quad \text{.....(11.16)}$$

- Limit state of serviceability

$$\delta_{des} <= \text{imposed limit of slip} \quad \text{.....(11.17)}$$

For safety factors γ the values reported by ACI-Committee 355, Table 11.1 can be used. The group and edge effect can also be taken into account in accordance with ACI 355 Sections 11.1.3, 11.1.4. The steps to follow in order to calculate the ultimate pull-out load and the anchor displacements are:

- Calculation of the fundamental pull-out value P_{uo} from the equation $(P_{uo}/\sqrt{f_{cc}})=6.9$ which relates to a 12 mm anchor with embedment length $l=(8.3)d$, $t=2$ mm, with an epoxy of low viscosity and $E_r=2200$ N/mm², poured into the annular gap and a hole drilled by percussive drilling device.

- The calculation of sets of coefficients μ, λ_e relating

to load and displacement, respectively:

$\mu_1 = 1.0, \lambda_{e1}$: for the effect of concrete strength on the values of $(P_u/\sqrt{f_{cc}})$ and $(\delta_{in1}(\sqrt{f_{cc}}))$ respectively, according to Fig.7.108, Fig.7.109. $(P_u/\sqrt{f_{cc}})$: ultimate pull-out values normalized with respect to concrete strength of 19.56 N/mm² and $\delta_{in1}\sqrt{f_{cc}}$: value of displacement at load level i normalized with respect to concrete strength of 19.56 N/mm²)

where:

$\lambda_{e10} = 1$, for the load P=10 kN

$\lambda_{e20} = 1-[(f_{ci}-19.56)/90.65]$, for P=20 kN

$\lambda_{e30} = 1-[(f_{ci}-19.56)/70]$, for P=30 kN

and

$(\delta_{20n1}\sqrt{f_{cc}}) = (\delta_{20}\sqrt{f_{cc}})/\lambda_{e20}$

$(\delta_{30ni}\sqrt{f_{cc}}) = (\delta_{30}\sqrt{f_{cc}})/\lambda_{e30}$

For values in between, the data of Section 7.12.3 Fig 7.109 can be used. Therefore:

$\delta_i\sqrt{f_{cc}} = (\delta_{in1})\lambda_{ei}$ .....(11.18)

μ_2, λ_{e2} : for the effect of the embedment length on the values of $(P_u/\sqrt{f_{cc}})$ and $(\delta_{in1}\sqrt{f_{cc}})$ respectively, according to Fig.7.110,7.111

μ_3, λ_{e3} : for the effect of the anchor diameter on the values of $(P_u/\sqrt{f_{cc}})$ and $(\delta_{in1}\sqrt{f_{cc}})$ respectively, according to Fig.7.112

μ_4 , λ_{e4} : for the effect of the resin thickness on the values of $(P_u/\sqrt{f_{cc}})$ and $(\delta_{inl}\sqrt{f_{cc}})$ respectively, according to Fig.7.113

μ_5 , λ_{e5} : for the effect of the type of anchor on the values of $(P_u/\sqrt{f_{cc}})$ and $(\delta_{inl}\sqrt{f_{cc}})$ respectively, according to Fig.7.114

μ_6 , λ_{e6} : for the effect of the type of resin on the values of $(P_u/\sqrt{f_{cc}})$ and $(\delta_{inl}\sqrt{f_{cc}})$ respectively, according to Fig.7.115

μ_8 , λ_{e8} : for the effect of the amount of reinforcement on the values of $(P_u/\sqrt{f_{cc}})$ and $(\delta_{inl}\sqrt{f_{cc}})$ respectively, according to Fig.7.117

μ_9 , λ_{e9} : for the effect of the method of insertion of resin on the values of $(P_u/\sqrt{f_{cc}})$ and $(\delta_{inl}\sqrt{f_{cc}})$ respectively, according to Fig.7.118

μ_{10} , λ_{e10} : for the effect of the method of drilling the hole on the values of $(P_u/\sqrt{f_{cc}})$ and $(\delta_{inl}\sqrt{f_{cc}})$ respectively, according to Fig.7.118

μ_{11} , λ_{e11} : for the effect of the possible eccentricity of the anchor in relation to the hole axis, on the values of $(P_u/\sqrt{f_{cc}})$ and $(\delta_{inl}\sqrt{f_{cc}})$ respectively, according to Fig.7.118

- Calculation of the ultimate pull-out load of the particular anchor as:

$$P_u=(P_{uo})[(\mu_1)(\mu_2)(\mu_3)(\mu_4)(\mu_5)(\mu_6)\quad(\mu_8)(\mu_9)(\mu_{10})(\mu_{11})]$$

- Calculation of the fundamental $\delta_{i,o}$ value, from the equation

$$\delta_{i,o}=(26.9)P_i^{1.047}\ \text{for anchor 3.01}$$

- Calculation of the $\delta_i\sqrt{f_{cc}}$ value of the anchor displacement at each load according to Eq.(11.18) as:

$$\delta_i=(\delta_{i,o})[(\lambda_{e1})(\lambda_{e2})(\lambda_{e3})(\lambda_{e4})(\lambda_{e5})(\lambda_{e6})\quad(\lambda_{e8})(\lambda_{e9})(\lambda_{e10})(\lambda_{e11})]$$

Then, the validity of the limit state of load carrying capacity and serviceability, Eq.(11.16), (11.17), can be proven.

The above calculations provide evidence that the quantification proposed by the thesis for the effect of the different variables on the values of ultimate pull-out load and the anchor displacement, normalized with respect to concrete strength, is simple and can therefore be applied to the design of adhesive anchors according to the modern aspects of structural safety.

12. REFERENCES

/1/ James R.W., Guardia C.D., McCreary Ch.R. Strength of Epoxy grouted anchor bolts in concrete, Journal of Structural Engineering, December 1987.

/2/ Biviridge R.L.W.. Repairs and extensions to concrete structures using resin anchored bars. Civil Engineering and Public Works Review, July 1973.

/3/ Biviridge R.L.W. Resin anchors. Civil Engineering, August 1976.

/4/ Sell R.Tragfaehigkeit von mit Reaktionsharz-moertelpatronen versetzen Betonankern und deren Berechnung. Die Bautechnik, 10/1973.

/5/ Eibl J.-Franke L.-Hjorth O. Versuche mit Kunstharz-moerteln. Die Bautechnik, 10/1972.

/6/ Farmer I.W. Stress distribution along a Resin grouted Rock Anchor. International Journal of Rock Mechanics and Mining Science. Anbstr, Vol. 12. Pergamon Press 1975.

/7/ Rehm G.-Franke L. Verankerung von Betonrippen-staehlen in Kunstharzmoerteln und Kunstharzbeton. Bauingenieur, 1978/53.

/8/ Daws G. An Introduction to the design of a resin anchor system. Concrete Beton, No. 20, 1980.

/9/ Lee N.K.- Mayfield B.- Snell C. Resin anchors in comcrete. Civil Engineering, April 1980.

/10/ Cannon R.W.-Godfrey D.A.-Moreadith F.L. Guide to the Design of Anchor Bolts and Other Steel Embedments. Concrete International, July 1981.

/11/ Wachtsmuth P.P.-Eligehausen R.Stand der Befestigungstechnik im Stahlbetonbau. IABSE Surveys S-19/82.

/12/ Kobarg J.Verbundfestigkeit von nachtraeglich reaktionsharzvermoertelten Betonstaehlen in Beton. Institut fuer Beton und Stahlbeton. Universitaet Karlsruhe. Bundesministerium fuer Bauordnung, Bauwesen und Staedtbebau. Forschungsbericht AZ:B15-800180, Juni 1982.

/13/ Peier W.H. Model for Pull-out Strength of Anchors in Concrete. ASCE. Journal of Structural Division, May 1983.

/14/ Eligehausen R.-Mallee R.-Rehm G. Stand der Befestigungstechnik im Stahlbetonbau. IABSE Surveys S-19/82.

/15/ Kinloch A.J. Adhesion and Adhesives Science and Technology. Chapman and Hall. London,1987./3.8.3/

/16/ Alner D.J. Aspects of adhesion. Procedings of the conferences held at the CITY University on 5 and 6 April 1967 and 9 and 10 April 1968. Volume 5. University of London Press Ltd, 1969.

/17/ Fiebrig M.Scientific Aspects of adhesion phenomena. State of the art report, unpublished. RILEM International Symposium on Adhesion between polymers and concrete". Aix en Provence, 16-19/9/86.

/18/ Eley D.D. Adhesion. Oxford University Press. London, 1961.

/19/ Good R.J. Intermolecular and Interatomic forces in "Treatise on Adhesion and Adhesives". Edited by R.L.Patrick. Volume 1. Marcel Dekker Inc. N.Y., 1967.

/20/ Young T. Cohesion of fluids. Philosophical Transactions of the Royal Society. London, 95 (1805).

/21/ Dupre' A. Theorie mechanique de la chaleur. Gauthier-Villars. Paris, 1869.

/22/ Kinloch A.J. Durability of Structural Adhesives. Applied Science Publishers, Essex, 1983.

/23/ Mouton Y. Reparation des structures en beton fissurrees par injection de liant epoxydiques. Laboratoir central des ponts et chaussees. Rapport de recherche LPC No8. PARI, Juin 1979.

/24/ Zisman, W.A. Adhesion. Industrial and Engineering Chemistry. 55(1953), No 1.

/25/ Wachtsmuth P.P. Tragverhalten vom Metallspreizduebeln in unbewehrten Beton unter zentrisher Zugbeansruchung. Dissertation. Institut fuer Werkstoffe im Bauwesen der Universitaet Stuttgart, 1982.

/26/ Mlodecki J. Adhesion forces of polymer modified concrete and plain concrete to steel in moulds and in reinforced concrete. RILEM international symposium on adhesion between polymers and concrete. Aix en Provence, 1986.

/27/ Fiebrig M. Zur Adhesion zwischen Polymeren Bindemitteln und Beton unter besonderer Berueck-sichtigung von Wasserwirkungen. Dissertation. R.W. Technische Hochschule Aachen, 1987.

/28/ Ramond G. Etude de la mouillabite de quelques materiaux routiers. Laboratoire Central des Ponts et chaussees Paris 1972. Internal report.

/29/ Zorll U. Mechanismus und Pruefung der Haftung von Beschichtungen. Tonindustriezeitung 99(1965).

/30/ Rehm G.-Franke L. Kleben im Konstruktiven Betonbau. Deutcher Auschuss fuer Sthalbeton Heft 331, 1982.

/31/ Hewlett P.C. Surface properties of substrate. State of the art report, unpublished. RILEM international symposium on adhesion between polymers and concrete. Aix en Provence, 1976.

/32/ Charnecki L. - Puterman M. Polymer materials for bonding tasks. State of the art report, unpublished. RILEM international symposium on adhesion between polymers and concrete. Aix en Provence, 1986.

/33/ Maier S. Kurzzeitverhalten von Giessharzen verschiedener Modifikationen mit Fuellstoffen im Hinblick auf die Verwendungsfaehigkeit im Bauwesen. Dissertation. T.U. Stuttgart, 1965.

/34/ Dahlquist G.A. The significance of Surface Energy in Adhesion. Proceedings of the conference held at the City University on 5, 6 April 1967 and 9, 10 April 1968. University of London press Ltd. London, 1969.

/35/ Allen K.W. Strength and structure. Aspects of adhesion. Proceedings of the conference held at Northampton College of Advanced Technology on 21,22 March 1963. University of London Press Ltd, 1965.

/36/ Griffith. The Phenomena of Fracture and Flow in Solids. Phlosophical Transactions of the Royal Society, London, 163/1920.

/37/ Williams J.G.. Fracture Mechanics of Polymers. Ellis Horwood Limited, Chichester 1984.

/38/ Irwin. Fracture Mechanics. Pergamon Press, N.Y., 1960.

/39/ Wu. Polymer interface and adhesion. Marcel Dekker Inc. N.Y., 1982.

/40/ Gent. Fracture Mechanics of Adhesive Bonds. Rubber Chemistry and Technology, 202/1974.

/41/ Arridge R.G.C. Mechanics of Polymers. Clarendon Press. Oxford, 1975.

/42/ Henning O.- Knofel D. Baustoffchemie. Eine Einfuerung fuer Bauingenieure und Architekten. Bauverlag. Wiesbaden, 1982.

/43/ Schutz R.J. On new ASTM standards - Epoxy resins. Concrete International. January 1982.

/44/ Shaw J.D.N. A review of resins used in construction. Adhesion and Adhesives, April 1982.

/45/ Furr H.L. Highway uses of epoxy with concrete. Transportation research board. National Research Council. Washington D.C,1984.

/46/ Krausse J. Reactionharzbeton als Werkstoff fuer hochbeanspruchte Maschinenteilen. Darmstadt, 1987.

/47/ Baoyu L. - Anoi L. - Geng R. Study of 3200 Vinylester resin mortar and its application. Proccedings of RILEM international symposium on adhesion between polymers and concrete. Aix en Provence, 1968 . Chapman and Hall. London, 1968.

/48/ Seidler P. Industriefussboeden. Expert Verlag, Grafenau 1 Wuertt, 1987.

/49/ Fiebrig M. Adhesion test procedures (unpublished). State of the art report. RILEM international symposium on adhesion between polymers and concrete. Aix en Provence, 1986.

/50/ Fiebrig .Epoxy resins for crack injection at joints of prestressed concrete bridges. International

conference on Polymers in Concrete. Darmstradt, 1984.

/51/ Conrad K.H. Beeinflussung von technologischen Eigenschaften zementgebundener Moerteln durch geeignete Epoxydharzsysteme unter Berueck-sichtigung der mehraxialen Festigkeiten. Dissertation. Grenoble 1986.

/52/ Lorman W.R. Engineering properties of epoxy resin as a structural adhesive for cracked reinforced concrete waterfront facilities. Naval Engineering Command.

/53/ Hertig P. Utilisation des resines epoxydique pour le collage acier-beton dans la construction mixte. Bulletin technique de la Suisse Romanche. 99, 1973.

/54/ Bresson J. Nouvelles recherces et applications concernant 1' utilisation des collages dans le structures. Beton plaque. Annales de 1' Institute Techniques du Batiment et des Travaux Publics, No 116, Paris Fevrier 1971.

/55/ Takaku A. - Arridge RGC. The effect of interfacial radial and shear stress on fibre pull-out in composite materials. Journal of Physics. D. Applied physics, Volume 6, 1973.

/56/ Laldji S. - Young AG. Bond between steel strand and cement grout in ground anchorages. Magazine of concrete reaearch. Volume 40, No 143, June 1988.

/57/ Robins P.J. - Standish I.G. The effect of lateral pressure on the bond of round reinforcing bars in concrete. International Journal Adhesion and Adhesives, April 1982.

/58/ Mindlin R. Force at a point in the interior of a

semi-infinite solid, Physics,volume 7, May 1936.

/59/ Probst.P. Ein Beitrag zum Bruchmechanismus von zentrisch gedruecktem Mauerwerk. Dissertation. Technische Universitaet Munchen, Februar 1981.

/60/ Rehm J. Ueber Die Grundlagen des Verbundes zwischen Stahl und Beton. Deutscher Auschuss fuer Stahlbeton. Heft 138, Berlin. Verlag von Wilhelm Ernst und Sohn.

/61/ Heilman H.G.-Hilsdorf H.-Finsterwalder K. Festigkeit und Verformung von Beton unter Zugspannungen. Deutscher Ausschuss fuer Stahlbeton. Heft 203, Berlin 1969. Verlag von Wilhelm Ernst und Sohn.

/62/ ACI Committe 355 - Anchorage to concrete. Draft state-of the art report. American concrete Institute, Detroit MI, September 1987.

/63/ ACI Committe 349 - Code requirements for nuclear safety related concrete structures (ACI 349-80) and commentary (ACI 349 R-80). American Concrete Institute, Detroit MI, April 1981.

/64/ P.C.I. (Prestressed Concrete Institute). PCI Design Handbook. Chikago, Illinois.

/65/ UEAtc. European union of agreement. UEAtc Directives for Assessment of Anchor Bolts - M.O.A.T. No 42/1986. December 1986.